EGE UNIVERSITY GRADUATE SCHOOL OF NATURAL AND APPLIED SCIENCES

(DOCTORATE THESIS)

POLYMER CLAY NANOCOMPOSITES

Esra Evrim YALÇINKAYA

Supervisors : Prof. Dr. Mehmet BALCAN

Prof. Dr. Çetin GÜLER

Chemistry Department

Department Code: 405.04.01

Presentation Date : 24.06.2011

Bornova-İZMİR

2011

Esra Evrim YALÇINKAYA tarafından doktora tezi olarak sunulan **"Polymer Clay Nanocomposites"** başlıklı bu çalışma E.Ü. Lisansüstü Eğitim ve Öğretim Yönetmeliği ile E.Ü. Fen Bilimleri Enstitüsü Eğitim ve Öğretim Yönergesi'nin ilgili hükümleri uyarınca tarafımızdan değerlendirilerek savunmaya değer bulunmuş ve **24.06.2011** tarihinde yapılan tez savunma sınavında aday oybirliği/oyçokluğu ile başarılı bulunmuştur.

Jüri Üyeleri:		**İmza**
Jüri Başkanı	**: Prof.Dr.Mehmet BALCAN…….**	**…….**
Raportör Üye	**: Prof.Dr. Kadir YURDAKOÇ…….**	**…….**
Üye	**:Yrd.Doç.Dr.Nursel ACAR SELÇUKİ**	**…….**
Üye	**: Doç.Dr. Armağan KINAL…….**	**…….**
Üye	**: Doç.Dr. Mustafa DEMİR.……**	**…….**

ÖZET

POLİMER KİL NANOKOMPOZİTLERİ

Esra Evrim YALÇINKAYA

Doktora Tezi, Kimya Bölümü
Tez Yöneticisi: Prof. Dr. Mehmet BALCAN
Prof. Dr. Çetin GÜLER

Haziran 2011, 100 sayfa

Bu çalışmada elektrik-elektronik endüstrisinde yaygın bir şekilde kullanılan polinorbornadien ile modifiye edilmiş montmorillonit kullanılarak polimer kil nanokompozitleri hazırlanmıştır. Bu amaçla montmorillonit, aynı zamanda polimerleşme reaksiyonlarında katalizör olarak kullanılabilecek olan kuaterner amonyum tuzu içeren rutenyum kompleksi ile modifiye edilmiştir. Norbornadien monomerinin polimerizasyon koşulları optimize edilmiştir. In-situ polimerizasyon yöntemiyle norbornadienin katmanlar arasında polimerleşmesi sağlanmıştır.

Çalışma süresince elde edilen malzemelerin spektroskopik (^{1}H-NMR, FTIR, XRD), kromatografik (GPC) ve termal (TG, DTG) analizleri gerçekleştirilerek yüzey özellikleri (TEM, SEM) ve dielektrik özellikleri incelenmiştir. Kil tabakalarının polimer içinde kısmen dağılmış (exfoliye) ve kısmen aralanmış (intercalated) yapılarda dağıldığı görülmüştür. Hazırlanan nanokompozitlerin termal kararlılıklarının saf polimere göre arttığı gözlenmiştir.

Uygulanan frekans arttıkça nanokompozitlerin dielektrik sabitleri ve dielektrik kayıpları azaldığı görülmüştür. Bu sonuçlar polinorbornadien-kil nanokompozitlerinin elektrik-elektronik endüstrisindeki kullanım alanlarının polinorbornadiene göre genişlemesine yol açacaktır.

Anahtar sözcükler: Halka açılma metatez polimerizasyonu, Polinorbornadien-kil nanokompozitleri, Polimerik malzemeler, Dielektrik özellikler.

ABSTRACT

POLYMER CLAY NANOCOMPOSITES

YALÇINKAYA, Esra Evrim

Ph.D. in Chemistry
Supervisor: Prof. Dr.Mehmet BALCAN
Prof.Dr.Çetin GÜLER
June 2011, 100 pages

In this study, polymer clay nanocomposites were prepared by using modified montmorillonite and polynorbornadiene that is used commonly in electric-electronic industry. To achieve this aim, the montmorillonite was modified by a Ruthenium complex containing a quaternary ammonium salt which was assigned as a catalyst in the polymerization reactions. Polymerization conditions of norbornadiene monomer were optimized. The norbornadiene monomers were polymerized among the montmorillonite layers by in-situ polymerization method.

The spectroscopic (^{1}H NMR, FTIR, XRD), chromatographic (GPC), thermal (TG, DTG) analyses of the materials synthesized throughout the study were made and also their surface (TEM, SEM) and dielectric properties were obtained. The clay layers were dispersed in the polymer matrix with partially exfoliated and partially intercalated structures. Thermal stabilities of the prepared nanocomposites were increased compared to pure polymer.

Dielectric constants and dielectric losses of the nanocomposites were decreased with increasing of the the applied frequency. These results will lead to the expansion of usage areas polynorbornadiene-clay nanocomposites in electric-electronic industry according to polynorbornadiene.

Keywords: Ring opening metathesis polymerization, Polynorbornadiene–clay nanocomposites, Polymeric materials, Dielectric properties.

ACKNOWLEDGMENT

I would like to give my best thanks to my supervisor, Prof. Dr. Çetin GÜLER for his precious suggestion, patience, enlightening me via his deep knowledge, experience and encouragement. He is a great mentor for me, who enriched my knowledge with his exceptional insights into chemistry. I would also like to thank Prof. Dr. Mehmet BALCAN for his help, suggestion, contribution and knowledge.

I would like to express my committee members, Prof. Dr. Kadir YURDAKOÇ and Assist. Prof. Dr. Nursel ACAR for their thoughtful comments.

Special thanks also go to the my dear friend Arş.Gör. Sıla BALCAN for her lasting frienships and support.

I want to thank to Research Grand Office of Ege University for supporting the 2007 Fen 046 numbered project. I also thank to TUBITAK for research funds (project number 108T101).

Finally, I am greatful to my family, especially my husband Selçuk YALÇINKAYA for his love, encouragement, encourange and supporting, my daughter dear Beril, who gave me so much happy time at home and my parents, especially my mother Süheyla ŞAKA, my grand mother for their great support of all my life.

İzmir / June 2011 **Esra Evrim YALÇINKAYA**

CONTENTS

Page

CONTENTS (continued)

Page

CONTENTS (continued)

Page

CONTENTS (continued)

Page

LIST OF FIGURES

Figure **Page**

LIST OF FIGURES (continued)

Figure **Page**

LIST OF FIGURES (continued)

Figure **Page**

LIST OF FIGURES (continued)

Figure **Page**

LIST OF FIGURES (continued)

Figure **Page**

LIST OF FIGURES (continued)

Figure **Page**

LIST OF TABLES

Table **Page**

ABBREVIATIONS

DCE	Dicholoroetane
DTG	Differential Thermal Analysis
FTIR	Fourier Transform Infrared Spectroscopy
GPC	Gel Permeation Chromatography
^{1}H NMR	Proton Nuclear Magnetic Resonance Spectroscopy
NBD	Norbornadiene
M_n	Number-average Molecular Weight
M_w	Weight- average Molecular Weight
PDI	Polydispersity Index
PNBD	Polynorbornadiene
ROMP	Ring Opening Metathesis Polymerization
SEM	Scanning Electron Microscopy
TEM	Transmission Electron Microscopy
TG	Thermogravimetry
TMSD	Trimethylsilyldiazomethane
XRD	X-Ray Diffraction Spectrometer

1. INTRODUCTION

Manufacturers fill polymers with particles in order to improve the stiffness and the toughness of the materials, to enhance their barrier properties, to enhance their resistance to fire and ignition or simply to reduce cost. Addition of particulate fillers sometimes imparts drawbacks to the resulting composites such as brittleness or opacity.

The marketplace is always looking for new products that have better performance at a lower cost, and such demands are very clearly seen in the composites arena where materials development is closely followed, or led, by newly developing microscopes. The fields of nanocomposites and nanostructure have seen parallel development during the past two decades, both with a focus on materials on the scale of nanometers (10^{-9}m). The electrical and electronics markets demand for miniaturization and for higher conductivity, antistatic additives and flame retardants is continuing. Whereas many argue that the cost for nano additives and their processing is too high, others point out the need and great promise of such new products. Every scientific journal and magazine has articles on this topic from every advantage point, and every major scientific conference has reported on the challenges and the opportunities sometime during the past few years (Stewart, 2006; Vaia and Wagner, 2004) making it impractical to review these references in this rapidly changing field. Whether the advance in microscopes came first or the nanomaterials themselves is not the issue here but simply that they have developed and this multidisciplinary topic is a must for the polymer microscopist to understand. Several texts and articles that describe information relevant to microscopy are cited here by way of example (Chernoff and Magonov, 2003; Zumbrunnen et al., 2002; Michler and Balta-Call, 2005; Magonov and Yerina, 2005; Wallenberger and Weston, 2004) as current work is best found by conducting an appropriate search on the specifics of interest.

Nanocomposites are a new class of composites that are particle-filled polymers for which at least one dimension of the dispersed particles is in the nanometer range. Polymer nanocomposites are a class of materials that generally contain less than 6% of nanometer sized additives. The nanofillers are of two general forms, plates (layered silicate nanoclays; mainly montmorillonite) or

carbon nanotubes (e.g., single and multiwall carbon nanotubes, respectively). The increasingly available nanoparticles create the opportunity for many different products in the future. The major differences between nanocomposites and traditional filled composites are the significantly smaller additive size and the lower concentration used in the product resulting in weight reduction, especially noteworthy for aerospace applications.

Applications that benefit from these improved properties include gas barriers for bottles (beer bottles), food packaging (boil-in bags, stand-up pouches), fuel tanks, automotive applications, electronics and electrical applications (components, printed circuit boards), electrically conductive parts, wires, cables, and many others. Most major plastics companies and compounders are developing, manufacturing, and marketing such products. Depending on the composite nature and structure, mechanical were greatly improved and sometimes the price went down.

The materials science focus is on the balance of the materials (polymer and filler), method of cost effective processing for good dispersion, fabrication of the product, and the final performance and thus the evaluation of the interaction of the matrix and filler (Vaia and Wagner, 2004).

Research has included the manufacture of nanomaterials such as clays by exfoliation and other methods to form finer, high aspect ratio particles. The range of polymers used has certainly increased with recent work done using natural or biopolymers (Wallenberger and Weston, 2004). The smaller size of the fillers results in significantly higher particle density and most importantly a larger interfacial area. This interface is responsible for the final properties. Thus, the nanofillers provide a means to "engineer and tailor morphology to achieve a desired property suite from the polymer nanocomposites" (Vaia and Wagner, 2004). Characterization methods used include TEM, SEM, and SPM, rheology, thermal analysis, and mechanical analyses. Although there can be major improvement in physical and mechanical properties, as with all materials the nature of the materials and the process used are key to limiting downsides, such as loss of toughness. Another potential downside is the fine sizes of the fillers themselves, and the possibility of their ingestion in the human lung and possible threat of disease such as is known for asbestiform materials. Finally, the patent

literature on nanocomposites gives a view of the breadth and importance of this new technology.

Clay materials have been related to our lives in many ways from a long time ago. For example food containers and vases were made from clay and the textile industry used clay to treat fabric well before the 20th century. Clay also is used in polymer compounding. With the development of polymer nanocomposites, montmorillonite clay has become widely investigated by many scientists and researchers. Nylon 6 MMT clay compounds later commercialized as nylon–clay hybrid was introduced by Toyota R&D Center in Japan (Usuki et al., 1993). 12-aminolauric organoclay absorbed ε-caprolactam monomers increasing its intersilicate layer basal spacing. The ε-caprolactam monomers between silicate layers were polymerized and produced polyamide 6–clay compound, which was referred to as a nanocomposite because it appeared that silicate layers were suspended in a polymer matrix.

The use of organoclays as reinforcing agents for nanocomposite preparation has been studied for various polymer systems including polypropylene (Gloaguen and Lefebvre, 2001), polyamide (Liu et al., 1999), poly(ethylene terephthalate) (Ke et al., 1999), polystyrene (Weimer et al., 1999), unsaturated polyesters (Suh et al., 2000), polyimide (Morgan et al., 2001), polyolefins (Hasegawa et al., 2000), poly(methyl methacrylate) (Huang and Brittain, 2001), ethylene-vinyl acetate copolymers (Zanetti et al., 2001; Alexandre et al., 2001) among others. This new type of material can be prepared by various techniques including exfoliation-adsorption, in situ intercalative polymerization, template synthesis and melt-intercalation and witnessed by X-ray diffraction measurements of silicate layer separation and transmission electron microscopy (TEM) observations (Okada et al., 1990).

In recent years polymer/layered silicate (PLS) nanocomposites have attracted great interest, both in industry and in academia, and represent a radical alternative to conventionally (macroscopically) filled polymers. Because of their nanometer size dispersion, the nanocomposites exhibit remarkable improvement in materials properties when compared with virgin polymer or conventional micro- and macro-composites. These improvements can include high module (Giannelis et al., 1999; LeBaron et al., 1999; Vaia et al., 1999; Biswas and Sinha

Ray, 2001), increased strength and heat resistance (Giannelis, 1998), decreased gas permeability (Bharadwaj, 2001; Messersmith and Giannelis,1995) and flammability (Gilman et al., 1997; Gilman et al., 2000), increased biodegradability of biodegradable polymers (Sinha Ray et al., 2002), large number of physical properties, increased barrier properties and increased thermal and environmental stability (Sinha Ray and Okamoto, 2003). In addition to their potential applications, PLS nanocomposites are also unique model systems to study the structure and dynamics of polymers in confined environments. Using both delaminated and intercalated hybrids, the statics and dynamics of polymers confined over distances ranging from the radius of gyration of the polymer to the statistical segment length of the chains can be studied.

On the other hand, there has been considerable interest in theory and simulations addressing the preparation and properties of these materials (Dabrowski et al., 2000), and they are also considered to be unique model systems to study the structure and dynamics of polymers in confined environments (Hackett et al., 1998). Although the intercalation chemistry of polymers when mixed with appropriately modified layered silicate and synthetic layered silicates has long been known (Theng, 1979), the field of PLS nanocomposites has gained momentum recently. The major findings have stimulated the revival of interest in these materials: first, the report from the Toyota research group of a Nylon-6 (N6)/montmorillonite (MMT) nanocomposite for which very small amounts of layered silicate loadings resulted in pronounced improvements of thermal and mechanical properties. Since then, many polymer/layered silicate nanocomposites have been prepared for various thermoplastic and thermosetting polymers. Today, efforts are being conducted globally, using almost all types of polymer matrices.

The main reason for these improved properties in polymer/layered silicate nanocomposites is the strong interfacial interactions between matrix and OMLS as opposed to conventional composites (Chen et al., 2002). These improvements are generally attained at lower silicate content ($\leq$5 wt%) compared to that of conventional filler filled systems. For these reasons polymer/layered silicate nanocomposites are far lighter in weight than conventional composites, and make them competitive with other materials for specific applications. Furthermore, the nanoscale morphology affords opportunity to develop model systems consisting

entirely of interfaces, and to study the structure and dynamics of confined and tethered chains using conventional bulk characterization techniques such as differential scanning calorimetry, thermally stimulated current, rheology, NMR, and various kinds of spectroscopy (VanderHart et al., 2001; Loo and Gleason, 2003).

Recently, the utility of inorganic nanoparticles as additives to enhance the polymer performance has been established. Various nano reinforcements currently being developed are nanoclay (layered silicates) (Sinha Ray and Okamoto, 2003), cellulose nanowhiskers (Mohanty et al., 2003), ultrafine layered titanate (Hiroi et al., 2004), and carbon nanotubes (Mitchell et al., 2002). Carbon nanotubes, however, are relatively clear cut case of new nanomaterials. Carbon nanotube based polymer composites are poised to exhibit exceptional mechanical, thermal and electrical properties.

The aim of this thesis is to obtain polymer-layered silicates nanocomposites and the improved properties that those materials can display. In this study, polymer clay nanocomposites will be prepared with polynorbornadiene used commonly in electric-electronic industry, and modified montmorillonite. To achieve this, the exchangeable ions between the layers of montmorillonite supplied pure will be replaced by a Ruthenium complex containing a quaternary ammonium salt which is a modified for cation exchange reaction. Then the norbornadiene monomers will be polymerized among the montmorillonite layers. Thus, clay layers are dispersed in polymers matrix and polymer-clay nanocomposites are obtained. The structures and properties of materials will be determined by spectroscopic (^{1}H-NMR, FTIR, XRD), chromatographic (GPC), thermal (TG, DTG) and surface analysis methods (TEM, SEM). Furthermore, the improvements in dielectric properties of nanocomposites and polymers will be investigated. So the polymer-clay nanocomposites will be produced by means of an economical single-step i.e. in situ polymerization method.

2. NANOCOMPOSITES

2.1. Structure and Properties of Nanocomposites

Nanotechnology is expected to play an important role in the twenty-first century, since it shows the characteristics of a key technology. It makes possible working tools and products that will effect sustainable change in our daily life and therefore our society. Nanotechnology goes far beyond miniaturization, constituting an independent approach. This is especially the case when new materials or products are obtained by effects which arise exclusively from the nanoscale. At this time, of all groups of materials these include, nanocomposites, which already offer the potential for industrial application.

The term ‘nanocomposite’ describes a two-phase material where one of the phases is dispersed in the second one on a nanometer (10^{-9}m) level. This term is commonly used in two distinct areas of material science: ceramics and polymers. Nanocomposites are commonly based on polymer matrices reinforced by nanofillers such as precipitated silica and silica-titania oxides synthesized by the sol-gel process, silica beads, cellulose whiskers, zeolits as well as colloidal dispersion of rigid polymers and many others.

Composites are already widely used in such diverse areas as transportation, construction, electronics and consumer products. They offer unusual combinations of stiffness, strength, and weight that are difficult to attain separately from the individual components. Nanocomposites, on the other hand, are a relatively new class of materials with ultrafine phase dimensions, typically of the order of a few nano-meters. Because of their nanometer size features nanocomposites possess unique properties typically not shared by their more conventional microcomposite counterparts and, therefore, offer new technology and business opportunities.

The physical mixture of a polymer and layered silicate may not form a nanocomposite. This situation is analogous to polymer composites, and in most cases separation into discrete phases takes place. In immiscible systems, which

typically correspond to the more conventionally filled polymers, the poor physical interaction between the organic and the inorganic components leads to poor mechanical, thermal properties and agglomeration in polymer matrix. In contrast, strong interactions between the polymer and the layered silicate in PLS nanocomposites lead to the organic and inorganic phases being dispersed at the nanometer level. As a result, nanocomposites exhibit unique properties not shared by their micro counterparts or conventionally filled polymers moduli (Okada et al., 1990; Giannelis, 1998; Giannelis et al., 1999; Le Baron et al., 1999; Vaia and Giannelis, 1997; Biswas and Sinha Ray, 2001).

2.2. Types of Nanocomposites

Layered silicates have layer thickness the order of 1 nm and a very high aspect ratio (e.g. 10–1000). A few weight percent of layered silicates that are properly dispersed throughout the polymer matrix thus create much higher surface area for polymer/filler interaction as compared to conventional composites. Depending on the strength of interfacial interactions between the polymer matrix and layered silicate (modified or not), the main two different types of PLS nanocomposites are thermodynamically achievable (Figure 2.1).

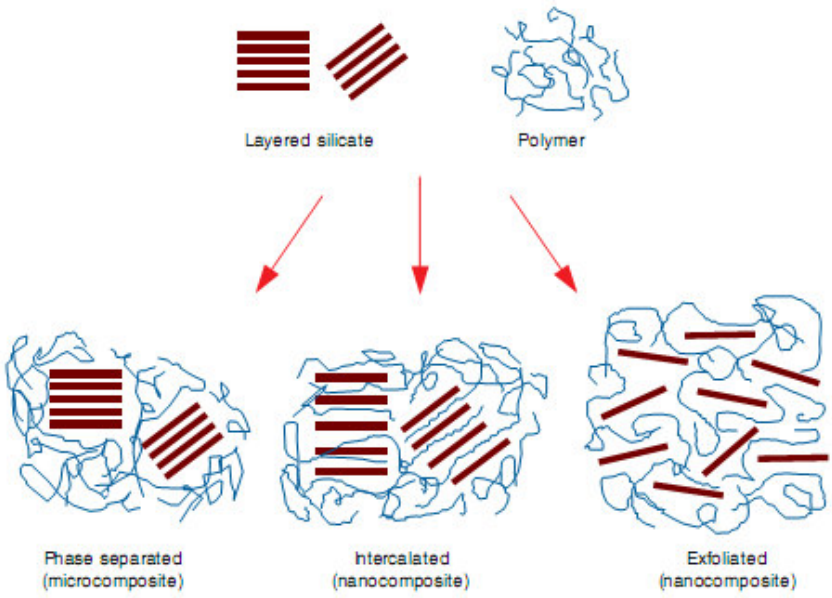

Figure 2.1. The Types of Nanocomposites.

2.2.1.Intercalated nanocomposites:In intercalated nanocomposites, the insertion of a polymer matrix into the layered silicate structure occurs in a crystallographically regular fashion, regardless of the clay to polymer ratio. Intercalated nanocomposites are normally interlayer by a few molecular layers of polymer. Properties of the composites typically resemble those of ceramic materials.

2.2.2. Exfoliated nanocomposites: In an exfoliated nanocomposite, 1 nm-thick the individual clay layers are dispersed in a continuous polymer matrix by an average distances that depends on clay loading. Usually, the clay content of an exfoliated nanocomposite is much lower than that of an intercalated nanocomposite. The latter configuration is of particular interest because it maximizes the polymer-clay interactions, making the entire surface of the layers available for the polymer. This should lead to most dramatic changes in mechanical and physical properties.

3. LAYERED SILICATES

3.1. Structure and Properties of Layered Silicates

The layered silicates commonly used in of Polymer Layered Silicate (PLS) nanocomposites belong to the same general family of 2:1 layered or phyllosilicates. Their crystal lattice consists of two-dimensional layers where a central octahedral sheet of alumina or magnesia is fused to two external silica tetrahedron by the tip so that the oxygen ions of the octahedral sheet do also belong to the tetrahedral sheets. The layer thickness is around 1 nm, and the lateral dimensions of these layers may vary from 30 nm to several microns or larger, depending on the particular silicate. These layers organize themselves to form stacks with a regular van der Walls gap in between them called the interlayer or the gallery. Isomorphic substitution within the layers (for example, Al^{3+} replaced by Mg^{2+} or Fe^{2+}, or Mg^{2+} replaced by Li^{1+}) generates negative charges that are counterbalanced by alkali and alkaline earth cations situated in the interlayer. As the forces that hold the stacks together are relatively weak, the intercalation of small molecules between the layers is easy (Bourbigot et al., 2000). In order to render these hydrophilic phyllosilicates more organophilic, the hydrated cations of the interlayer can be exchanged with cationic surfactants such as alkylammonium or alkylphosphonium. The modified clay (or organoclay) being organophilic, its surface energy is lowered and is more compatible with organic polymers. These polymers may be able to intercalate within the galleries, under well defined experimental conditions.

Montmorillonite, hectorite, and saponite are the most commonly used layered silicates. Layered silicates have two types of structure: tetrahedral-substituted and octahedral substituted. In the case of tetrahedrally substituted layered silicates the negative charge is located on the surface of silicate layers, and hence, the polymer matrices can react interact more readily with these than with octahedrally-substituted material. Details regarding the structure and chemistry for these layered silicates are provided in Figure 3.1 and Table 3.1.

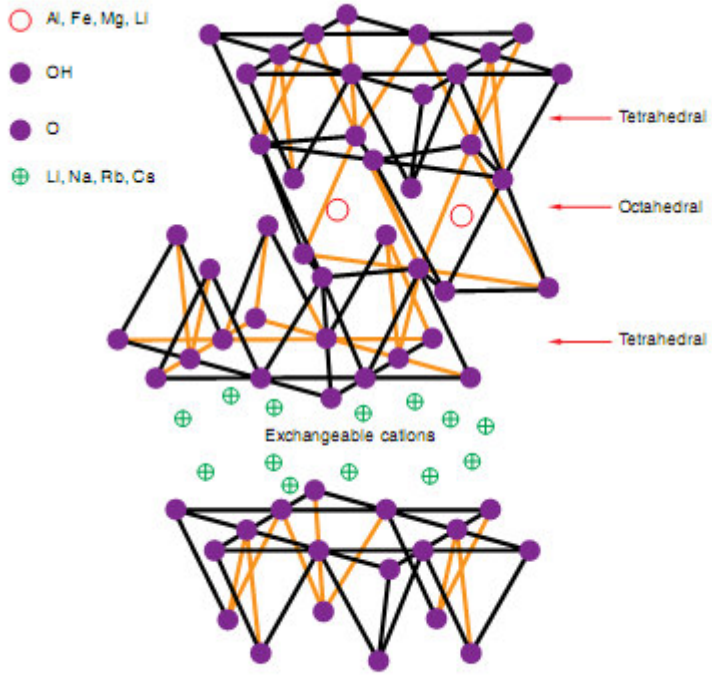

Figure 3.1. The Structure of Montmorillonite Mineral.

Table 3.1. Chemical formula and characteristic parameter of commonly used 2:1 phyllosilicates.

2:1 phyllosilicates	Chemical formula	CEC (mequiv/100 g)	Particle length (nm)
Montmorillonite	$Mx(Al_{4-x}Mg_x)Si_8O_{20}(OH)_4$	110	100–150
Hectorite	$Mx(Mg_{6-x}Li_x)Si_8O_{20}(OH)_4$	120	200–300
Saponite	$MxMg_6(Si_{8-x}Al_x)Si_8O_{20}(OH)_4$	86.6	50–60

M, monovalent cation; x, degree of isomorphous substitution (between 0.5 and 1.3).

These types of layered silicates are characterized by a moderate surface charge known as the cation exchange capacity (CEC), and generally expressed as mequiv/100 g. This charge is not locally constant, but varies from layer to layer, and must be considered as an average value over the whole crystal.

Layered silicates have two particular characteristics, which are generally considered for PLS nanocomposites. The first is the ability of the silicate particles to disperse into individual layers. The second characteristic is the ability to fine-tune their surface chemistry through ion exchange reactions with organic and inorganic cations. These two characteristics are, of course, interrelated since the

degree of dispersion of layered silicate in a particular polymer matrix depends on the interlayer cation.

3.2. Structure and Properties of Organically Modified Layered Silicates

To render layered silicates miscible with other polymer matrices, one must convert the normally hydrophilic silicate surface to an organophilic one, making the intercalation of many engineering polymers possible. Generally, this can be done by ion-exchange reactions with cationic surfactants including primary, secondary, tertiary, and quaternary alkylammonium or alkylphosphonium cations. Alkylammonium or alkylphosphonium cations in the organosilicates lower the surface energy of the inorganic host and improve the wetting characteristics of the polymer matrix, and result in a larger interlayer spacing. Additionally, the alkylammonium or alkylphosphonium cations can provide functional groups that can react with the polymer matrix, or in some cases initiate the polymerization of monomers to improve the strength of the interface between the inorganic and the polymer matrix (Krishnamoorti and Giannelis, 1996).

In order to describe the structure of the interlayer in organoclays, determine the orientation and arrangement of the alkyl chain was performed using X-ray diffraction (XRD). Depending on the packing density, temperature and alkyl chain length, the chains were thought to lie either parallel to the silicate layers forming mono or bilayers, or radiate away from the silicate layers forming mono or bimolecular arrangements as in the Figure 3.2 (Lagaly, 1986). However, these idealized structures have been shown to be unrealistic (Vaia et al., 1994) using FTIR experiments. By monitoring frequency shifts of the asymmetric CH_2 stretching and bending vibrations, they found that the intercalated chains exist in states with varying degrees of order. In general, as the interlayer packing density or the chain length decreases (or the temperature increases), the intercalated chains adopt a more disordered, liquid-like structure resulting from an increase in the gauche/trans conformer ratio (Figure 3.3). When the available surface area per molecule is within a certain range, the chains are not completely disordered but retain some orientation order similar to that in the liquid crystalline state.

This interpretation has been recently confirmed by molecular dynamics simulations where a strong layering behavior with a disordered liquid-like arrangement has been found, that can evolve towards a more ordered arrangement by increasing the chain length (Hackett et al., 1998). As the chain length increases, the interlayer structure appears to evolve in a stepwise fashion, from a disordered to more ordered monolayer then 'jumping' to a more disordered pseudo-bilayer.

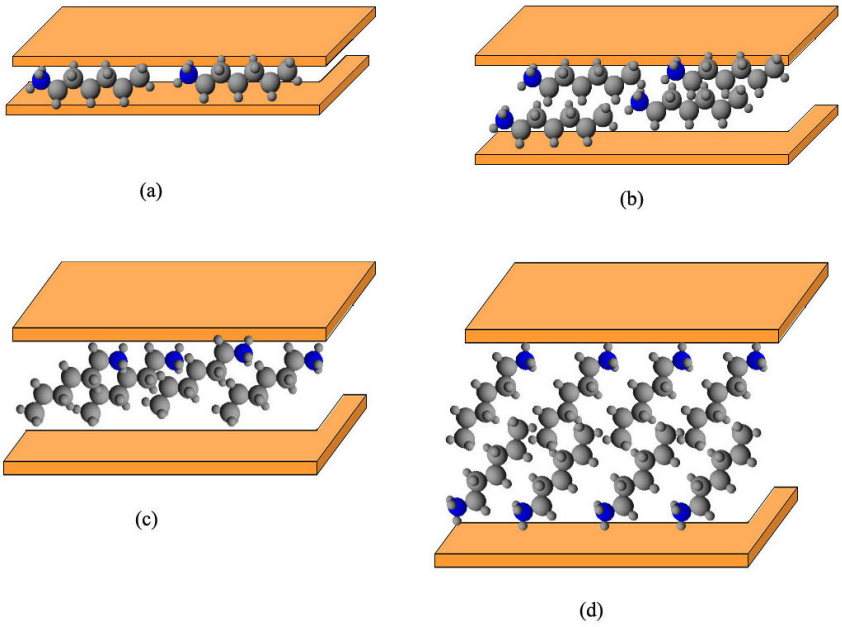

Figure 3.2. Alkyl Chain Aggregation In Layered Silicates: (a) lateral monolayer; (b) lateral bilayer; (c) paraffin-type monolayer and (d) paraffin-type bilayer

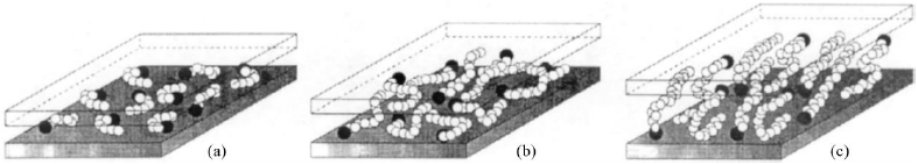

Figure 3.3. Alkyl Chain Aggregation Models: (A) Short Chain Lengths, The Molecules Are Effectively Isolated From Each Other, (B) Medium Lengths, Quasi-Discrete Layers Form With Various Degree Of In Plane Disorder And Interdigitation Between The Layers And (C) Long Lengths, Interlayer Order Increases Leading To A Liquid-Crystalline Polymer Environment. Open Circles Represent The CH_2 Segments While Cationic Head Groups Are Represented By Filled Circles (Vaia et al., 1994).

4. RING OPENING METATHESIS POLYMERIZATION

The olefin metathesis reaction is of great synthetic utility in polymer chemistry. The ability to simultaneously cleave and reform carbon–carbon double bonds has led to its widespread use in the design of useful organic molecules (Murdzek and Schrock, 1987) and polymers (Bazan et al., 1989). Although olefin metathesis was discovered as early as 1955 (Bazan et al., 1990), it has only achieved a leading role in synthetic methodology in the last decade. Ring-opening metathesis polymerization (ROMP) (Hafner et al., 1996), acyclic diene metathesis (ADMET) (Wagener et al., 1991), and ring-closing metathesis (RCM) (Grubbs et al., 1995), are transition-metal-catalyzed reactions of prime importance for both cleaving and forming C=C double bonds (Ivin et al., 1997). Since the visionary proposition by He´risson and Chauvin in 1970 that metal alkylidenes are active species in this type of reactions (He´risson et al., 1970), significant advances in the design of efficient, well-defined, one component olefin metathesis catalysts have been achieved. A milestone was laid in the mid-1980s with the discovery by Schrock et al. of relatively stable, well characterized alkylidene complexes based on early transition metals, in particular, molybdenum and tungsten (Schrock, 1990). Another strong impetus came from the development of ruthenium-based catalysts in the early 1990s. The most notorious representative of this new generation of olefin metathesis catalysts is the metal-alkylidene complex $RuCl_2(=CHPh)(PCy_3)_2$ developed by Grubbs and co-workers (Schwab et al., 1995). This complex, along with applications in both ROMP and RCM over the past few years (Schneider et al., 1997; Kinoshita et al., 1997; Ghosh et al., 1998; Pitarch et al., 1998). They have also found many applications in the synthesis of natural products (Leeuwenburgh et al., 2003; Manning et al., 1997; Biagini et al., 1997)

Cyloalkenes undergo ring-opening polymerization in the presence of coordination initiators based on transition metals to yield polymers containing a double bond, for instance, cyclopentene yields polypentenamer. The polymerization is referred to as ring-opening metathesis polymerization (ROMP) by analogy to the olefin metathesis reaction, which results in a transalkylidenation between two alkenes:

$$RCH=CHR + R'CH=CHR' \rightarrow 2RCH=CHR'$$

Both olefin metathesis and ROMP require similar initiators and proceed by the same reaction mechanism. The initiating and propagating species are metal-alkylidene (carbene) complexes. The original initiators used for ROMP were two component systems, composed of a halide or oxide of an early transition metal such as W, Mo, Rh, or Ru with an alkylating agent (Lewis acid) such as R_4Sn or $RAlCl_2$, which generate metal- carbenes in situ. These initiator systems have limitations- the strong Lewis acids make MW control more difficult, there is incompatibility with a variety of functional groups, the actual metal-carbene initiators are formed in low concentrations, and temperatures of 100 ^{0}C are needed. Since these initiators are relatively inexpensive, they still find use in commercial applications.

Better control of the reactions is achieved by using stable, isolable metal-carbene complexes, such as the Schrock initiators based on molybdenum and tungsten (M = W, Mo) and the Grubbs initiators based on Ruthenium (Figure 4.1).

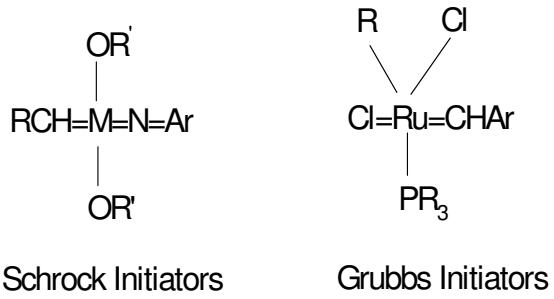

Figure 4.1. Schrock and Grubbs Initiators.

The Schrock initiators are limited compared to the Grubbs initiators, because of their sensitivity to air and moisture and their intolerance of monomers with oxygen – containing functional groups such as carbonyl, carboxyl, and hydroxyl. The Grubbs initiators are relatively tolerant to a variety of functional groups and reaction conditions. There has been and still is considerable effort in finetuning the initiator by variations in the ligands attached to the metal to allow one to achieve good polymerization rates with control of side reactions. For example, activity of the Grubbs initiators increases with larger and more electron-

donating halides, and these trends have been rationalized in terms of the ROMP mechanism (Trnka and Grubbs, 2001). ROMP proceeds as a living polymerization for most of the metal – carbene initiators. Narrow MWD and block copolymers can be obtained. Only modest temperatures of 25- 50 ^{0}C are required with the Schrock and Grubbs initiators.

Initiation involves coordination of the double bond of monomer with the transition metal (imino and OR' ligands not shown), cleavage of the π- bond with formation of a 4- membered metallocyclobutane intermediate, followed by rearrangement to form a metal – carbene propagating center (Figure 4.2):

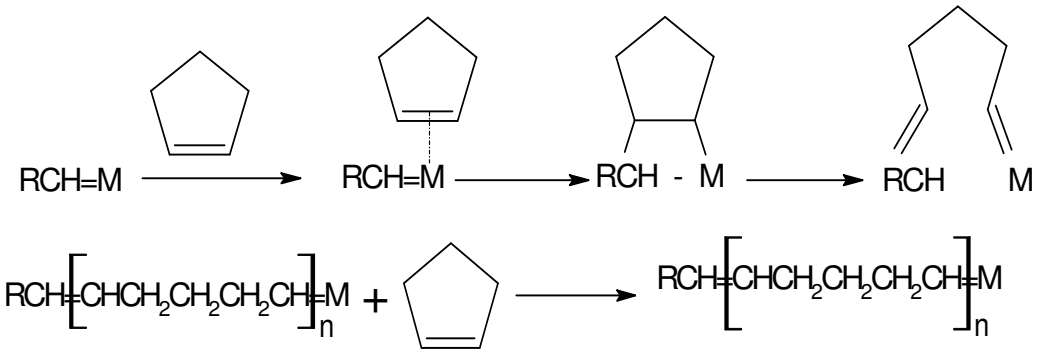

Figure 4.2. Mechanism for the formation of the Ring Opening Metathesis Polymerization.

Propagation follows in a similar manner, and the overall result is the insertion of the halves of the double bond of monomer into the metal- carbene bond. Evidence for cleavage of the double bond instead of an adjacent single bond comes from analysis of the ozonolysis products from a copolymer of cyclooctene and 1- ^{14}C-cyclopentene. The metal- carbene propagating centers can be terminated by conversion to double bonds by a Witting-type reaction with an aldehyde. The final polymer has terminal double bonds at both chain ends as well as a double bond in the repeat unit (Odian, 2004).

4.1. Ruthenium-Based Ring Opening Metathesis Polymerization Catalyst

Over the last decade, a tremendous amount of scientific research has focused on the development of new catalysts for polymer synthesis. The potential applications of a polymer are determined by its physical and mechanical

properties, which are defined by the polymer morphology. The polymer morphology largely depends on the composition and architecture of the polymer. Therefore, the development of well identified catalysts for the polymerization of a wide range of monomers with control over the stereochemistry, molecular weight and co-monomer incorporation has been a long-standing goal. These challenges can be achieved by using a living polymerization process in which there is neither chain transfer nor termination (Opstal et al., 2003).

In the late 1950s, heterogeneous catalysts based on Mo, Ru, W or Re oxides and halides were capable of breaking the double bond of a cyclic olefin and converting the ring-opened molecule into a polymer with double bonds in the main-chain (Ivin and Mol, 1997). This process, called ring- opening metathesis polymerization (ROMP), has been studied in great detail since these initial discoveries. It is now known that olefin metathesis reactions are initiated by transition metal complexes. Furthermore, since these early heterogeneous catalysts were difficult to characterize, a lot of research has been focused on the development of single site these complexes. Two of the most representative catalysts that have emerged the last 10 years are based on Mo (Schrock et al., 1990; Schrock et al., 1988) and Ru (Nguyen et al., 1992; Nguyen et al., 1993).

The development of olefin metathesis catalyzed by transition metals experienced an increase in the 1990s after the discovery of the well-defined Grubbs carbene–phosphine complexes (Ivin and Mol, 1997), $[RuCl_2(PR_3)_2(=CRR')]$, which have been appropriate for synthesis of new formulations. Besides the importance of the presence of the carbene in the starting catalyst for the initiation of the reaction, the ligands also play a role as an additional key ligand when dealing with ring opening metathesis polymerization (ROMP) (Love et al., 2003). Thus, the properties of the polymers depend on the ligands coordinated to the metal center not directly engaged in reaction. These ligands are well known as ancillary ligands. Besides phosphines, amine ligands can also drive the activity of metals by controlling the electronic density or steric effects in the coordination metal sphere (Brow et al., 1993; Seligson et al., 1991). Despite their importance, these ligands are not widely explored in homogeneous catalysis. It is well known results that the ligand nature can have profound and largely unpredictable effects

on the catalytic of the coordination complexes and present results strongly support this fact.

Besides of Grubbs catalysts, recent publications have shown that the multivariate ligand environment around Ru, bearing a large diversity in functional groups provides multifaceted reactive sites, which can be exploited by various substrates and thus can lead to numerous interesting organic products with the same catalyst (Schrock et al., 1990). In our investigation is about synthesis and activity of new synthesized ruthenium-based systems in the field of ROMP. New synthesized ruthenium-based catalyst is shown Figure 4.3.

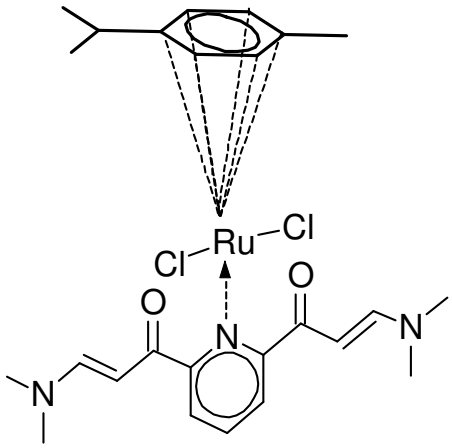

Figure 4.3. Ruthenium catalyst that is active in ring opening metathesis polymerization.

New synthesized ruthenium-based catalyst show high activity for ROMP after activation with trimethylsilyldiazomethane (TMSD) to generate the active species. Our new synthesized ruthenium-based catalyst is versatile and efficient promoters for the ROMP of both strained and low-strain olefins like norbornadiene when activated by a suitable carbene precursor such as trimethylsilyldiazomethane (TMSD) (Stumpf et al., 1995; Demonceau et al., 1997).

When a diazo compound was added to the reaction mixture, polymerization took place with no apparent induction time and high yields of polynorbornadiens were obtained (Demonceau et al., 1997). Strikingly, attempts to polymerize norbornadiene (bicyclo[2.2.1]hepta-2,5-diene-) gave unexpected results. Not only was the corresponding ROM polymer formed in higher yields, but also it had a highly stereoregular structure, as evidenced by NMR analysis (Noels et al., 1998). In our investigation is about synthesis and activity of new

synthesized ruthenium-based systems in the field of ROMP with and without the need for TMSD activation.

5. POLYNORBORNADIENE

Polynorbornadienes with low dielectric constant are of importance in use in integrated circuits, insulation of microchips, production of micro channels on circuits as an electronic packaging material. Ruthenium (Ru), Molybdenum (Mo), Tungsten (W) are used ring opening polymerization of norbornadiene various transition metal catalysts (Matos and Lina-Neto, 2004; Czelusniak and Szymanska-Buzar, 2004; Szymanska-Buzar et al., 2001). In our study, a different Ruthenium complex which is not present in literature as catalyst was used.

The rapid development of microelectronic industry creates high demand for low dielectric constant (low-k) materials. Polynorbomadiene (AvatrelTM) is a new photodefinitable dielectric material developed by B. F, Goodrich Company (Bai et al., 2001). Low dielectric constant interlevel dielectrics have been identified in the National Technology Roadmap for Semiconductors as being critical to the realization of high performance interconnections. Dielectric constant targets for the interlevel metal insulator were set at 4.1 in 1997, and are anticipated to drop to 2.5 in 2001. In an effort to reduce the permittivity of interlevel dielectrics, new organic films are being developed. In addition to a low dielectric constant, these films must meet all the performance characteristics for integrated circuits or electronic packages, which include good adhesion to a variety of films and substrates, thermal stability, high elongation-to-break values, and low stress (Grove et al., 1999). This polymer has several desirable properties. First, its dielectric constant and moisture absorption are low because the molecule consists mainly of saturated hydro-carbon bonds. Second, it has high T_g, and good thermal stability due to its stiff polymer backbone. Third, the side groups, "R", can be tailored to improve the properties of thin films using this polymer. An alkyl side group is added in the polymer to increase the intrachain mobility, resulting in an improvement in mechanical properties. Decyl chains are chosen to provide higher elongation-to-break (Bai et al., 2001). It can absorb up to several times its own weight of plasticizer oil and still retain useful properties. It has high tear strength and high dynamic damping properties and finds applications in noise control (e.g., under the hoods of diesel – powered automobiles) and vibration

damping (automobile- body mounts and instrument isolation pads). It has also been used for cleaning up oil spills.

Polynorbornadiene belongs to the class of cycloaliphatic polyolefins. These polymers, because of their rigid repeat structures, exhibit a combination of desirable properties, such as chemical resistance, high heat-distortion temperatures, stiffness and strength, optical transparency, and often low dielectric constants. These properties render them suitable for optical applications, such as lenses, compact discs, wave guides, and photoresists, electronic packaging, medical applications, and so forth. Furthermore, the tricyclic repeat unit of PNBD is regarded as a potential solar energy storage device. Low dielectric constant materials are under intensive investigations for the fabrication of integrated circuits (Peetz et al., 2003).

Polynorbornadiene is produced through polymerization with a transition metal catalyst Ruthenium (Ru), Molybdenum (Mo), Tungsten (W) are used ring opening polymerization of norbornadiene various transition metal catalysts (Figure 5.1).

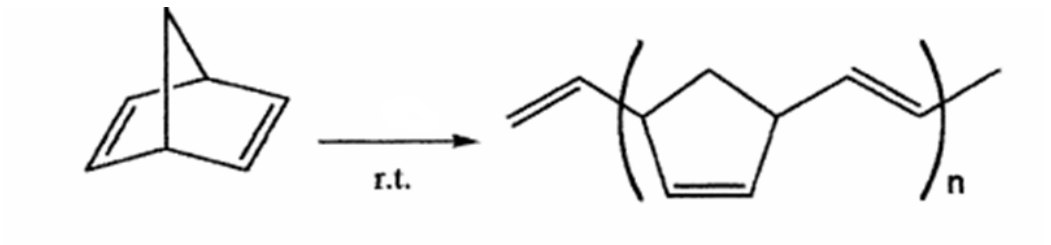

Figure 5.1. Polymerization Scheme of Norbornadiene.

Norbornadiene and their derivatives can serve as monomers for the synthesis of highly molecular mass polymers with widely varying structure. This group of cyclic compounds gives an example, how quite different chemical polymer structures and the resulting variation of properties can be achieved not only by a choice of monomer structure but also by a selection of catalyst systems. Depending on the type of catalysts, norbornadiene and its derivatives can be polymerized in accordance with A or B directions (Ivin and Mol, 1997; Makovetsky, 1999) (Figure 5.2).

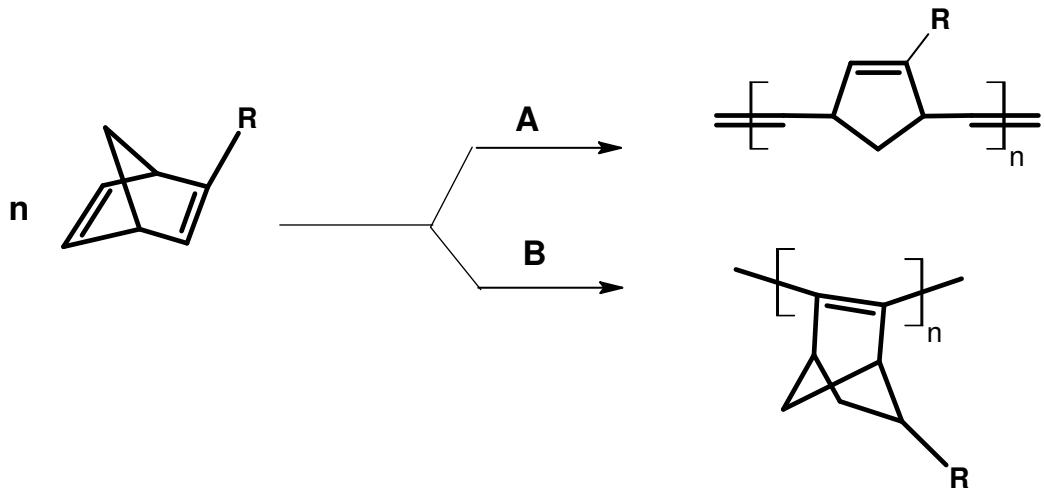

Figure 5.2. Polymerization types of Norbornadiene.

In the presence of ROMP catalysts (e.g. based on W-, Re-, or Ru-compounds) cyclo-linear structures formed by opening of the strained norbornadiene five-membered-cycle can be synthesized (A) In this way, norbornene polymers with different alkyl-, F, and Si-containing substituents (including alkoxy, carbazolyl, and other groups) have been prepared. On the other hand, polymers with entirely different structure can be prepared from the same monomers using Ni- and Pd containing catalysts (B). In this case the reaction proceeded as a classical addition olefin polymerization retaining strained rings unchanged. Properties of the resulting polymers (e.g. the glass transition temperature) are quite different from those of polynorbornadienes obtained by ROMP (Finkelshtein et al., 2003).

6. PREPERATION OF NANOCOMPOSITES

6.1 Modification of the Clay Particles

Normally, when organic and inorganic materials are mixed with each other, interactions between organic and inorganic materials may not be strong. Namely, inorganic particles can not be dispersed in polymer matrix. For that reason, to achieve of best dispersion compatibilizing agents are used. The compatibilizing agents used in the synthesis of nanocomposites (polyamide 6-clay hybrids) were amino acids (Okada et al., 1990), alkylammonium ions, phosphonium ions, silanes, aminomethylstyrene (Laus et al., 1998) and living free radical polymerizations initiator (LFRP) (Weimer et al., 1999). Modification process based on cation exchange basis. The cation-exchange process is occurred between alkylammonium ions and cations initially intercalated between the clay layers (Figure 6.1).

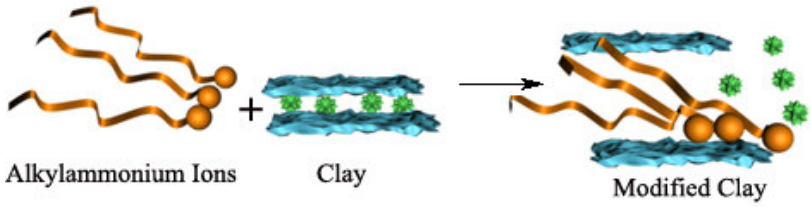

Figure 6.1. The Cation-Exchange Process (Spheres Represent NH_3^+ and Stars Represent Exchangeable Cations).

Polymer intercalation or exfoliation depends on silicate functionalization and constituent interactions. An optimal interlayer structure on the OMLS, with respect to the number per unit area and size of surfactant chains, is most favorable for nanocomposite formation, and (b) polymer intercalation depends on the existence of polar interactions between the OMLS and the polymer matrix (Figure 6.2).

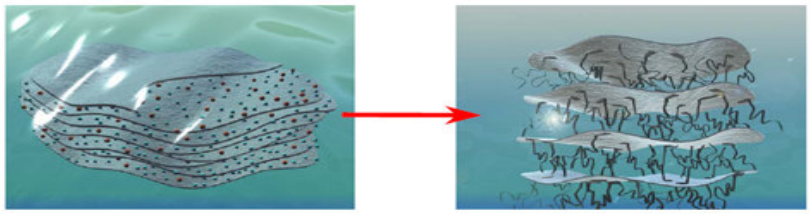

Figure 6.2. The Cation-Exchange Representation (Okada Et Al., 1990), a) C^{+n}mmt b)Alkylammonium Ions Exchanged MMT (modified MMT).

Polymer-layered silicate nanocomposites have been prepared various methods. They include four main processes (Oriakhi et al., 1998).

6.2. In Situ Intercalative Polymerization Method

In situ polymerization is the first method used to synthesize polymer-clay nanocomposites based on polyamide 6. First, the layered silicate is swollen in the monomer. This swelling process is related to mixing time, polarity of the monomer molecules, the surface treatment of the layered silicates, and temperature. Clay which has the high surface energy attracts polar monomer. Monomer can diffuse between the clay layers. When equilibrium is reached the diffusion stops and the clay has been swollen in the monomer to a certain extent corresponding to a perpendicular orientation of the alkyl ammonium ions (Messersmith et al., 1994). Polar monomers are easily driven between the clay layers than less polar monomers. As this mechanism occurs, the organic molecules can eventually delaminate the clay. After the swelling initiator is added, then the polymerization reaction is initiated by an increase of temperature or radiation, by the diffusion of a suitable initiator or by an organic initiator or catalyst fixed through cationic exchange inside the interlayer before the swelling step by the monomer. (Messersmith et al., 1995) (Figure 6.3).

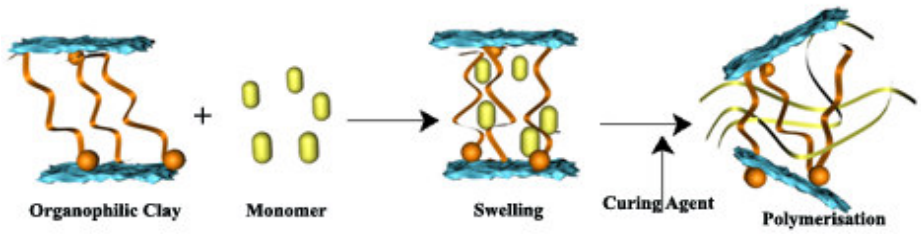

Figure 6.3. The In-Situ Polymerization Process.

6.3. Melt Intercalation

In this method, only thermoplastic polymers are used because of the preparation method. The layered silicate is mixed with polymer via extrusion and injection molding. The mixture is then annealed at a temperature above the glass transition temperature (Tg) of the polymer and forms a nanocomposite.

As shown in Figure 6.4 the polymer chains dramatic loss of conformational entropy during the intercalation. The proposed driving force for this mechanism is the important enthalpic contribution of the polymer/organoclay interactions during the blending and annealing steps. The polymer chains loose conformational entropy as they get intercalated between the clay layers. The loss of conformational entropy of the polymer chains during the intercalation is possibly compensated by enthalpic interactions between the clay and the polymer.

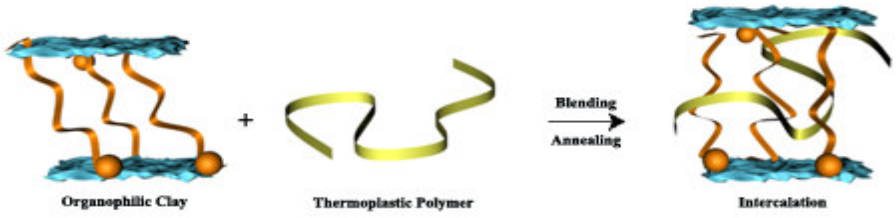

Figure 6.4. The Melt Intercalation Process.

The melt intercalation process has become increasingly popular because of its great potential for application in industry economically and easiness of process. This method is environmentally benign due to the absence of organic solvents.

Recently, the melt intercalation technique has become a main stream for the preparation of polymer/organophilic layered silicate nanocomposites because it is quite compatible with the recent industrial techniques. This method involves the annealing, statically or under shear, a mixture of the polymer and organophilic layered silicate above the softening point of the polymer. During the annealing, the polymer chains diffuse from the bulk polymer melt into the galleries between the silicate layers.

6.4 Intercalation of Polymer from Solution

The layered silicate is exfoliated into single layers using a solvent in which the polymer (or a prepolymer in case of insoluble polymers such as polyimide) is soluble. It is well known that such layered silicates, owing to the weak forces that stack the layers together can be easily dispersed in an adequate solvent, such as water, chloroform, or toluene. The polymer then adsorbs onto the delaminated sheets and when the solvent is evaporated (or the mixture precipitated), the sheets reassemble, sandwiching the polymer to form, in the best case, an ordered multilayer structure (Figure 6.5) (Green Cones Solvent Molecules and Red Curve Polymer Backbone). Under this process are also gathered the nanocomposites obtained through emulsion polymerization where the layered silicate is dispersed in the aqueous phase. Nanocomposites based on high-density polyethylene (Jeon et al., 1998), polyimide (Yano et al., 1993), and nematic liquid crystal polymers (Kawasumi et al., 1998) have been synthesized by this method.

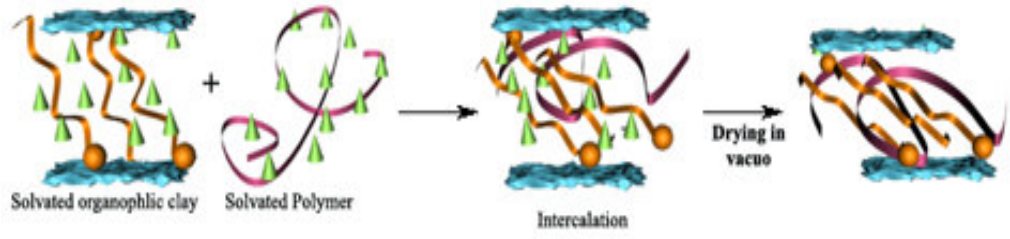

Figure 6.5. The Intercalation of the Polymer by the Solution Method.

For the overall process, in which polymer is exchanged with the previously intercalated solvent in the gallery, a negative variation in the Gibbs free energy is required. The driving force for the polymer intercalation into layered silicate from solution is the entropy gained by desorption of solvent molecules, which compensates for the decreased entropy of the confined, intercalated chains (Vaia and Giannelis, 1997). Using this method, intercalation only occurs for certain polymer/solvent pairs. This method is good for the intercalation of polymers with little or no polarity into layered structures, and facilitates production of thin films with polymer-oriented clay intercalated layers. However, from commercial point of view, this method involves the copious use of organic solvents, which is usually environmentally unfriendly and economically prohibitive.

On the other hand, during polymer intercalation from solution, a relatively large number of solvent molecules have to be desorbed from the host to accommodate the incoming polymer chains. The desorbed solvent molecules gain one translational degree of freedom, and the resulting entropic gain compensates for the decrease in conformational entropy of the confined polymer chains.

6.5 Template Synthesis

This technique, where the silicates are formed in situ in an aqueous solution containing the polymer and the silicate building blocks has been widely used for the synthesis of double-layer hydroxide-based nanocomposites (Wilson Jr et al., 1999; Oriakhi et al., 1997) but is far less developed for layered silicates. In this technique, based on self-assembly forces, the polymer aids the nucleation and growth of the inorganic host crystals and gets trapped within the layers as they grow. The following sections review the four aforementioned preparation techniques that will be illustrated with representative examples.

7. MATERIALS AND METHODS

7.1 Materials

2,6-Diacetylpyridine (Sigma-Aldrich), α-terpinene (Fluka), $RuCl_3 \times 3H_2O$ (Alfa Aesar), Trimethylsilyldiazomethane (TMSD, Sigma-Aldrich), Norbornadiene (NBD) (Sigma-Aldrich), acetone (technic), NaOH (Merck), dichloromethane (Sigma-Aldrich), toluene (Sigma-Aldrich), ethanole (Sigma-Aldrich), 1,2-dichloroethane (Fluka), tetrahydrofuran (Sigma-Aldrich), dimethylsulfoxide (Sigma-Aldrich). Dichloromethane (Sigma-Aldrich) was vacuum distilled. All of the chemicals are reagent grade. Commercial grade solvents were also dried under argon atmosphere and distilled prior to use. Solutions of the catalyst were freshly prepared for each reaction. Trimethylsilyldiazomethane (TMSD, from Aldrich) supplied as 2M solution in hexanes. This solution was further diluted by addition of a reaction solvent as dichloromethane.

Norbornadiene was extracted with % 5-10 NaOH solution to remove stabilizator (250 ppm Butylatedhydroxytoluene) from the monomer. Then it was dried over $MgSO_4$, and distilled from CaH_2.

7.2 Methods

All reactions and manipulations were performed under an argon atmosphere by using conventional schlenck tube techniques. Argon gas was dried by passing through P_2O_5 (Aldrich 97%).

^{1}H-NMR (400 MHz) and ^{13}C-NMR (100 MHz) spectra were recorded o a Varian Unity 400 Spectrometer. NMR chemical shifts are reported downfield from tetramethylsilane (TMS) as the internal standard in chloroform ($CDCl_3$) or dimethylsulfoxide (DMSO) as solvents.

FTIR spectra were taken with a Perkin Elmer Pyris 1 FTIR Spectrometer on KBr plates.

The number and weight average molecular weights ($\bar{M}_n$ and $\bar{M}_w$) and polydispersity index (PDI) ($\bar{M}_w$ /$\bar{M}_n$) of the polymers were determined by gel

permeation chromatography (GPC). GPC analysis of the polymers was performed on a Hewlett-Packard (HP) HPLC system with a differential refractometer detector. Tetrahydrofurane (THF) served as the eluent at a flow rate of 1.0 mL/min. The molecular weights and polydispersities are reported versus monodisperse polystyrene standards.

Thermal degradation was studied with a thermogravimetric analyzer (Perkin Elmer Pyris 1 TGA/DTA) by the heating of samples from ambient temperature to 1000^0C at 10^0C/min under a 10 bar dry air atmosphere and N_2. All of the products were dried in vacuum oven at 55^0C on 10 mbar pressure before the thermal analyses.

Montmorillonite was supplied by Southern Clay Products, Inc (ion-exchange capacity = 92 meq/100g). Characterization of montmorillonite mineral and determination of the interlayer spacing of the silicate layers for unmodified montmorillonite, modified montmorillonite and description type of the nanocomposites were performed by X-Ray Diffraction Spectrometers (Philips E'xpert Pro; Cu-Kα ray, λ=1.54056 Å). The basal spacing values of montmorillonite mineral calculated by Bragg' Law.

The structure of nanocomposites typically was proved using X-ray diffraction (XRD) analysis and transmission electron micrographic (TEM) images. Both TEM and XRD are essential tools for evaluating nanocomposite structure. Basically XRD studies yielded quantitative characterization of nanostructure and TEM gives qualitative information about the nanostructure.

TEM allows a qualitative understanding of the internal structure, spatial distribution of the various phases, and views of the defect structure through direct visualization. This method was used in our studies to description type of the nanocomposites. TEM images diagrams were taken from a Jeol 6355 by TÜBİTAK MAM. The samples were prepared by using of ultramicrotome method.

8. RESULTS AND DISCUSSION

8.1. Synthesis and Characterization of (2E,2'E)-1,1'-pyridine-2,6-diylbis[3-(dimethylamino)prop-2-en-1-one] as a Amine Ligand (1)

This compound was synthesized according to a modified procedure (Gamez et al., 2002). 0.5 g (3 mmol) 2,6-Diacetylpyridine was dissolved in 10 mL of toluene in the schlenk tube. Then 3 mL N,N-dimethylformamide dimethylacetal was added and stirred over night at 80-90 ^{0}C in Ar atmosphere (Figure 8.1). The solvent was filtered by cannula wire and the residue was dried in vacuum at room temperature. The yield obtained was 80% and orange colour. The FTIR spectrum of the amine ligand was given in Figure 8.2.

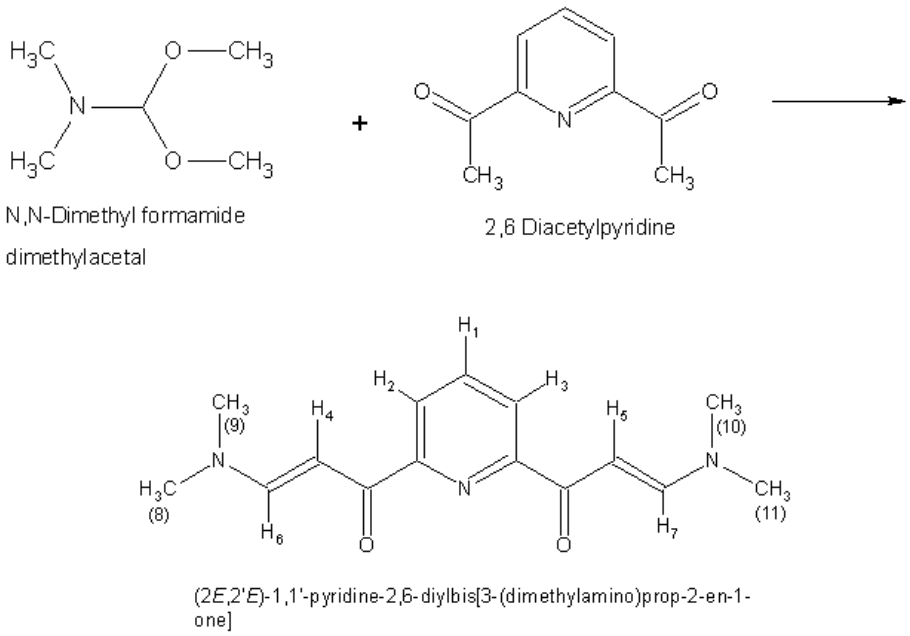

Figure 8.1. Synthetic route of (2*E*,2'*E*)-1,1'-pyridine-2,6-diylbis[3-(dimethylamino)prop2-en-1- one] (**1**).

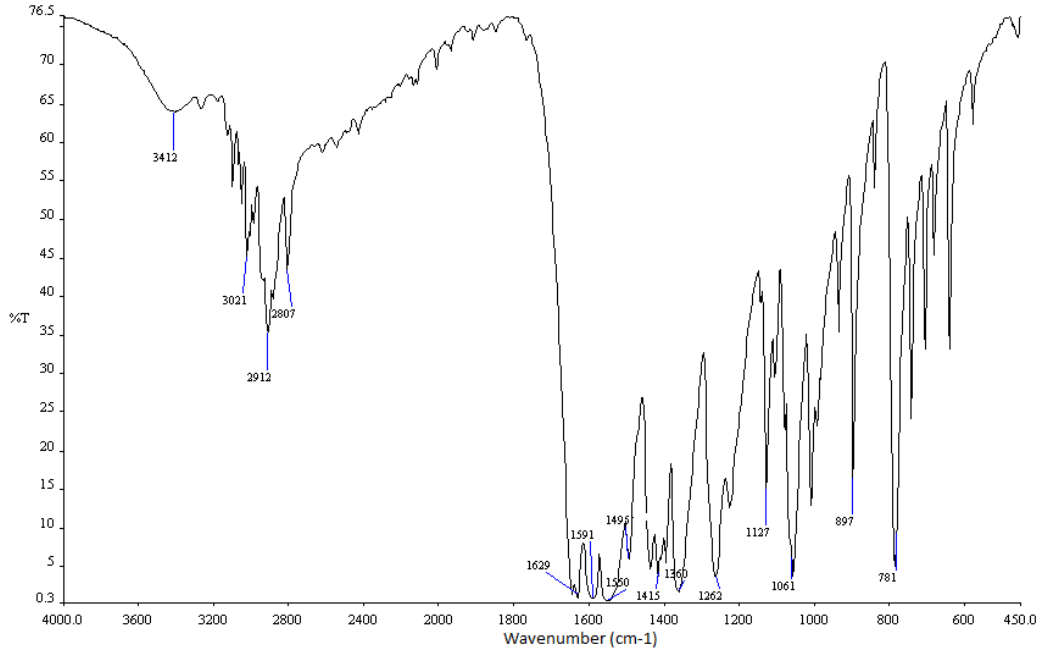

Figure 8.2. FTIR Spectrum of the (2*E*,2'*E*)-1,1'-pyridine-2,6-diylbis[3-(dimethylamino) prop-2-en 1- one] (**1**).

The characteristic FTIR spectrum of (2E, 2'E)-1,1'-pyridine-2,6 diylbis[3-(dimethylamino)prop-2-en-1-one] (1) as an amine ligand was shown in Figure 8.2. The band assignment for the FTIR spectrum of ligand was as follows: olefinic C-H stretching band in C=CH and aromatic C-H stretching band at about 3000 cm^{-1}; C-H stretching in CH_3 and C-H stretching in CH_2 at about 2900 cm^{-1}; C-H stretching in N-CH_3 at about 2800 cm^{-1}; C=O diketones carbonyl absorption band at 1655-1635 cm^{-1}; C=C in pyridine ring at 1600-1585 cm^{-1}; C=C in chain and C=N in pyridine ring at 1680-1620 cm^{-1}; C-C in pyridine ring at 1500-1400 cm^{-1}; C-N in ring at 1335-1020 cm^{-1}. Further bands were shown by aromatic rings in the fingerprint region between 1225 and 950 cm^{-1}.

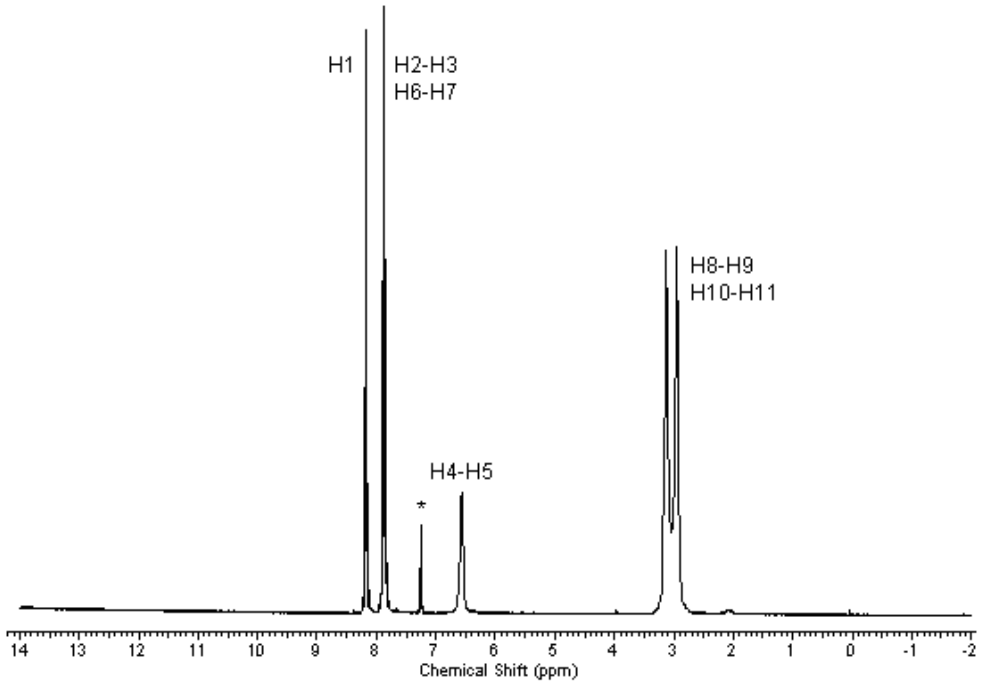

Figure 8.3. ^{1}H-NMR Spectrum of the (2*E*,2'*E*)-1,1'-pyridine-2,6-diylbis[3-(dimethylamino)prop-2 en-1- one] (**1**).

The ^{1}H-NMR spectrum of amine ligand was shown in Figure 8.3. The peak at 8.12 ppm was assigned to CH group of pyridine ring that was represented as (H_1) proton. The peaks at 7.91 ppm were assigned to four CH groups that were represented as (H_2, H_3, H_6, H_7) protons. The δ value of two CH groups protons that were represented as (H_4, H_5) was shown at 6.59 ppm. The signals on 3.21-2.98 ppm were assigned to four CH_3 groups of chain.

All of the analysis data about the amine ligand were represented as below.

^{1}H-NMR ($CDCl_3$) (ppm) 8.12 (t, 1H, H_1), 7.91 (m, 4H, H_2, H_3, H_6, H_7), 6.59 (d, 2H, H_4, H_5), 3.21-2.98 (ss, 12H, H_8, H_9, H_{10}, H_{11}). FTIR (cm^{-1}) 3099, 3053, 2911, 1645, 1632, 1584, 1494, 1395, 1261, 1129, 1057, 993, 897, 783.

8.2 Synthesis and Characterization of Ruthenium salt $[RuCl_2$ (p-cymene)$]_2$ (2)

$RuCl_3 \times 3H_2O$ (0.91 g; 3.48 mmol) and (3-isopropyl-6-methylcyclohexa-1,4-diene) (4.93 g; 35.5 mmol) is dissolved in 70 mL ethanol in the schlenk tube (Figure 8.4). The reaction mixture is refluxed for 5 hours. The resulting orange

precipitate is collected by filtration and washed with ethanol (20 mL×5) and dried in vacuo at room temperature. The yield obtained was 70% and red colour.

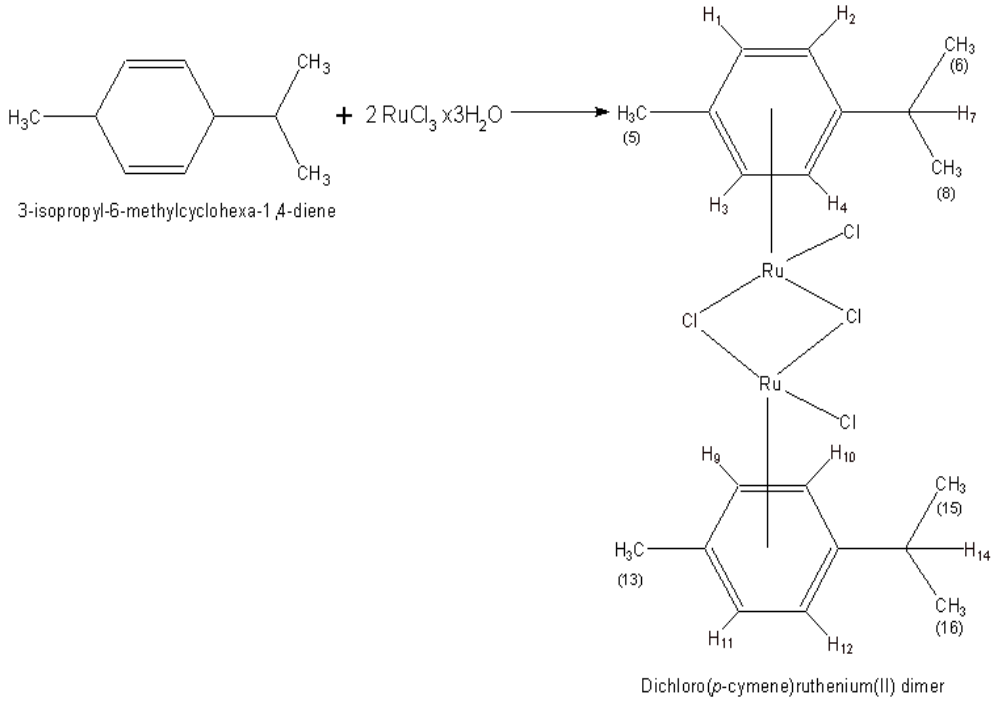

Figure 8.4. Synthetic route of $[RuCl_2\ (p\text{-cymene})]_2$ **(2).**

The FTIR spectrum of the $[RuCl_2\ (p\text{-cymene})]_2$ was given in Figure 8.5. The band assignment for the FTIR spectrum of the $[RuCl_2\ (p\text{-cymene})]_2$ was as follows: aromatic C-H stretching band at about 3000 cm^{-1}; C-H stretching in CH_3 and C-H stretching band at about 2900 cm^{-1}; C=C in pyridine ring at about 1600 cm^{-1}; C-C in pyridine ring at 1500-1400 cm^{-1}; Further bands were shown by aromatic rings in the fingerprint region between 1225 and 950 cm^{-1}.

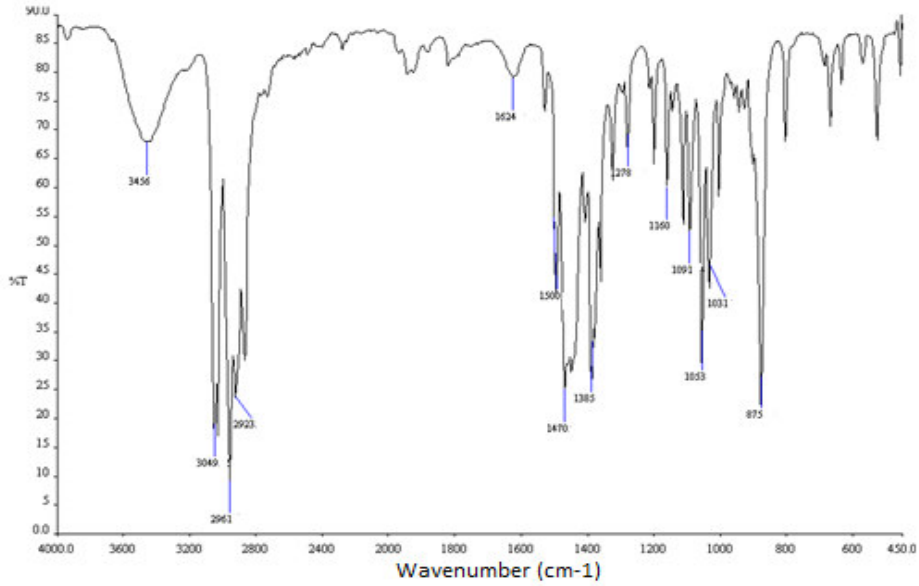

Figure 8.5. FTIR Spectrum of the $[RuCl_2\ (p\text{-cymene})]_2$ **(2).**

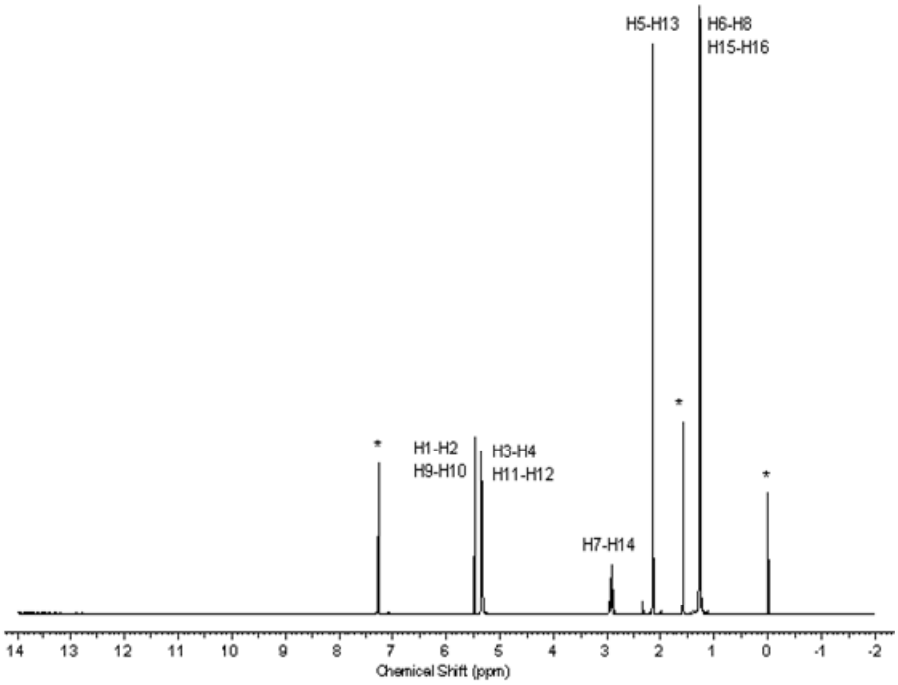

Figure 8.6. ^{1}H-NMR Spectrum of the $[RuCl_2\ (p\text{-cymene})]_2$ **(2).**

The ^{1}H-NMR spectrum of the [$RuCl_2$ (p-cymene)]$_2$ **(2)** was given in Figure 8.6. The doublet doublet peaks at 5.46 ppm was assigned to four CH groups of benzene rings that was represented as (H_1, H_2, H_9, H_{10}) protons. The doublet doublet peaks at 5.32 ppm was assigned to other four CH groups of benzene rings that were represented as (H_3, H_4, H_{11}, H_{12}) protons. The δ value of two CH groups protons that were represented as (H_7, H_{14}) was shown at 2.92 ppm. The singlet signal on 2.16 ppm was assigned to two CH_3 groups of chain (H_5, H_{13}). The doublet doublet peaks at 1.29 ppm was assigned to four CH_3 groups of chain that was represented as (H_6, H_8, H_{15}, H_{16}) protons.

All of the analysis data about the amine ligand were represented as below.

^{1}H-NMR ($CDCl_3$) δ (ppm) 5.46 (dd, 4H, H_1, H_2, H_9, H_{10}), 5.32 (dd, 4H, H_3,H_4,H_{11},H_{12}), 2.92 (m, 2H, H_7,H_{14}), 2.16 (s, 2H, H_5,H_{13}), 1.29 (dd, 4H, H_6, H_8, H_{15},H_{16}). FTIR (cm^{-1}) 3029, 3049, 2961, 1624, 1495, 1467, 1388, 1360, 1325, 1278, 1198, 1160, 1091, 1053, 1034, 1004, 877, 801, 669, 526.

8.3. Synthesis and Characterization of Amine Ligand Substituted Ruthenium (II) Complex (3)

0.1 g [$RuCl_2$ (p-cymene)]$_2$ (**2**) (0.16 mmol) was dissolved in dry dichloromethane (10 mL) and subsequently 0.088 g (0.32 mmol) of amine ligand (**1**) was added slowly. The reaction mixture was stirred at room temperature for two nights in Ar atmosphere (Figure 8.7). The solution is concentrated by removing half of the solvent in vacuum. The final product was precipitated in diethylether, filtered and dried in vacuum at room temperature. The yield obtained was 90% and brown colour.

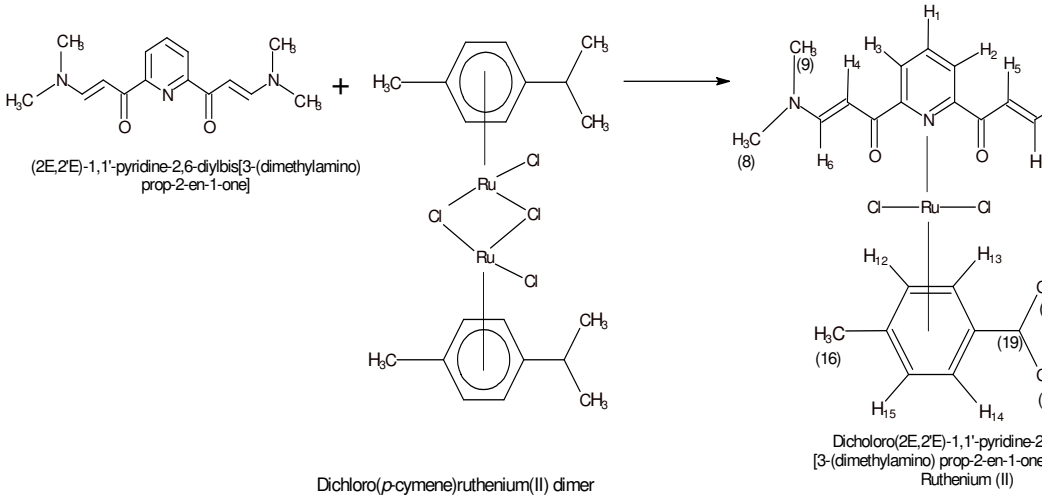

Figure 8.7. Synthetic route of Ruthenium (II) Complex (**3**).

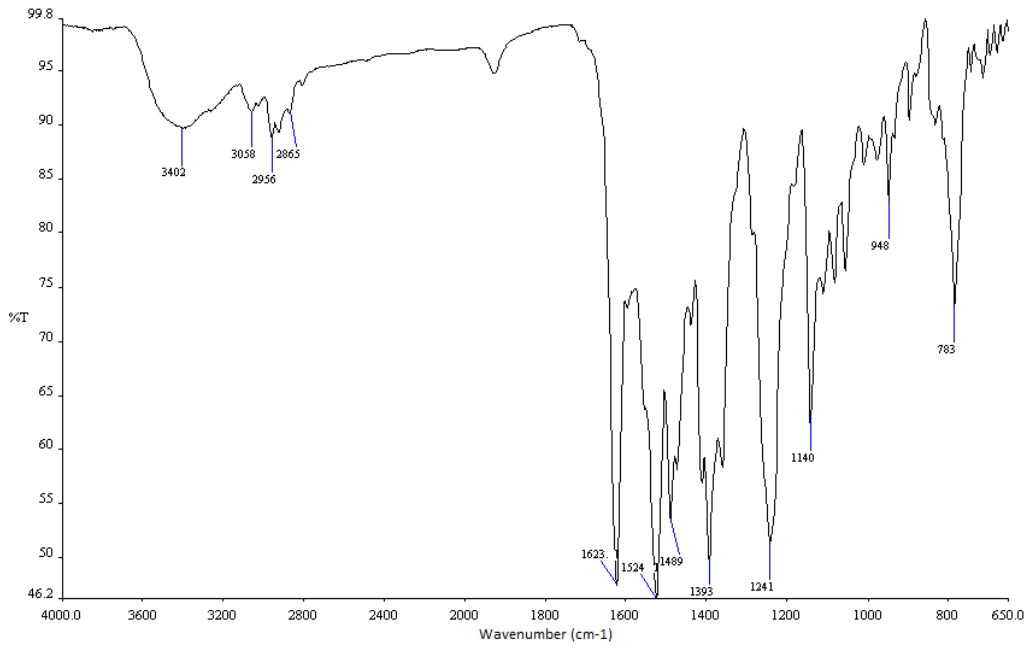

Figure 8.8. FTIR Spectrum of the Ruthenium (II) Complex (**3**).

The band assignment for the FTIR spectrum of the catalyst (Figure 8.8) was as follows: olefinic C-H stretching in C=CH and aromatic C-H stretching at about 3000 cm^{-1}; C-H stretching in CH_3 and C-H stretching in CH_2 at about 2900 cm^{-1}; C=C in pyridine ring at about 1600 cm^{-1};C-H stretching in N-CH_3 at about

2800 cm^{-1}; C=O diketones carbonyl absorption band at 1655-1635 cm^{-1}; C=C in pyridine ring at 1600-1585 cm^{-1}; C=C in chain and C=N ring at 1680-1620 cm^{-1}; C-C in pyridine ring at 1500-1400 cm^{-1}; C-N in ring at 1335-1020 cm^{-1}. Further bands were shown by alkanes and alkenes in the fingerprint region between 1400 and 800 cm^{-1}. Further bands were shown by aromatic rings in the fingerprint region between 1225 and 950 cm^{-1}.

The ^{1}H-NMR spectrum of the Ruthenium (II) Complex **(3)** was given in Figure 8.9. The triplet peaks at 8.75 ppm was assigned to CH group of pyridine ring that was represented as (H_1) proton. The doublet peaks at 8.20 ppm was assigned to other two CH groups of pyridine ring that were represented as (H_2, H_3) protons. The δ value of two CH groups protons that were represented as (H_6, H_7) was shown at 7.60 ppm. The doublet signal on 6.30 ppm was assigned to other two CH groups of chain (H_4, H_5). The double doublet peaks at 5.25-5.45 ppm were assigned to four CH groups of benzene ring that was represented as (H_{12}, H_{13}, H_{14}, H_{15}) protons. The peaks at 3.05-3.15 ppm were assigned to four CH_3 groups of N-CH_3 protons that were represented as (H_8, H_9, H_{10}, H_{11}). From calculating of peak areas, the δ value of CH group proton that was represented as (H_{19}) was shown at 2.75 ppm, CH_3 group protons that was represented as (H_{16}) was shown at 2.20 ppm and two CH_3 group protons that were represented as (H_{17},H_{18}) were shown at 1.15-1.20 ppm. These are indicative that synthesis of amine ligand substituted Ruthenium complex from amine ligand and [$RuCl_2$ (p-cymene)]$_2$ was achieved with a small slip in ^{1}H-NMR spectrum.

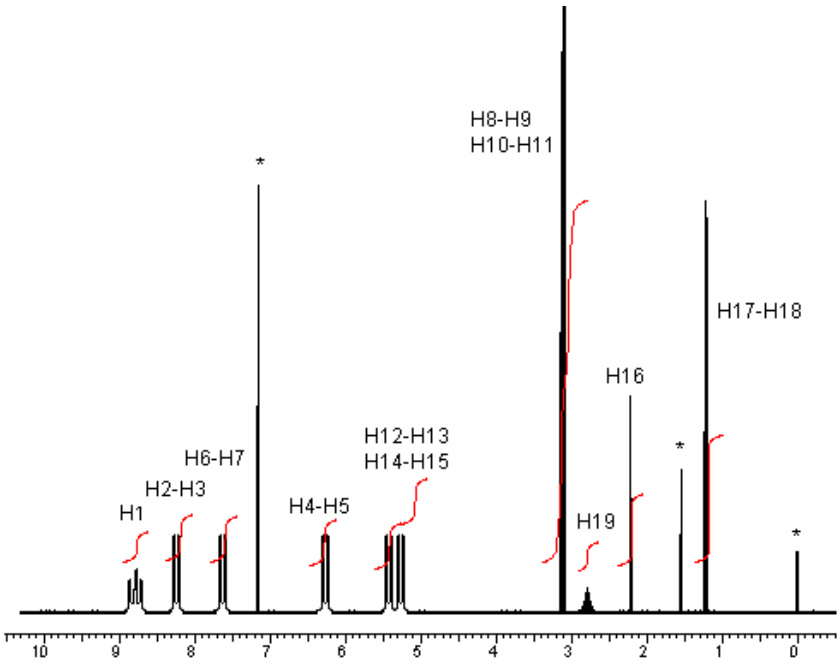

Figure 8.9. ^{1}H-NMR Spectrum of the Ruthenium (II) Complex (**3**).

All of the analysis data about the amine ligand were represented as below:

^{1}H-NMR ($CDCl_3$) δ (ppm) 8.75 (t, 1H, H_1), 8.20 (d, 2H, H_2,H_3), 7.60 (d, 2H, H_6,H_7), 6.30 (d, 2H, H_4,H_5), 5.25-5.45 (dd, 4H, H_{12},H_{13},H_{14},H_{15}), 3.05-3.15 (ss, 12H, H_8,H_9,H_{10},H_{11}), 2.75 (m, 1H, H_{19}), 2.20 (s, 3H, H_{16}), 1.15-1.20 (dd, 6H, H_{17},H_{18}). FTIR (cm^{-1}) 2962, 1930, 1623, 1489, 1473, 1394, 1362, 1242, 1142,1083, 1056, 1010, 976, 949, 897, 784, 714. Anal.calcd.for $RuC_{25}H_{33}Cl_2N_3O_2$ (579.52): C 51.75, H 5.69, N 7.24 %; found: C 49.80, H 5.35, N 6.81 %.

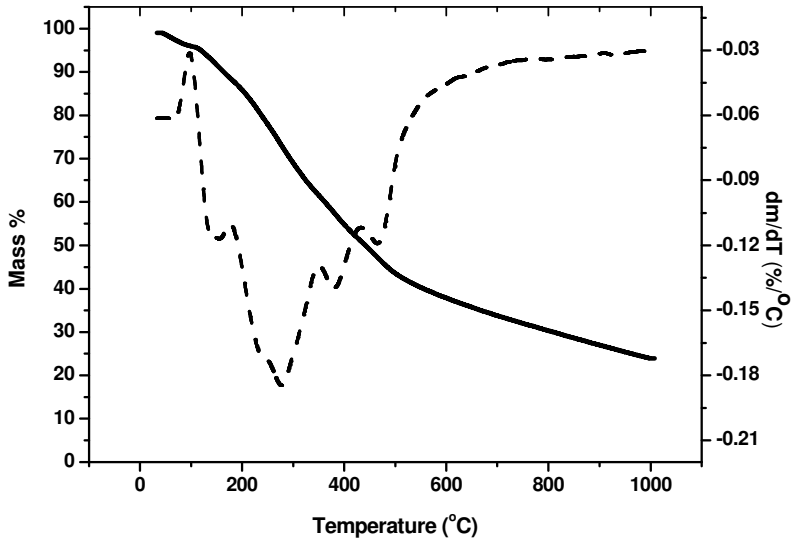

Figure 8.10. TG-DTG Thermograms of the Ruthenium (II) Complex (in N_2 atmosphere) (**3**).

The TG-DTG thermograms of the Ruthenium (II) Complex (**3**) in N_2 atmosphere was shown in Figure 8.10. According to TG-DTG thermograms, there are several degradation stages for Ruthenium (II) Complex (**3**) between 100-800 ^{o}C. The total mass loss was about 60% at this temperature range. Degradation started at 100 ^{o}C and continued up to about 275 ^{o}C. The maximum peak temperature of DTG thermogram was about 275 ^{o}C. After this temperature, two small degradation stages were occurred until 800 ^{o}C. They occurred at about 380 and 470 ^{o}C. It was observed that, the rate of degradation standed firm ever after 800 ^{o}C.

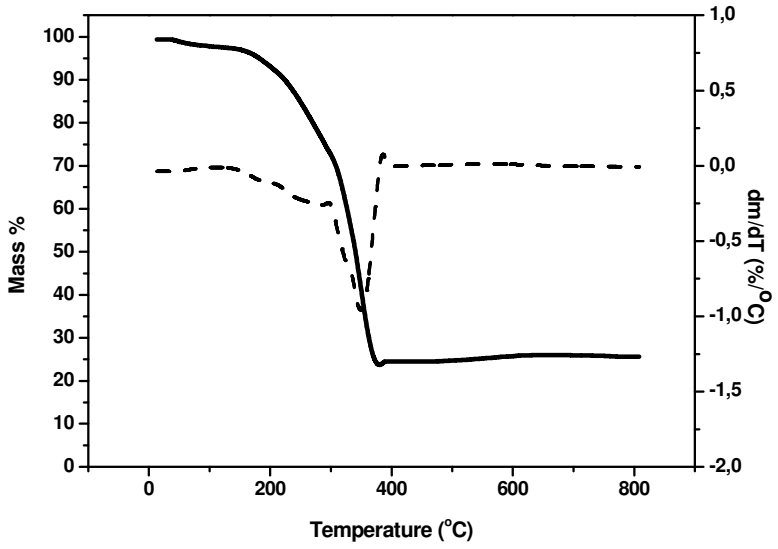

Figure 8.11. TG-DTG Thermograms of the Ruthenium (II) Complex (in O_2 atmosphere) (**3**).

The TG-DTG thermograms of the Ruthenium (II) Complex (**3**) in O_2 atmosphere was shown in Figure 8.11. According to TG-DTG thermograms, there is one degradation stage for Ruthenium (II) Complex (**3**) between 100-400 ^{o}C. The total mass loss was about 80% at this temperature range. Degradation started at 100 ^{o}C and continued up to about 345 ^{o}C. The maximum peak temperature of DTG was about 345 ^{o}C. It was observed that the rate of degradation standed firm ever after 400 ^{o}C.

8.4. Characterization of Montmorillonite Mineral

X-Ray diffractogram of Na-montmorillonite was presented in Figure 8.12. The basal spacing values of montmorillonite mineral calculated by Bragg' Law ($n\lambda=2dSin\theta$) (Table 8.1) (Grim, 1968; Brown, 1961). Also, the minerals that montmorillonite contains was shown at this table. The basal spacing value (d_{001}) of montmorillonite was calculated as 11.4 Å.

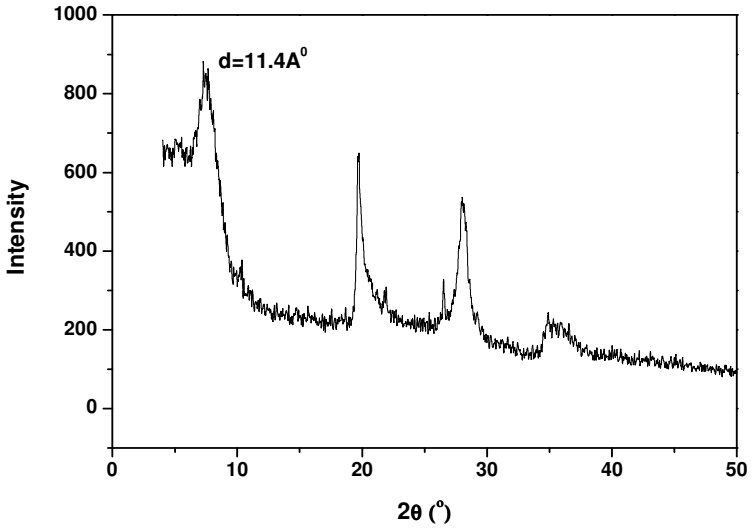

Figure 8.12. X-Ray Diffraction Diagram of Montmorillonite.

Table 8.1. The basal spacing values of Na-montmorillonite.

2θ (^{o})	**d** (Å)	**Structure**
7.657	11.40	Montmorillonite
19.756	4.98	Montmorillonite
28.011	3.18	Montmorillonit+Ouartz
35.999	2.49	Montmorillonite
36.568	2.45	Montmorillonite

The FTIR absorption spectrum of Na-montmorillonite was presented in Figure 8.13. Na-montmorillonite showed a typically broad OH stretching band at 3633 cm^{-1}. Absorption bands of adsorbed molecular water were appeared at 1642 and 3451 cm^{-1}. They showed a broadly similar pattern of adsorption at the 1047 cm^{-1} arising from Si-O stretching vibrations. More characteristic, however, were the well-resolved OH deformation bands at 917 cm^{-1}. The absorption bands in the region below 526 cm^{-1} arise from Si-O stretching vibrations.

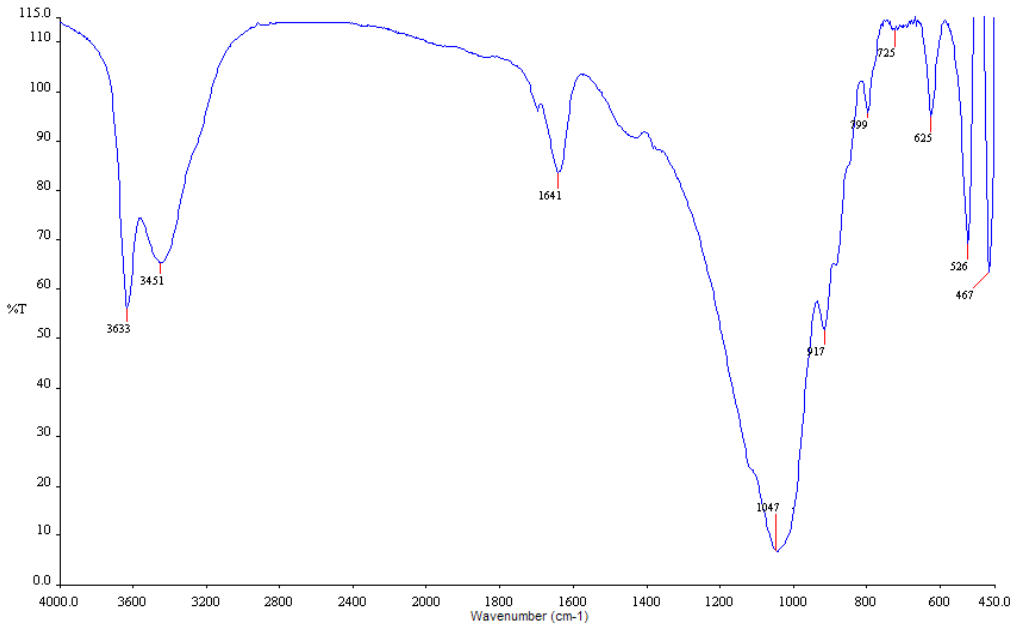

Figure 8.13. FTIR Spectrum of the Montmorillonite.

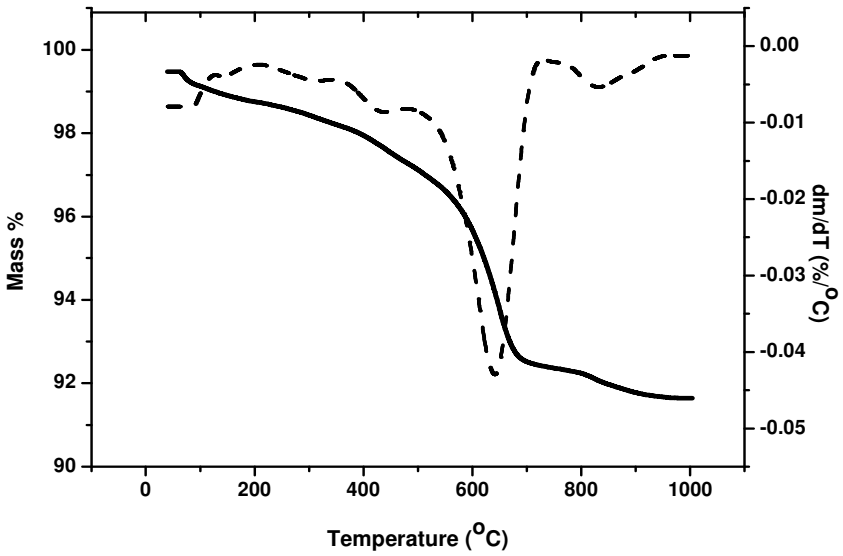

Figure 8.14. TG-DTG Thermograms of the Montmorillonite (in N_2 atmosphere).

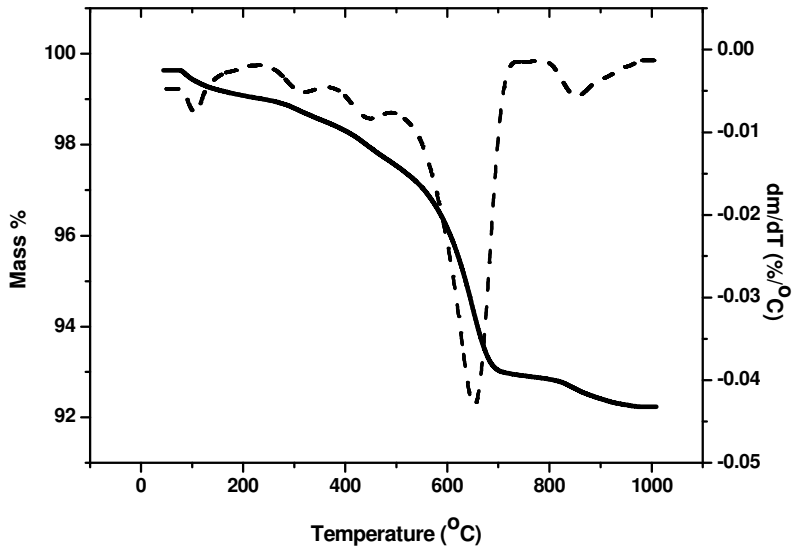

Figure 8.15. TG-DTG Thermograms of the Montmorillonite (in O_2 atmosphere).

The TG-DTG thermograms of the unmodified montmorillonite in N_2 and O_2 atmosphere were shown in Figure 8.14 and Figure 8.15, respectively. The same thermogram was obtained in these conditions because of not containing any organic materials. According to TG-DTG thermograms, one decomposition stage was obtained. The weight loss of unmodified montmorillonite was found as 8.5 wt % that has volatile materials. Degradation started at 100 ^oC due to unbound H_2O and continued up to about 800 ^oC due to chemically bound H_2O. The maximum peak temperature of DTG thermogram was about 645 ^oC.

8.5. Modification and Characterization of Montmorillonite with Catalyst

In this section, sodium montmorillonite (Cloisite Na^+) was modified with modificator that was also used as a catalyst in preparation of nanocomposites. For the purpose of well dispersed clay mineral, amount of sodium montmorillonite was dispersed in distilled water for 24 hours at room temperature. Equivalent amount of cation exchange capacity (CEC) of montmorillonite 0.02 mmol modificator was stirred with 0.15 mmol HCl in another schelenk under Ar at room temperature. This solution was poured into montmorillonite dispersion slowly.

The final dispersion was stirred for else 24 hours at room temperature. Then the mixture was separated by filtration washed with 1:1 ratio of distilled water-methanol several times. After this washing no further chloride can be detected in the wash water with a silver nitrate solution. Modified clay (Mod-MMT) was dried overnight under vacuum (Figure 8.16).

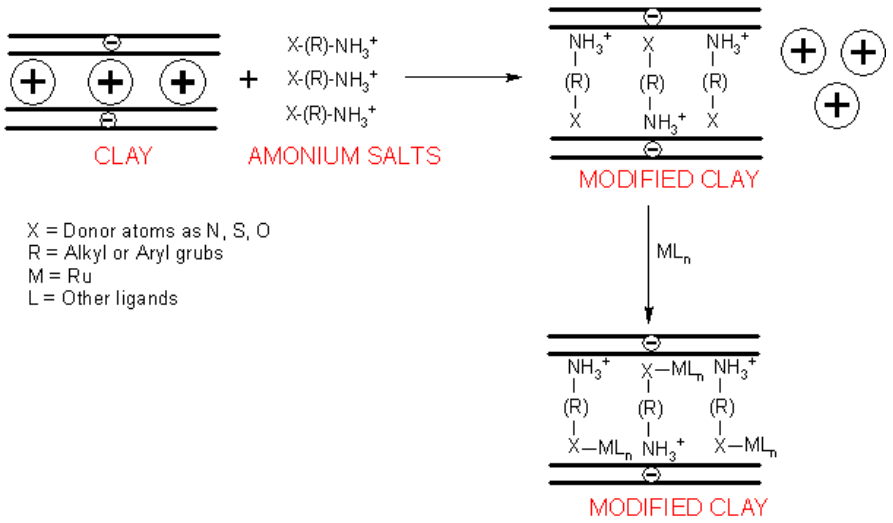

Figure 8.16. Schematic present of Modification of Montmorillonite with Ru complex (**3**).

In general, the modifications were examined with regard to literature; the excess equivalent amount modificator was used in modification process according to calculated from the Cation Exchange Capacity (CEC) the montmorillonite. This is well known that when the modificator amount in solution is increased, cation exchange equilibrium is change towards to products. For the purpose determination of optimum modificator amount for modification of montmorillonite, modified montmorillonites that containing modificator calculated amount from Cation Exchange Capacity (CEC) of 1 folds (0.016 mmol), 2 folds (0.032 mmol), 3 folds (0.048 mmol), 5 folds (0.080 mmol), 7 folds (0.112 mmol) were prepared. Montmorillonite was modified with 1 folds (Mod-MMT 1), 2 folds (Mod-MMT 2), 3 folds (Mod-MMT 3), 5 folds (Mod-MMT 5), 7 folds (Mod-MMT 7) modificator with stirred 24 hours. The interlayer distance of modified montmorillonite was determined with X-Ray Diffraction Spectrometers.

X-Ray diffractogram of Na-MMT and modified montmorillonites (Mod-MMT 1), (Mod-MMT 2), (Mod-MMT 3), (Mod-MMT 5) and (Mod-MMT 7)

were presented in Figure 8.17. Generally, the pure montmorillonite exhibits a broad XRD peak and similar phenomenon was observed in Na-montmorillonite. The basal spacing d_{001} for the Na-MMT was 11.40 Å (1.14 nm), calculated according to the Bragg formula $n\lambda=2d\sin\theta$. For the Mod-MMT 1, Mod-MMT 2, Mod-MMT 3, Mod-MMT 5 and Mod-MMT 7, the basal spacing was expanded to 16.25, 17.73, 18.72, 19.70, 20.00 Å, respectively. As the sodium cations in the interlayer galleries are replaced by different amount of Ru complex. It is interesting that the XRD peaks sharpen after intercalation, suggesting increased ordering by exchanging with the organic modifiers. From this diffractogram, the increasing of basal spacing values of montmorillonite was seen clearly.

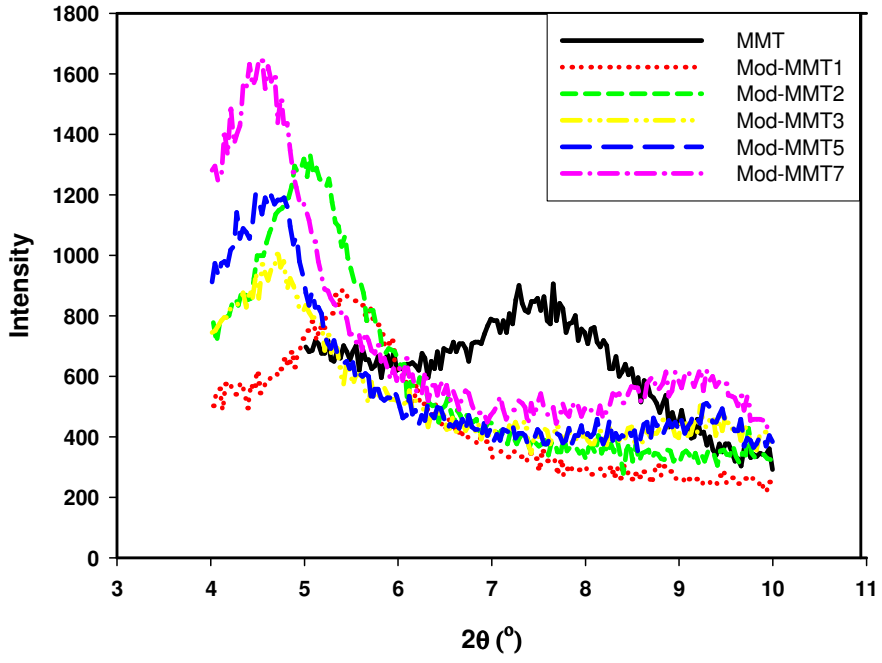

Figure 8.17. XRD diffractograms of Na- MMT, Mod-MMT1, Mod-MMT2, Mod-MMT3, Mod-MMT5 and Mod-MMT7.

The basal spacing values (d_{001}) of Na-montmorillonite and modified montmorillonite calculated by Bragg' Law were summarized in Table 8.2.

Table 8.2. The basal spacing values of Na- montmorillonite and modified montmorillonite (MC)

Structure	**2θ (^{o})**	**d** (Å)
Na-MMT	7.657	11.40
Mod-MMT 1	5.431	16.25
Mod-MMT 2	5.064	17.43
Mod-MMT 3	4.716	18.72
Mod-MMT 5	4.482	19.70
Mod-MMT 7	4.415	20.00

The change of the d-values (basal spacing) with the amount of modificator was shown graphically in Figure 8.18. As shown in that figure, when the amount of modificator increased, d-values of the montmorillonite were increased. However, the growth rate was reduced after Mod-MMT3. Although measured d-values for Mod-MMT5 are larger than Mod-MMT3, the modified clay which one will use in the polymerization stage was decided to compare of polymerization yield and the price of catalyst. When the Ruthenium complex was prepared in the laboratory, the $RuCl_3 * 6H_2O$ salt was used. The price of this salt was so high. Therefore there was not significant change between the polymerization yield of Mod-MMT5 and Mod-MMT3. Because of this important reason, Mod-MMT3 (3 fold modificator) was been decided to use in the modification of the montmorillonite.

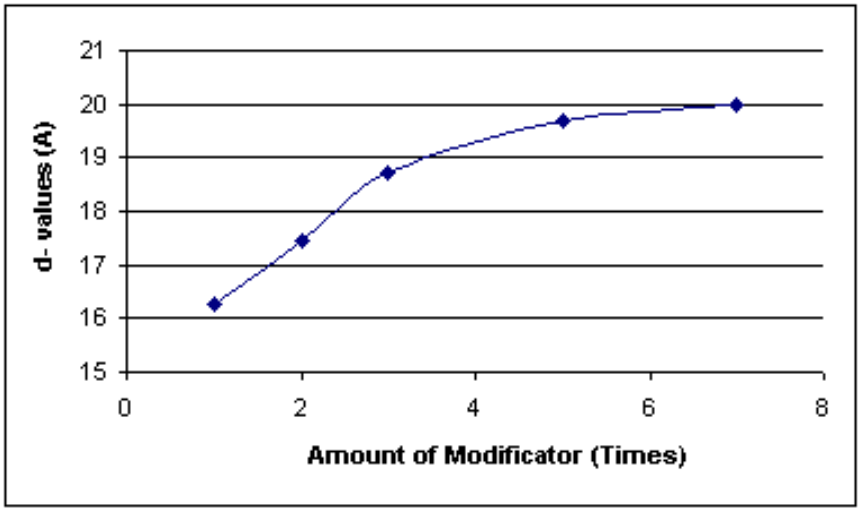

Figure 8.18. Variation of d- values with the amount of the modificator.

For the determination of the optimum time for the modification process, montmorillonite was modified with the modificator for different times. For the obtaining of well dispersed clay mineral in distilled water, a certain amount of sodium montmorillonite in distilled water were mixed with magnetic stirrer respectively 2, 4, 6, 12, 24 and 48 hours at room temperature. Then 0.02 mmol modificator that the equivalent amounts to Cation Exchange Capacity (CEC) of montmorillonite mixed with 0.15 mmol HCl in schelek at room temperature to obtain a homogeneous mixture. In this way, Cl-salt of Ruthenium complex was obtained to enter between the layers of montmorillonite. The Ruthenium complex is sensitive to air. So, modification was achieved under Ar gas against any degradation. This solution was added slowly into the montmorillonite dispersion under Ar gas and the dispersion was mixed 24 hours at room temperature. The mixture was separated by filtration washed with 1:1 ratio of distilled water-methanol several times. After this washing no further chloride could be detected in the wash water with a silver nitrate solution. Then filter paper products were dried in the vacuum oven for a night.

The 2θ values of modified montmorillonite at the different mixing time were determined with X-Ray Diffraction Spectrometer and the basal spacing values were calculated by Bragg' Law (Table 8.3).

Table 8.3. The d- values of Modified Montmorillonite for different mixing times.

Time (h)	**2θ (^{o})**	**d** (Å)
2	5.387	16.39
4	5.454	16.19
6	5.688	15.52
12	5.253	16.81
24	5.431	16.26
48	5.053	16.09

The change of the d-values (basal spacing) with the mixing time was shown graphically in Figure 8.19. According to this figure, there was no significant change in the d-values with the increasing of mixing time especially after 24 hours. So the optimum mixing time was determined as 24 hours for modification of montmorillonite with the Ruthenium complex.

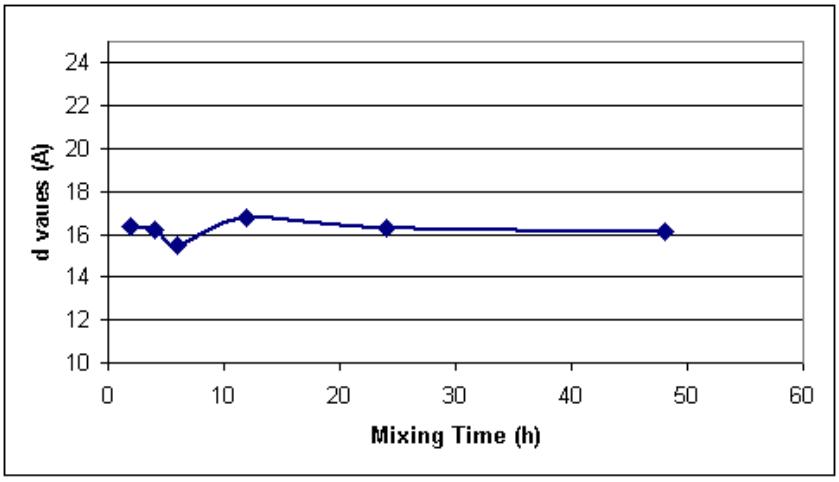

Figure 8.19. Variation of d- values with the mixing time.

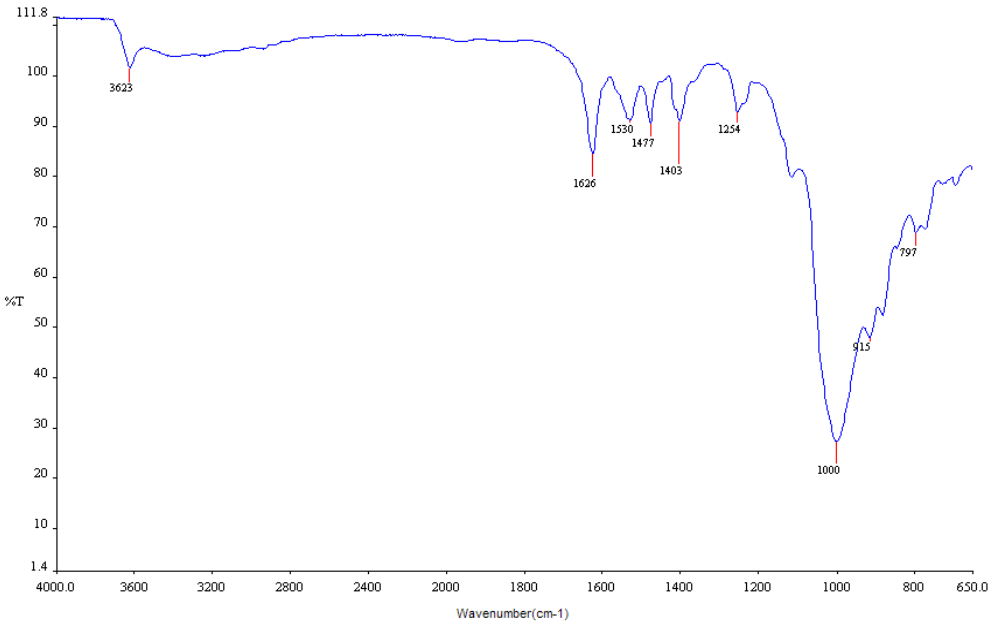

Figure 8.20. FTIR Spectrum of the Modified Montmorillonite.

The FTIR absorption spectrum of the modified montmorillonite was presented in Figure 8.20. When the FTIR spectrum of the montmorillonite is compared with modified montmorillonite, new bands can be seen like, C=N stretching band in ring at about 1600-1500 cm^{-1}; C-C in pyridine ring at 1500-1400 cm^{-1}; C-N in ring at 1335-1020 cm^{-1}.

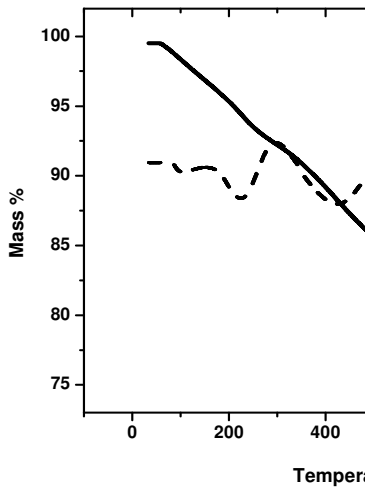

Figure 8.21. TG-DTG Thermograms of the Modified Montmorillonite (in N_2 atmosfere).

The TG-DTG thermograms of the modified montmorillonite in N_2 atmosphere was shown in Figure 8.21. According to this TG-DTG thermograms, the three decomposition stages of modified montmorillonite were between 100-800 ^oC. The total mass loss was about 24% at this temperature range. Degradation started at 100 ^oC and continued up to about 225 ^oC. The second degradation stage was occurred at about 415 ^oC due to the degradation of remained catalyst. The maximum peak temperature was about 545 ^oC. It was observed that, the rate of decomposition standed firm ever after 800 ^oC.

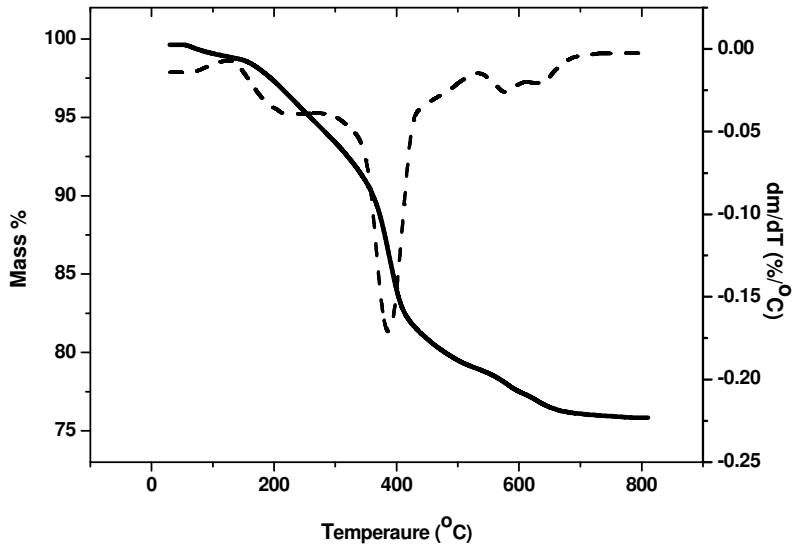

Figure 8.22. TG-DTG Thermograms of the Modified Montmorillonite (in O_2atmosphere).

The TG-DTG thermograms of the modified montmorillonite in O_2 atmosphere was shown in Figure 8.22. According to this TG-DTG thermograms, the decomposition stages of modified montmorillonite were between 100-800 ^oC. The total mass loss was about 26% at this temperature range. The maximum peak temperature was about 385 ^oC. It was observed that, the rate of decomposition standed firm ever after 800 ^oC.

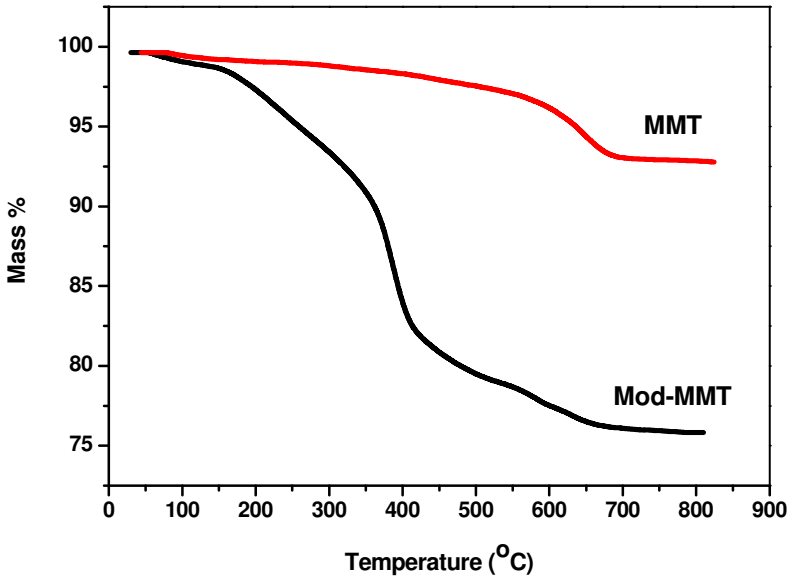

Figure 8.23. TG Thermograms of the Montmorillonite and Modified Montmorillonite (in O_2 atmosphere).

The TG thermograms of the unmodified montmorillonite and modified montmorillonite were shown in Figure 8.23. According to TG thermograms, the weight loss of modified montmorillonite was found as 26 wt % due to the organic materials, Ru complex, as a modificator at 800 ^{o}C. Unmodified montmorillonite exhibited about 8.5 wt % weight loss at same temperature. So, it was indicated that 17.5 wt % modificator was hold on to the montmorillonite. This result was compatible with that calculated of amount of modificator from CEC of the montmorillonite.

8.6. Synthesis of Polynorbornadiene with Ring Opening Metathesis Polymerization (ROMP)

8.6.1. Synthesis of Polynorbornadiene with ROMP Catalyzed by Ruthenium Complex

In a typical ROMP experiment, 0.023 g (0.04 mmol) catalyst was dissolved under Ar in about 5 mL of dry reaction solvent and stirred for a few minutes. 0.8 mL (8 mmol) monomer was injected into the catalyst solution and stirred overnight at room temperature ([Ru] / [NBD]=1/200). Then, the polymer was precipitated in large amount of vigorously stirred methanol by adding dropwise. However, the polymer could not be isolated in high yield with only using catalyst. So we decided to use co-catalyst in reactions as in several literatures (Delaude et al., 1999; Demonceau et al., 1997). The general mechanism scheme of norbornadiene polymerization that catalyzed by Ruthenium complex was given in Figure 8.24. In the synthesis of polynorbornadiene by ROMP experiments, ratio of [C] / [M], temperature, reaction time, precipitation reagent were changed The main experiment parameters were presented in Table 8.4.

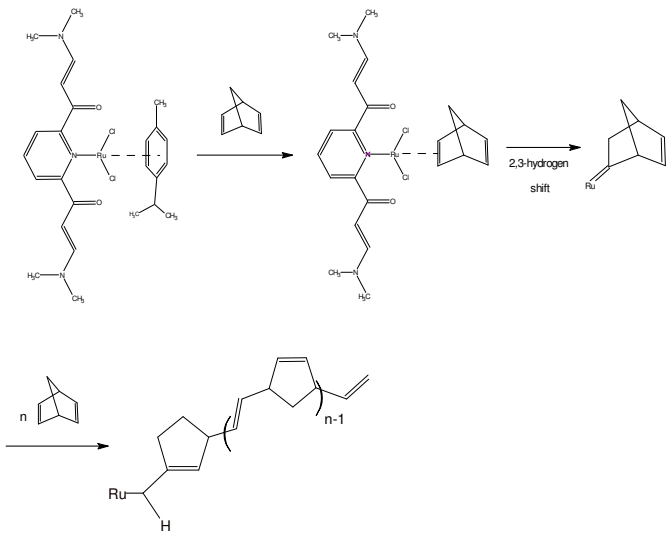

Figure 8.24. Possible mechanism for the formation of the initial metal-carbene in the absence of co-catalyst.

Table 8.4. The main experiment parameters that were used of synthesis of polynorbornadine with Ru complex (**3**) C: Ru complex, M:Monomer.

[C] / [M]	**Temperature**	**Reaction time**	**Precipitation Reagent**	**Solvent**	**Quantity of Solvent**
1/50	25 °C	0.5h	Methanol	CH_2Cl_2	3 mL
1/100	40 °C reflux	2h	Hexane	$CHCl_3$	5mL
1/200		6h		THF	10 mL
1/500		8h		Toluene	15 mL
1/1000		10h		DMSO	20 mL
1/1500		12h		1,2 DCE	25 mL
1/2000		18h		DMF	
		24h			

8.6.2. Synthesis of Polynorbornadiene with ROMP Catalyzed by Ruthenium Complex and co-catalyst (TMSD)

We used trimethylsilydiazomethane (TMSD) as a co-catalyst in our system for high yield. Diazo compounds are usually used as a co-catalyst in ROMP. The detailed structure of TMSD was given in Figure 8.25.

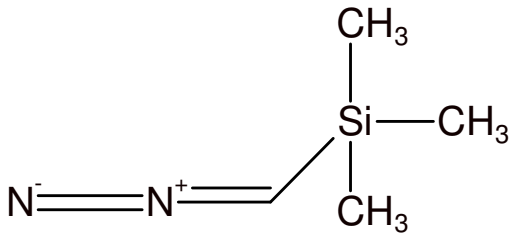

Figure 8.25. Structure of Trimethylsilydiazomethane (TMSD).

Possible mechanism for the formation of the catalytically active species in ROMP reactions was given in Figure 8.26.

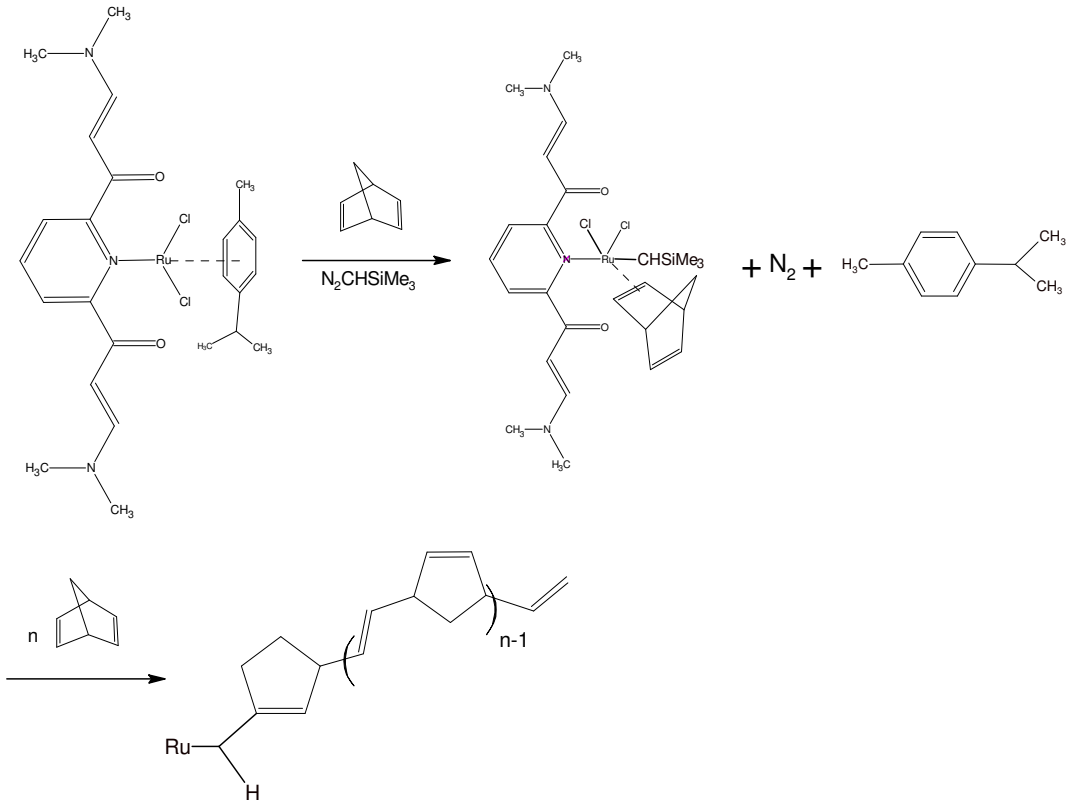

Figure 8.26. Possible mechanism for the formation of the initial metal-carbene in the presence of TMSD.

The most likely process for the initiation of the ROMP of NBD involves the coordination of the diene to the metal centre followed by ring-opening, 1,2-hydrogen shift and alkylidene ligand formation. Such a transformation can result from the different type of coordination of NBD ligand to the metal centre. In the presence of an excess of NBD the weakly coordinating alkene bond can be substituted by NBD molecule leading to the formation of alkylidene ligand and next metallacyclobutane unit.

0.023 g (0.04 mmol) catalyst was dissolved under Ar in about 5 mL of dry CH_2Cl_2 and stirred for a few minutes. 0.8 mL (8 mmol) monomer was injected into the catalyst solution and stirred a few minutes before 1 mL of 0.1 M TMSD diluted in the reaction solvent (in ether/ CH_2Cl_2) (0.1 mmol) was added dropwise over a 30 min period. The reaction mixture was kept at R.T. and 40^0C reflux overnight ([Ru] / [NBD]=1/200). Then, the polymer was precipitated in large amount of vigorously stirred methanol by adding dropwise. The precipitated polymer was separated by filtration washed with small portions of methanol several times and dried overnight under vacuum. In this experiment, effect of the ratio of [C] / [M], temperature, reaction time, precipitation reagent, quantity of solvent, type of solvent and quantity of co-catalyst were investigated like presented above and optimize polymerization conditions were determined.

8.6.2.1. The Effect of [C] / [M] Ratio

For the assessment of optimum catalyst/monomer, the reactions were carried out for 1 / 200, 1 / 500, 1 / 1000, 1 / 1500 and 1 / 2000 for 18 hours at room temperature (Table 8.5). The other variables were kept constant. The obtained polymerization yield was very low for the 1 / 50 and 1 / 100 catalyst / monomer ratio. As a result of the experiments, Figure 8.27 shows the effect of the catalyst / monomer on the polymerization yield. From this figure, the optimum [C] / [M] ratio was identified as 1 / 1000.

Table 8.5. Polymerization of Norbornadiene with Various [C] / [M] Ratio [a].

Entry	[C] / [M]	Yield %
1	1/200	25
2	1/500	35
3	**1/1000**	**55**
4	1/1500	56
5	1/2000	57

[a]Reactions at room temperature, in 3 mL CH_2Cl_2; 18 h; 1 mL co-catalyst.

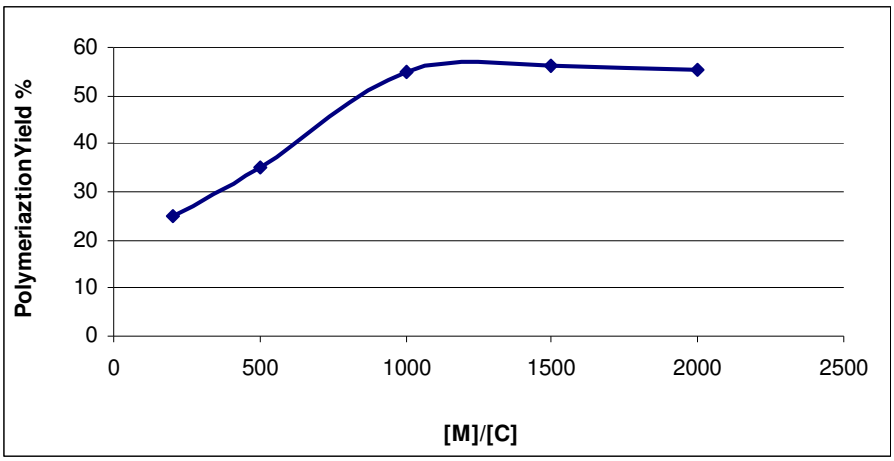

Figure 8.27. The effect of [C] / [M] Ratio on the polymerization yield of norbonadiene.

8.6.2.2. The Effect of Reaction Time

For the assessment of optimum polymerization time, the reactions were performed for 2, 6, 8, 10, 12, 18 and 24 hours at 25 ^{o}C, at constant [C] / [M] as 1/1000. The results of polymerization yields were given at Table 8.6. The effect of the catalyst / monomer on the polymerization yield was shown at Figure 8.28. From this figure, the polymerization yield was constant since 18 hours. Optimum reaction time was identified as 18 hours.

Table 8.6. Polymerization of Norbornadiene at various Reaction time [a].

Entry	Reaction time (h)	Yield %
1	24	56
2	**18**	**55**
3	12	30
4	10	23
5	8	15
6	6	13
7	2	10

[a]Reactions at room temperature, in 3 mL CH_2Cl_2; [Ru] / [NBD] = 1/1000; 1 mL co-catalyst.

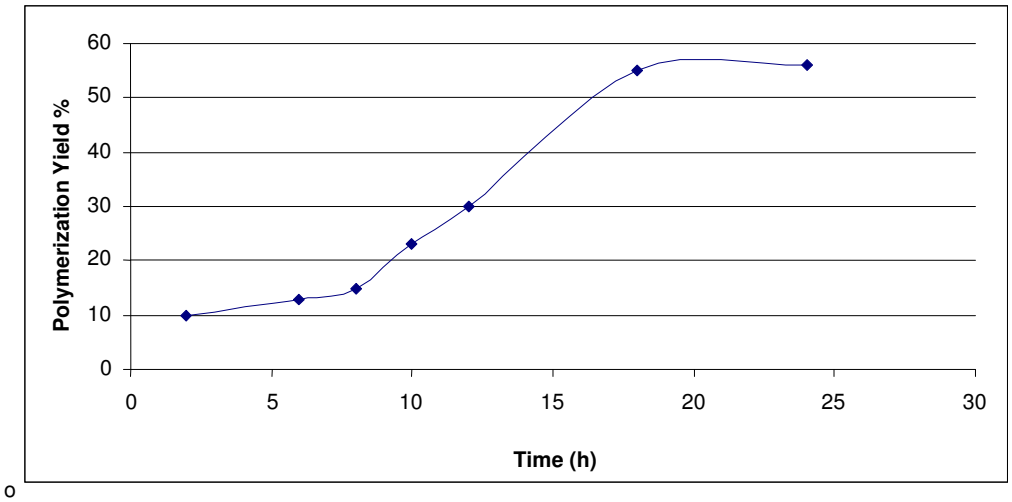

o

Figure 8.28. The effect of Reaction time on the polymerization yield of norbonadiene.

8.6.2.3. The Effect of the Temperature

For the determination of the optimum temperature, the reactions were carried out at room temperature and 40 ^{o}C, the reflux for 18 hours in 3 mL CH_2Cl_2 at constant [C] / [M] and other variables were kept constant. The results of polymerization yields were given at Table 8.7. As a result of the experiments, the polymerization yield was raised to 80% that the reaction was performed at reflux for 18 hours. It was observed that, the reaction was carried out for 6 hours at reflux, the yield was not changed. Therefore, due to shorter reaction time, optimum temperature was decided as for 6 hours at 40^{0}C reflux temperature.

Table 8.7. Polymerization of Norbornadiene at various Temperature [a].

Entry	Temperature	Reaction Time (h)	Yield %
1	**40 ^{o}C, reflux**	**6**	**80**
2	25 ^{o}C	18	55
3	40 ^{o}C, reflux	18	80

[a]Reactions in 3 mL CH_2Cl_2; [Ru] / [NBD] = 1/1000; 1 mL co-catalyst.

8.6.2.4. The Effect of the Quantity of co-catalyst

For the assessment of the optimum quantity of co-catalyst, the reactions were performed at different amounts of co-catalyst (0.2 mL, 0.4 mL, 0.6 mL, 0.8 mL and 1 mL) and other variables were kept constant. The results of polymerization yields were given at Table 8.8. The effect of the catalyst / monomer on the polymerization yield was shown at Figure 8.29.As a result of the experiments, the optimum quantity of co-catalyst was identified as the amount of 1 mL. For the determination of the optimum amount of co-catalyst, it was not tested more than amount of 1 mL. In general, 1 mL was used as quantity of co-catalyst in the literature, using of more than 1 mL co-catalyst had no significant change in the yield of polymerization. So, 1 mL was used as the optimum co-catalyst with considering the high price of co-catalyst.

Table 8.8. Polymerization of Norbornadiene at various Quantity of co-catalyst [a].

Entry	Quantity of co-catayst	Yield %
1	**1 mL**	**80**
2	0.8 mL	30
3	0.6 mL	20
4	0.4 mL	15
5	0.2 mL	10

[a]Reactions at 40 °C, reflux, in 3 mL CH_2Cl_2; [Ru] / [NBD] = 1/1000; 6h.

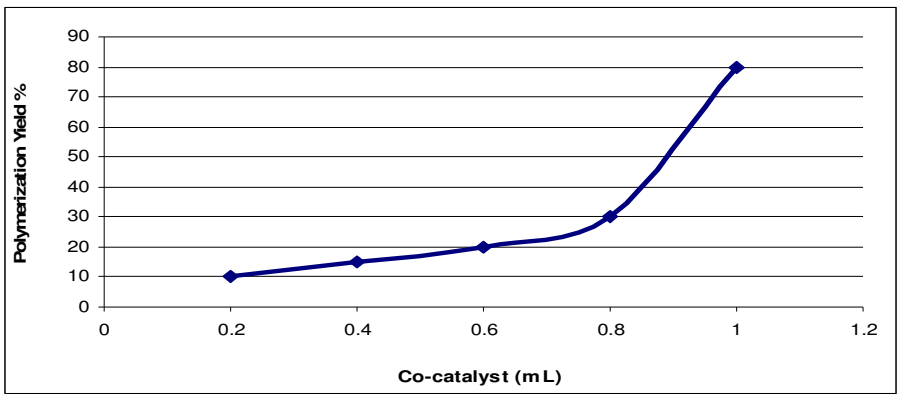

Figure 8.29. The effect of quantity of co-catalyst on the polymerization yield of norbonadiene.

Our concern was to emphasize the role of the carbene precursor on the polymerization process. When the polymerization of norbornadiene was tested with pure TMSD (no addition of catalyst, 1mL of NBD solution in dichloromethane and [TMSD]/ [NBD] = 1/200, 1/500, 1/1000; tested at room temperature and 40^0 C, 6 h) no polymerization was observed. However, when norbornadiene was tested with ruthenium catalyst without activation with TMSD ([Ru]/[NBD] = 1/200, 1/500, 1/1000, 3 mL dichloromethane, 6 h), a conversion of 6% was observed. Because there was no TMSD activation, the initiating metal–carbene complex must result from a reaction between the catalyst and the substrate olefin.

We have also varied the amount of diazo compound introduced and its rate of addition to the monomer and catalyst solution at room temperature. It appears from these trials that the reaction is most efficient when the original standard conditions are followed (0.1 mmol of TMSD, 30 min addition time). Modifying the concentration of the TMSD solution or the rate of the syringe pusher used to add TMSD, or both, did not result in any dramatic improvement and sometimes had a detrimental influence on the polymerization outcome. Instantaneous addition of TMSD led to polymers with a relatively narrow distribution of high molecular weights but the yield stagnated lower.

As a result of committed experiments, optimum conditions for polymerization were detected. Polymerization was carried out 1/1000 [C] / [M] ratio, in 3 mL dry dichloromethane, at 40 ^oC reflux temperature and for 6 hours.

8.6.3. Characterization of Polynorbornadiene with ROMP Catalyzed by Ruthenium Complex and co-catalyst (TMSD)

The FTIR spectra of norbornadiene and polynorbornadiene were presented in Figure 8.30 and Figure 8.31.

According to the FTIR spectrum of norbornadiene (NBD), C-C and C=C (in ring) bands can be seen at 2986 cm^{-1} , 1641 cm^{-1}, 1543 cm^{-1}, 1310 cm^{-1}, 930 cm^{-1} and 800 cm^{-1}. According to FTIR spectrum of polynorbornadiene, we can see cyclo structure bands at 2962 cm^{-1}, 1681 cm^{-1}, 1425 cm^{-1}, 1259 cm^{-1}, 1080 cm^{-1}, 1010 cm^{-1} and 800 cm^{-1}. Unlike from norbornadiene, strongly C=C (on chair)

band at about 1620 cm^{-1} and C-H stretching band of CH=CH (on chair) at about 1016 cm^{-1} were appeared of spectrum of polynorbornadiene.

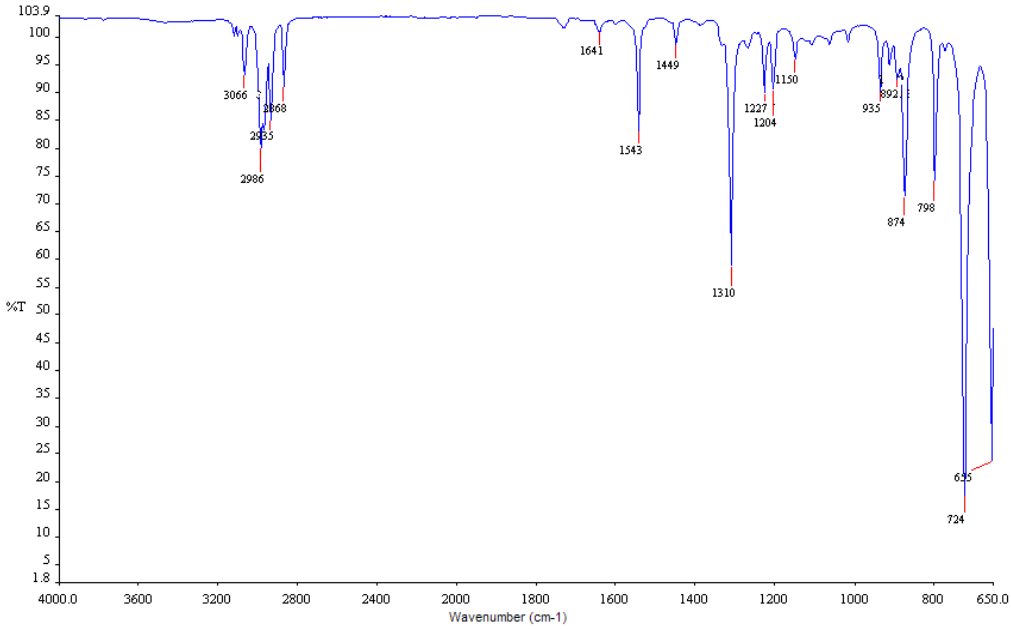

Figure 8.30. FTIR Spectrum of the Norbornadiene (NBD)

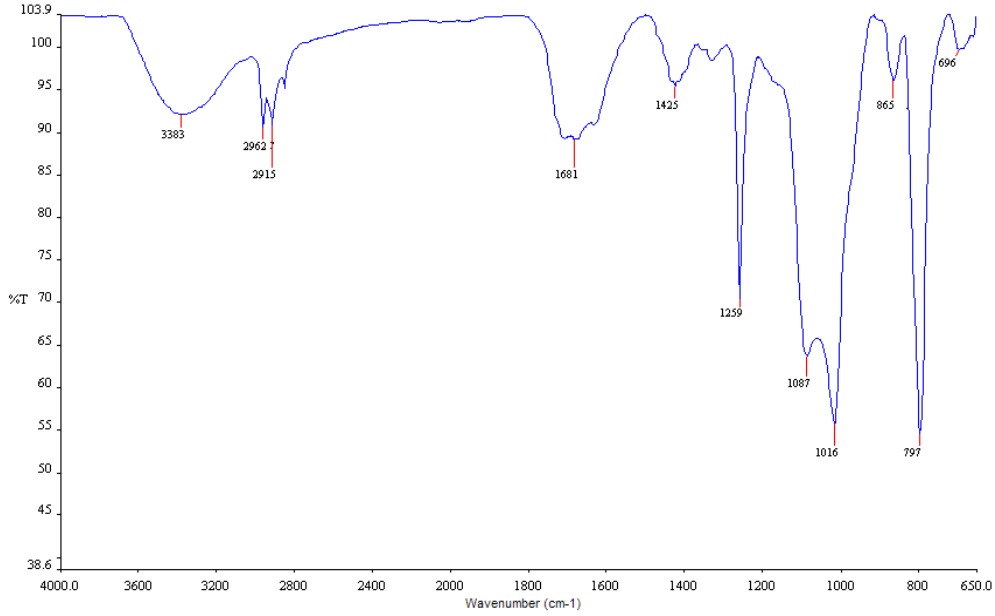

Figure 8.31. FTIR Spectrum of the Polynorbornadiene (PNBD)

FTIR analysis was not enough for structure analysis. ^{1}H-NMR analysis must be tested for polynorbornadiene.

The ^{1}H-NMR spectrum of polynorbornadiene was presented at Figure 8.32. The ^{1}H-NMR spectrum of polynorbornadiene shows five well-seperated groups of signals. Simultaneously the formation of an unsaturated polynorbornadiene with characteristic signals of the olefinic protons at ca. 5.6 and 5.4 ppm appeared. (protons denoted 5,6 and 2,3). From integral ratio of signal due to protons denoted 1,4 at δ 3.6 (*cis* double bond) and δ 3.2 (*trans* double bond) ppm appeared. Two protons denoted 7 were appeared at δ 2.4 and 1.3 ppm.

^{1}H-NMR data of the polynorbornadiene were represented:

^{1}H-NMR (400 MHz, $CDCl_3$): δ *5.6-5.2* (m, 4H), *3.6* (s, 1H), *3.2* (s, 1H), *2.3* (s, 2H), *1.2* (s, 2H).

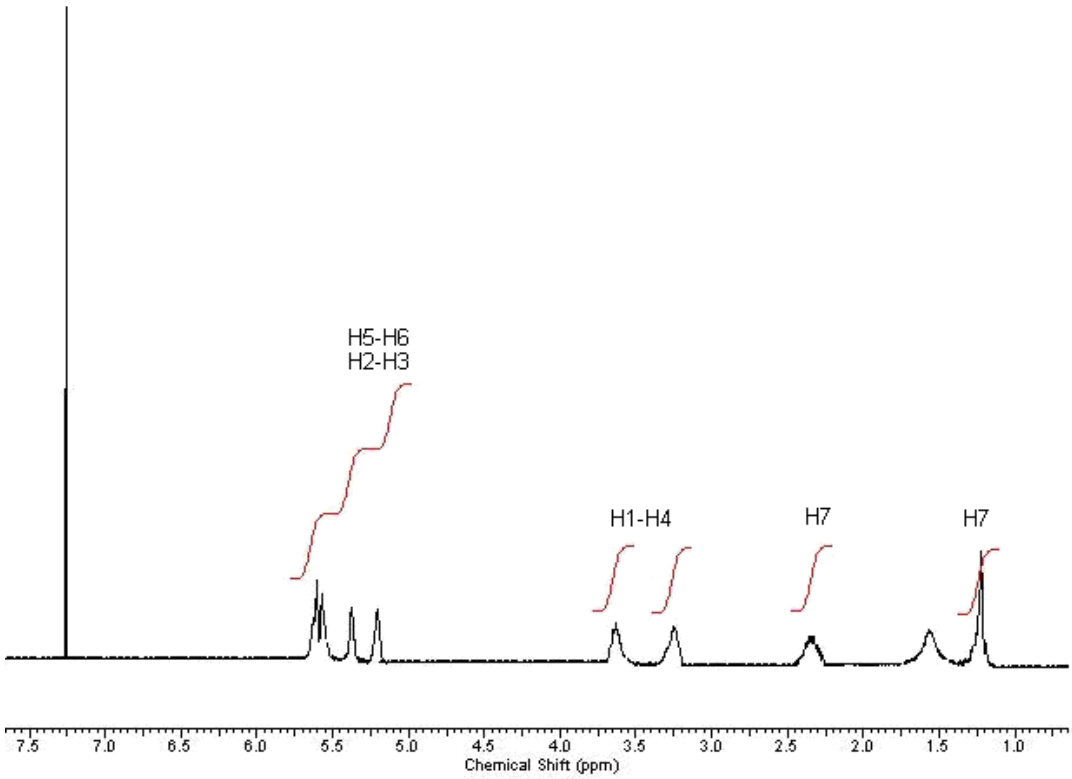

Figure 8.32. ^{1}H-NMR Spectrum of the Polynorbornadiene (PNBD).

M_n, M_w and M_w/ M_n (polydispersity index, PDI) of the polynorbornadiene were measured by GPC (Figure 8.33). The polymer formed in high yield and had a simple unimodal molecular weight distribution as evidenced by GPC analysis of polymers. According to GPC trace, M_n=34320 g/mol (the number average

molecular weight), M_w= 121380 g/mol (weight-average molecular weight) and M_w/M_n=3.53 results were obtained.

The ruthenium complex was treated with TMSD to generate a Ru-carbene. A conversion of 80% was reached which is so higher than in the case when no activator is used but the polymer exhibits a broad molecular weight distribution (M_w/M_n=3.53). The broadening of the molecular weight distribution is caused by the generation of multi-reactive sites (those activated in situ and those activated by TMSD). Because of strong macromolecular chains, solubility of these polymers is not good in some solvents.

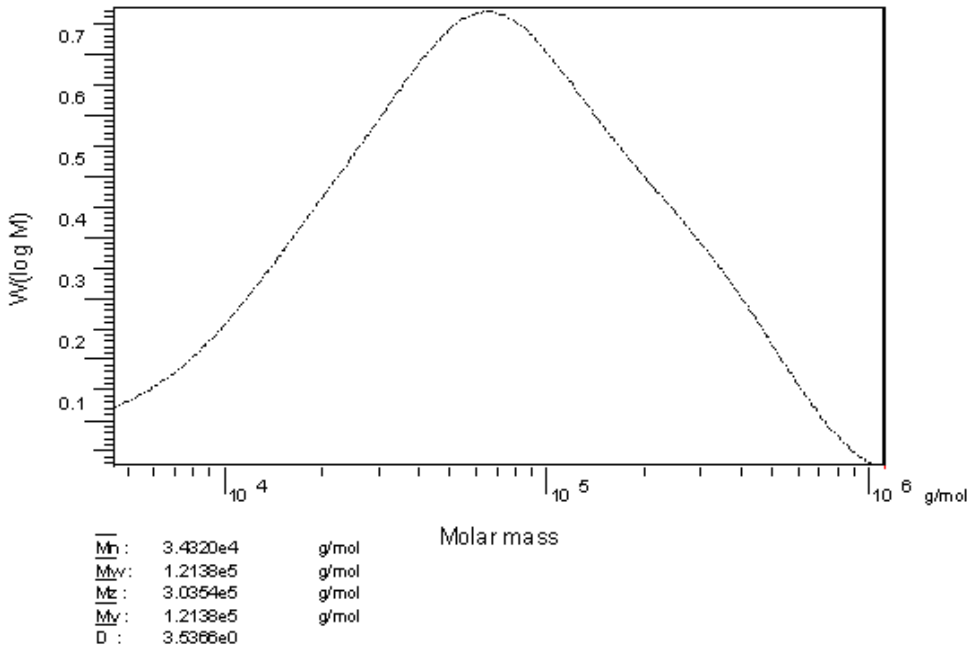

Figure 8.33. GPC Traces of the Polynorbornadiene (PNBD).

The thermogravimetric analyses (TG-DTG) of polynorbornadiene under N_2 atmosphere were determined and the results were shown in Figure 8.34. According to these thermograms, the polymer began to decompose the gradual at 100 ^oC, important part of the polymer was decomposed at about 500 ^oC, and decomposition was completed at about 700 ^oC. There was a small decomposition peak at about 245 ^oC because of remaining catalyst at the time of polymerization. The maximum peak temperature was about 425 ^oC. The total weight loss was

about 86% at this temperature range. The remaining 14% portion of the organic material is carbonized.

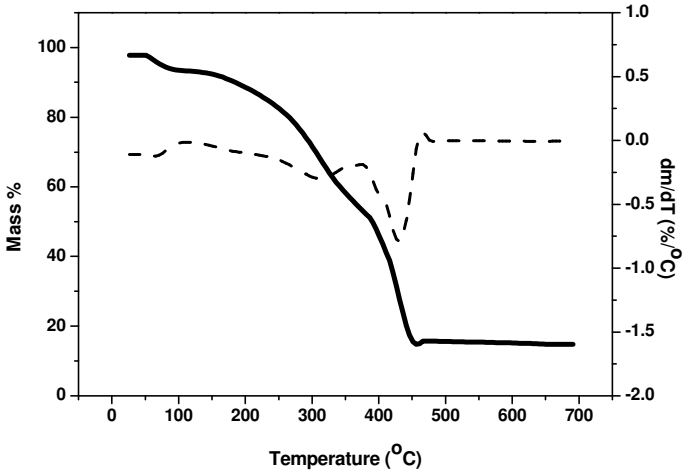

Figure 8.34. TG-DTG Thermogram of Polynorbornadiene (PNBD) (in N_2 atmosphere).

The thermograms (TG-DTG) of polynorbornadiene under O_2 atmosphere were shown in Figure 8.35. According to these thermograms, degradation started at about 130 ^oC and continued up to about 480 ^oC. There was a small decomposition peak at about 305 ^oC because of remaining catalyst at the time of polymerization. The maximum peak temperature was about 440 ^oC. All polymer sample was burned at this temperature range. Namely, the carbonized residue that remained under N_2 atmosphere was completely burned.

The maximum peak temperature of the polymer was increased under O_2 atmosphere according to N_2 atmosphere.

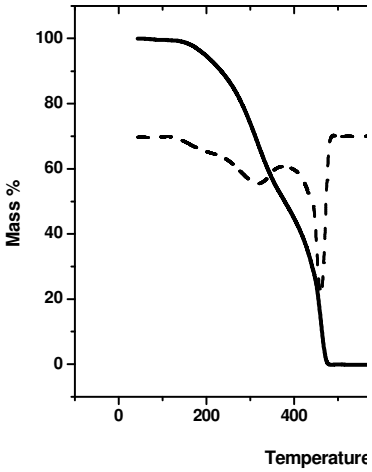

Figure 8.35. TG-DTG Thermogram of Polynorbornadiene (PNBD) (in O_2 atmosphere).

8.7. Synthesis and Characterization of Polynorbornadiene-Clay Nanocomposites

Firstly, 1 mL (0.9 g, 9.76 mmol) norbornadiene monomer was placed to shelenk under Ar atmosphere. Modified clay that 1% amount of monomer was added and mixed for a night. The next day, 1 mL, 0.1 M TMSD (ether / CH_2Cl_2) (0.1 mmol) trimetilsilydiazometan (TMSD) and 3 mL dry dichloromethane were added and mixed one more night. Then the obtained nanocomposites were precipitated in the large amount of methanol and separated by filtration washed with methanol several times. It was dried a night in a vacuum.

8.7.1. XRD Analysis of Nanocomposites

Polynorbornadiene-montmorillonite clay nanocomposites were prepared that containing different percentages of montmorillonite. For this purpose, 1%, 3% and 5% polynorbornadiene-clay nanocomposites were prepared. X-ray diffraction (XRD) was often been used for determining the degree of intercalation and/or exfoliation of clay in the polymer matrix. Montmorillonite interlayer distance had been increased from 11.40 Å to 18.72 Å with modificator that also will be used as a polymerization catalyst. The aim of this study is that, to perform of polymerization of the norbornadienes among the layers of montmorillonite that

separated with modificator. In this way, the layers of montmorillonite will be dispersed as much as possible in the polymer matrix. In other words, the d_{001} peak that is expected to be seen at $2\theta=4\text{-}10^0$ must be disappeared in the XRD spectrum.

XRD patterns of polynorbornadiene-clay nanocomposites that were content 1%, 3% and 5% MMT were given in Figure 8.36, Figure 8.37, Figure 8.38, respectively.

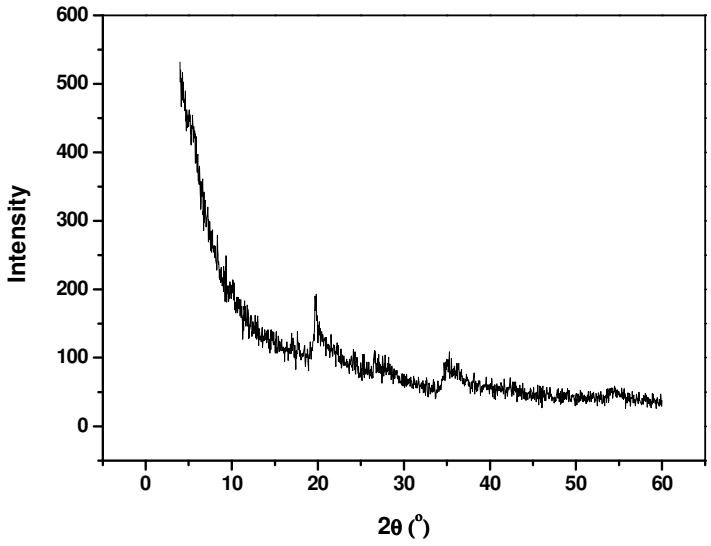

Figure 8.36. XRD Pattern of PNBD-1% MMT nanocomposite.

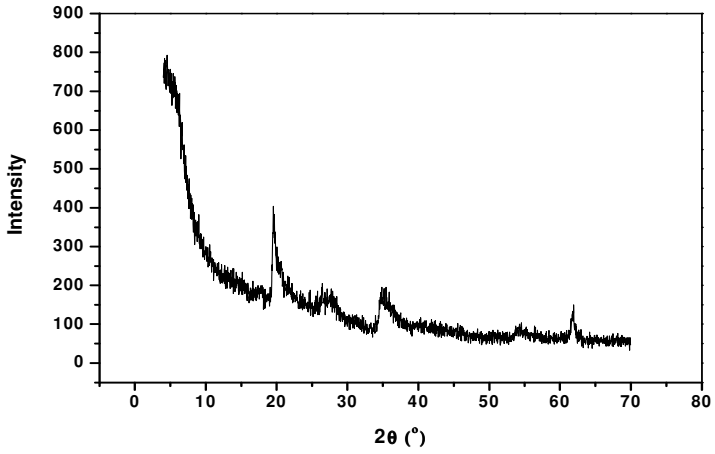

Figure 8.37. XRD Pattern of PNBD-3% MMT nanocomposite.

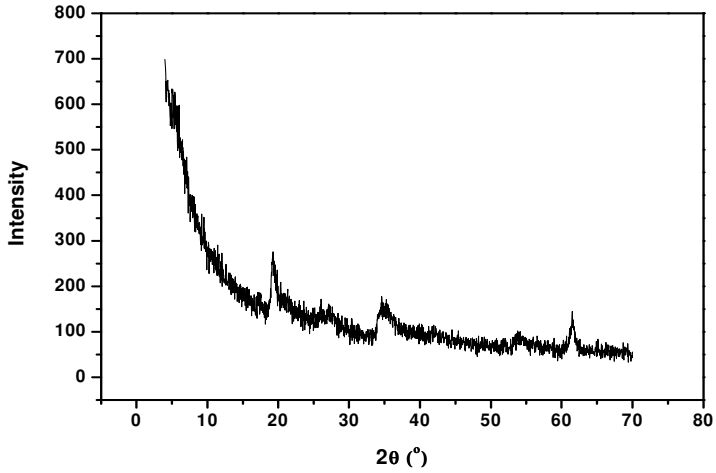

Figure 8.38. XRD Pattern of PNBD-5% MMT nanocomposite.

As shown from these figures, there is a lack of any diffraction peak in $2\theta=4\text{-}10^0$ as opposed on the diffraction peak at $2\theta=4.71^0$ (d_{001}=18.7 Å) for organophilic clay, indicating the possibility of having exfoliated silicate nanolayers of organophilic clay dispersed in a PNBD matrix. Namely, the 001 diffraction peak on XRD spectra disappeared, which implies that the layered structure in the clay particles is largely destroyed by in situ polymerization.

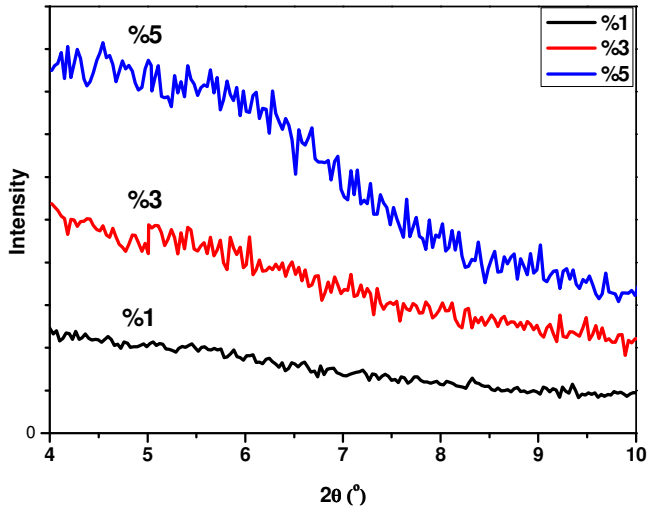

Figure 8.39. XRD Patterns of PNBD- MMT nanocomposites at low angles.

The XRD patterns of all PNBD nanocomposites which were obtained by dispersing organically modified clay in NBD monomer with in-situ polymerization was illustrated with the more detailed in the same pattern at low angles (2θ=4-10^0) in Figure 8.39. As it can be seen from this figure that, for the nanocomposite PNBD-1%MMT and PNBD-3%MMT, an exfoliated structure was obtained with absence of any d_{001} reflection in the XRD region. The existence of exfoliation may be due to good compatibility of PNBD with monomer at low concentration that might result from interaction of clay surface with the PNBD. On the other hand, PNBD-5%MMT exhibited small and broad peaks that might be probably resulting from partially exfoliated or intercalated structures. It was indicating that there is a small amount of organoclay existing in the form of an intercalated layer structure. In other words, this small and broad peak was indicating that PNBD chains are intercalated into the gallery of clay layers. Based upon this information it seems that there might be relatively more attractive forces between the clay layers at higher loading which may lead to some intercalated clays with a small peak in XRD analysis.

8.7.2. TG-DTG Analysis of Nanocomposites

The thermal stability of the materials usually was also examined by thermogravimetric analysis with a heating rate of 10 ^{0}C/min. The mass loss due to the formation of volatile degradation products were monitored as a function of temperature.

The thermal stability of a material is usually assessed by thermogravimetric analysis where the sample mass loss due to volatilization of degraded by-products is monitored as a function of a temperature rise.

Thermal parameters are related to both particle size of the inorganic filler and mobility of the polymer chains in the matrix. The sizes of the fillers lead to an exceptionally large effect on interfacial area in the composite. The interfacial region is extremely large in nanocomposites. The polymer–particle interaction is occurred in this area. The interaction of the polymer with the nanoparticles gives significant opportunity for changing the polymer mobility and relaxation dynamics. Small size means that the particles do not create large stress

concentrations and thus do not compromise the ductility of the polymer. The small size of nanofillers can also lead to unique properties of the particles themselves.

The thermal stability of 1%, 3% and 5% polynorbornadiene-clay nanocomposites under O_2 atmosphere were determined by TG-DTG method. TG-DTG thermograms were given in Figure 8.40, Figure 8.41 and Figure 8.42, respectively.

According to TG-DTG thermogram of PNBD-1% MMT nanocomposite (Figure 8.40), there were two degradation stages between 150-510 ^{o}C. The total weight loss was about 96% at this temperature range. The remaining part was due to presence of montmorillonite (4%). Degradation was started at 150 ^{o}C and continued up to about 340 ^{o}C. There was a small degradation peak at 340 ^{o}C due to presence of the catalyst. The maximum peak temperature was about 450 ^{o}C. It was observed that, the rate of degradation standed firm ever after 510 ^{o}C.

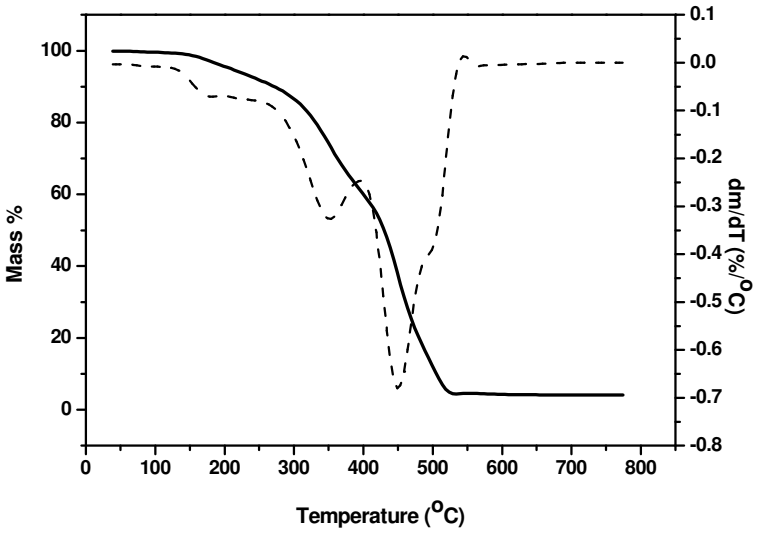

Figure 8.40. TG-DTG Thermograms of PNBD-1% MMT nanocomposite (in O_2 atmosphere).

According to TG-DTG thermogram of PNBD-3% MMT nanocomposite (Figure 8.41), there was two degradation stages between 120-560 ^{o}C. The total weight loss was about 93.5 % at this temperature range. The remaining part was due to presence of montmorillonite (6.5 %). Degradation was started at 100 ^{o}C

and continued up to about 345 ^{o}C. There was a small degradation peak at 345 ^{o}C due to presence of the catalyst. The maximum peak temperature was about 530 ^{o}C. It was observed that, the rate of degradation standed firm ever after 560 ^{o}C.

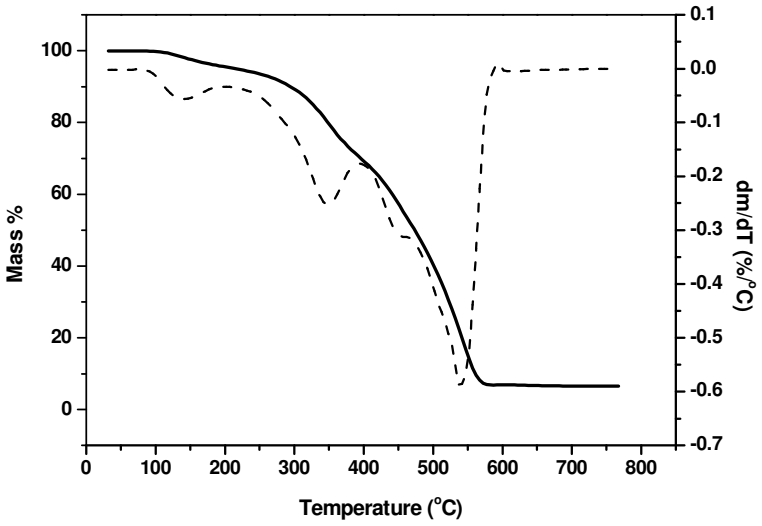

Figure 8.41. TG-DTG Thermograms of PNBD-3% MMT nanocomposite (in O_2 atmosphere).

According to TG-DTG thermograms of PNBD-5% MMT nanocomposite (Figure 8.42), there was two degradation stages between 150-580 ^{o}C. The total weight loss was about 92 % at this temperature range. The remaining part was due to presence of montmorillonite (8 %). Degradation was started at 120 ^{o}C and continued up to about 345 ^{o}C. There was a small degradation peak at 345 ^{o}C due to degradation of the residue catalyst. The degradation peaks at 450-500 ^{o}C due to degradation of the polymer. Also, there was a small decomposition peak at about 600 ^{o}C due to decomposition of the clay. The maximum peak temperature was about 570 ^{o}C. It was observed that, the rate of degradation standed firm ever after 580 ^{o}C.

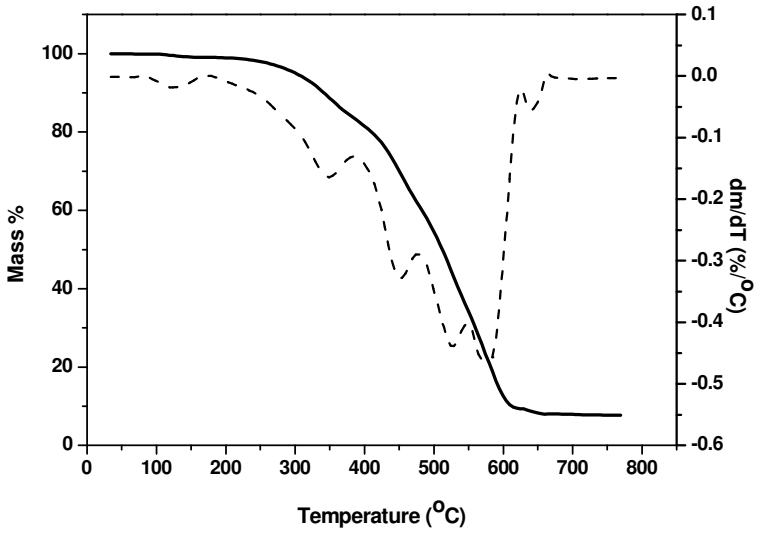

Figure 8.42. TG-DTG Thermograms of PNBD-5% MMT nanocomposite (in O_2 atmosphere).

TG thermograms of the all nanocomposites and polynorbornadiene were given in Figure 8.43. All nanocomposite structures exhibited enhanced thermal stabilities compared to the pure polymer, PNBD. From the DTG data, it is clear that the maximum peak temperature and residual weight after complete volatilization both increased. In general, there appeared to be a few stages of weight loss, starting at approximately 150 ^{o}C and ending at 600 ^{o}C, which might correspond to the degradation of the catalyst, structural degradation of the polymer and decomposition of clay mineral. The maximum peak temperatures of the nanocomposites are higher than pure PNBD, and shift toward higher temperature as the amount of Na-MMT increases, indicating an enhancement of the thermal stability upon intercalation. The maximum peak temperatures of the PNBD, PNBD-1% MMT, PNBD-3% MMT and PNBD-5% MMT were 440, 450, 530, 570 ^{o}C, respectively. The maximum peak temperature (in air) increased by 130 ^{o}C in comparison of PNBD with the PNBD-5% MMT nanocomposite. This enhancement of the thermal stability may be caused by the 'barrier effect' of the montmorillonite layer structure, which hinders mobility of the small molecules produced during the thermal degradation of the PNBD.

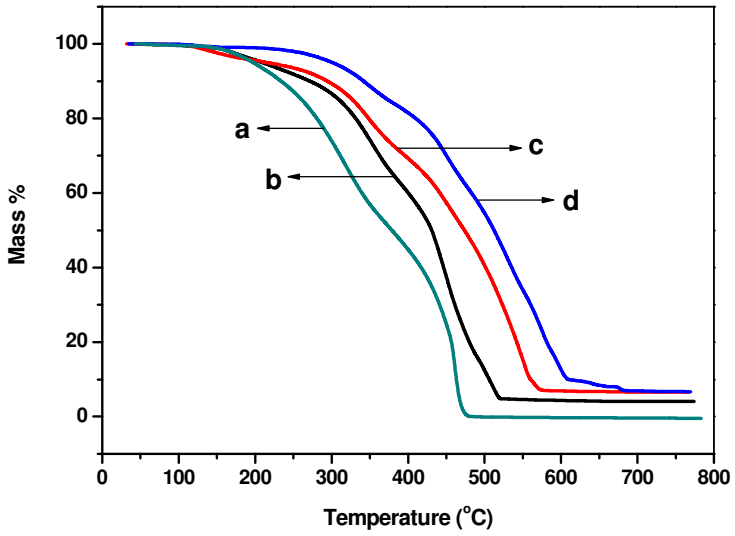

Figure 8.43. TG Thermograms of (a) PNBD, (b) PNBD-1%MMT, (c) PNBD-3%MMT, (d) PNBD-5%MMT (in O_2 atmosphere).

For the assessment of thermal stability of 1%, 3% and 5% polynorbornadiene-clay nanocomposites under N_2 atmosphere, TG-DTG analysis's carried out. TG-DTG thermograms were given in Figure 8.44, Figure 8.45, Figure 8.46, respectively.

According to TG-DTG thermogram of PNBD-1% MMT nanocomposite under N_2 atmosphere (Figure 8.44), there were two degradation stages between 130-550 ^{o}C. The total mass loss was about 84% at this temperature range. The remaining part was due to presence of montmorillonite (16%). Degradation was started at 130 ^{o}C and continued up to about 450 ^{o}C. There was a degradation peak at 450 ^{o}C due to degradation of the polymer. The maximum peak temperature was about 450 ^{o}C. It was observed that, the rate of degradation standed firm ever after 550 ^{o}C.

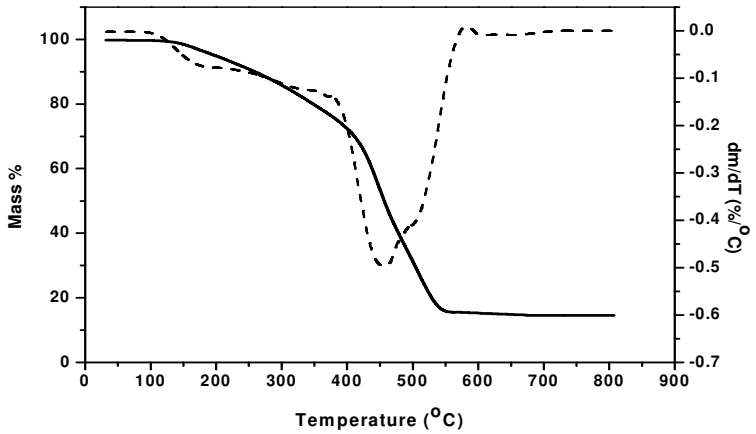

Figure 8.44. TG-DTG Thermograms of PNBD-1% MMT nanocomposite (in N_2 atmosphere).

According to TG-DTG thermogram of PNBD-3% MMT nanocomposite (Figure 8.45), the degradation stage between 120-600 ^{o}C. The total weight loss was about 81% at this temperature range. The remaining part was due to presence of montmorillonite (19%). Degradation was started at 120 ^{o}C and continued up to about 450 ^{o}C. There was a degradation peak at 450 ^{o}C due to degradation of the polymer. Also, there was a small decomposition peak at 590 ^{o}C due to decomposition of the clay mineral. The maximum peak temperature was about 465 ^{o}C. It was observed that, the rate of degradation standed firm ever after 600 ^{o}C.

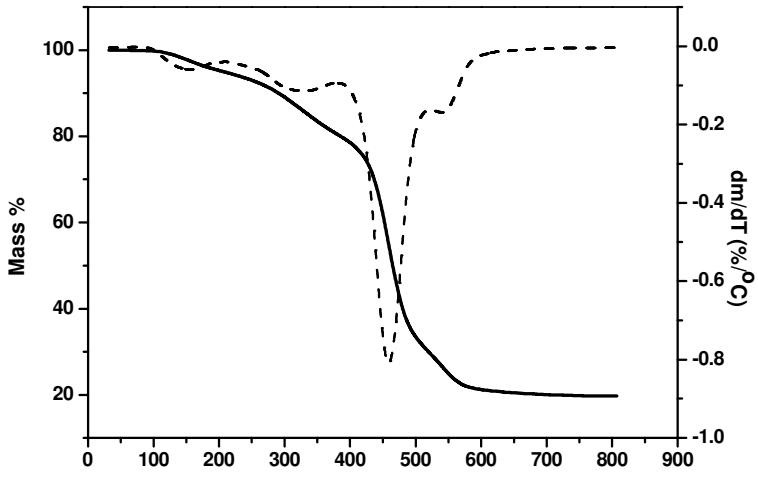

Figure 8.45. TG-DTG Thermograms of PNBD-3% MMT nanocomposite (in N_2 atmosphere).

According to TG-DTG thermogram of PNBD-5% MMT nanocomposite (Figure 8.46), there was two degradation stages between 120-600 ^{o}C. The total weight loss was about 80% at this temperature range. The remaining part was due to presence of montmorillonite (20%). Degradation was started at 120 ^{o}C and continued up to about 345 ^{o}C. There was a small degradation peak at 345 ^{o}C due to presence of the catalyst. The degradation peaks at 450 ^{o}C and 550 ^{o}C due to the degradation of polymer and the decomposition clay minerals. It was observed that, the rate of degradation standed firm ever after 600 ^{o}C.

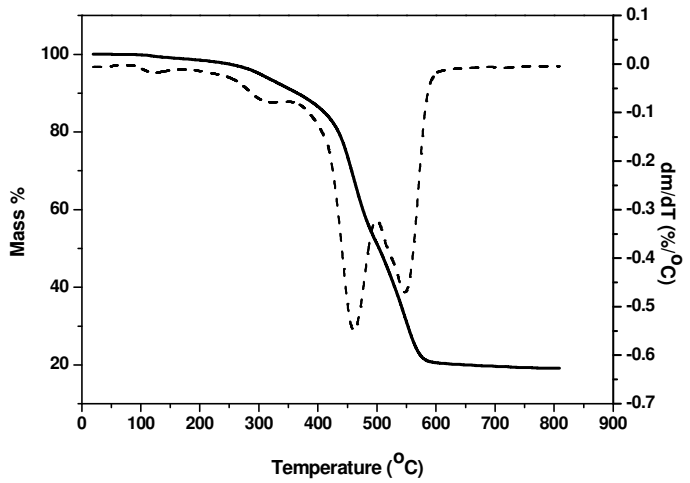

Figure 8.46. TG-DTG Thermograms of PNBD-5% MMT nanocomposite (in N_2 atmosphere).

TG thermograms of the all nanocomposites under N_2 atmosphere were given in Figure 8.47. All nanocomposite structures exhibited to enhanced thermal stabilities with the increasing of the clay content.

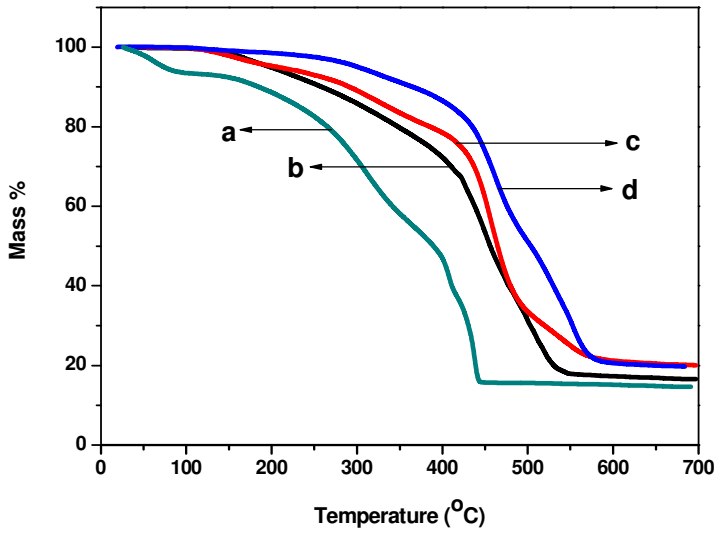

Figure 8.47. TG Thermograms of (a) PNBD, (b) PNBD-1%MMT, (c) PNBD-3%MMT, (d) PNBD- 5%MMT (in N_2 atmosphere).

8.7.3. FTIR Analysis of Nanocomposites

1%, 3% and 5% polynorbornadiene-clay nanocomposite were characterized by FTIR method. FTIR spectrum of 1% polynorbornadiene-clay nanocomposite was given in Figure 8.48. The same spectra were carried out with 3% and 5% polynorbornadiene-clay nanocomposites. It was observed that characteristic montmorillonite absorption bands (1150 cm^{-1}) were collide with characteristic polymer absorption bands. And due to the small content of clay particles, clay absorption bands could not be observed clearly.

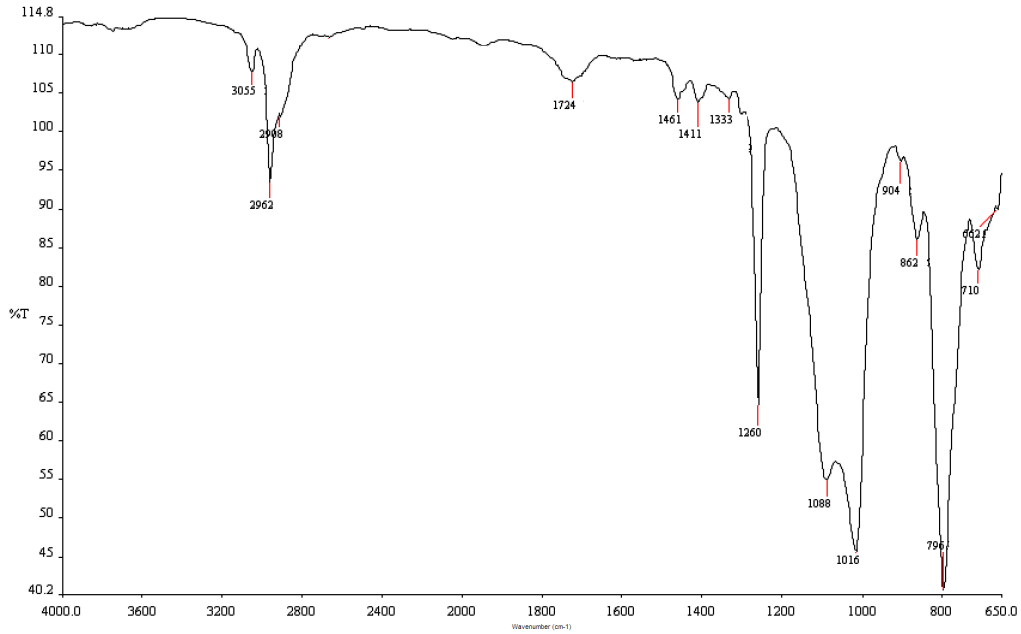

Figure 8.48.FTIR Spectrum of PNBD-1% MMT nanocomposite.

8.7.4. SEM Analysis of Nanocomposites

Surface properties of 1%, 3% and 5% polynorbornadiene-clay nanocomposites could be characterized by SEM (Scanning Electron Microscopy) method. SEM images of them are given in Figure 8.49, Figure 8.50, Figure 8.51, respectively.

The surface morphologies of the nanocomposites are compared by SEM analyses. The morphological images of the nanocomposites at magnification 5000× and 10.000× were shown at Figure 8.49-8.51 in which the bright regions correspond to clay aggregates. The SEM images show that the all nanocomposites had the nanoporous morphology. For the PNBD-3%MMT and PNBD-5%MMT nanocomposites, one can see big aggregated particles together with small aggregates which may be attributed to intercalated or partially exfoliated structure. This may be most probably due to the poor interaction of MMT layers with polymer matrix in the interlayer galleries. On the other hand, PNBD-1%MMT nanocomposite has relatively small clusters of the clay particles that are homogeneously dispersed in the PNBD matrix.

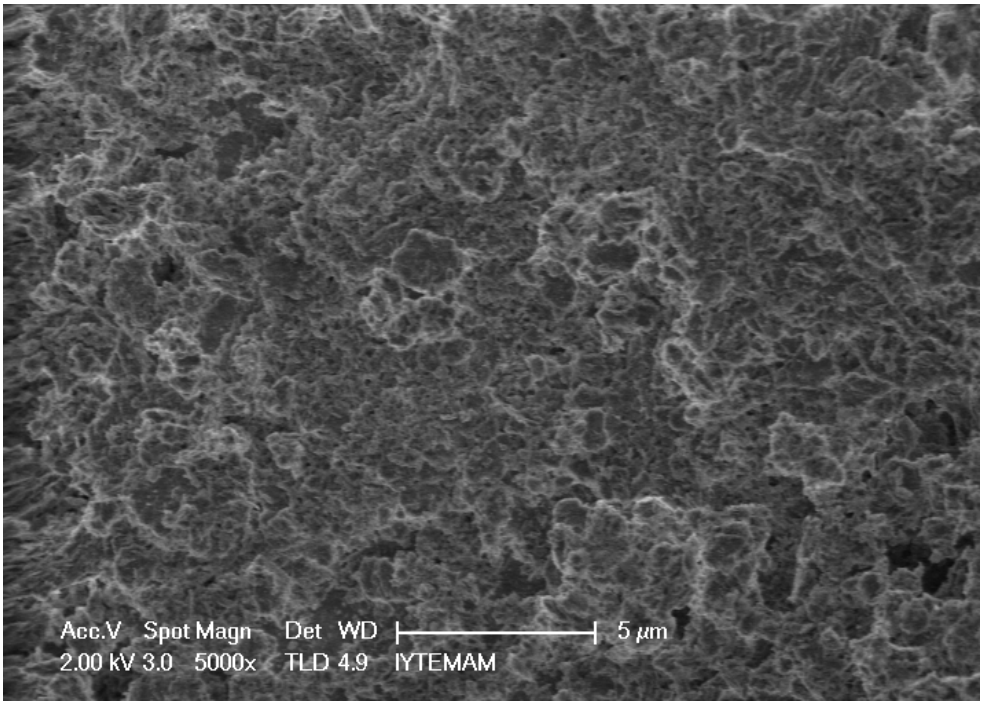

(a)

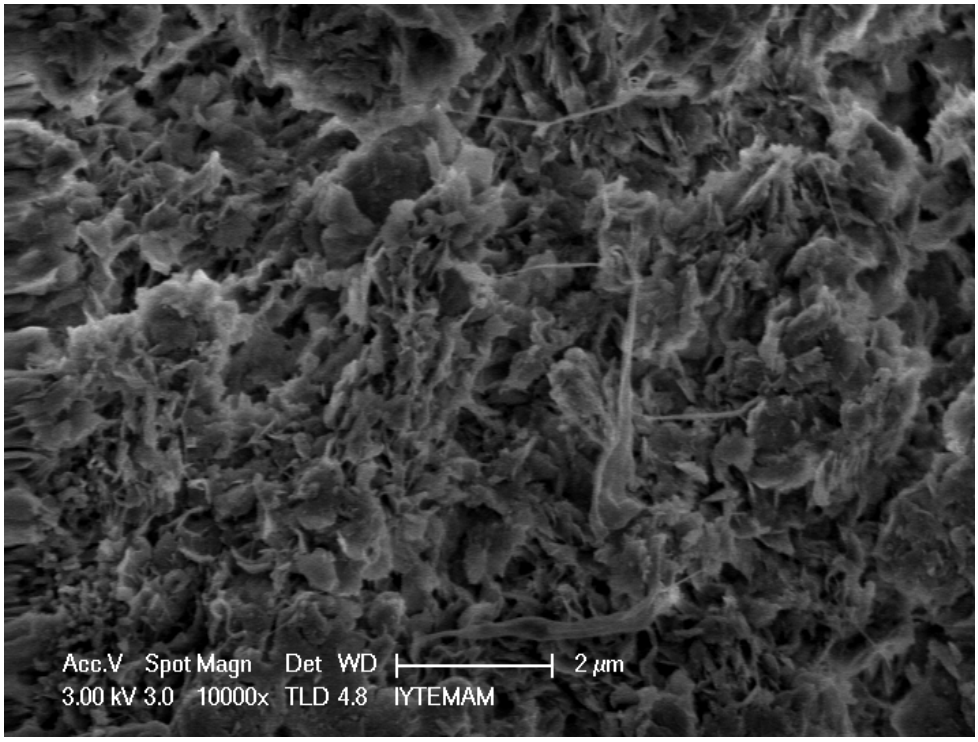

(b)

Figure 8.49. SEM Micrograph of PNBD-1% MMT nanocomposite magnification with (a) 5000× (b) 10000×.

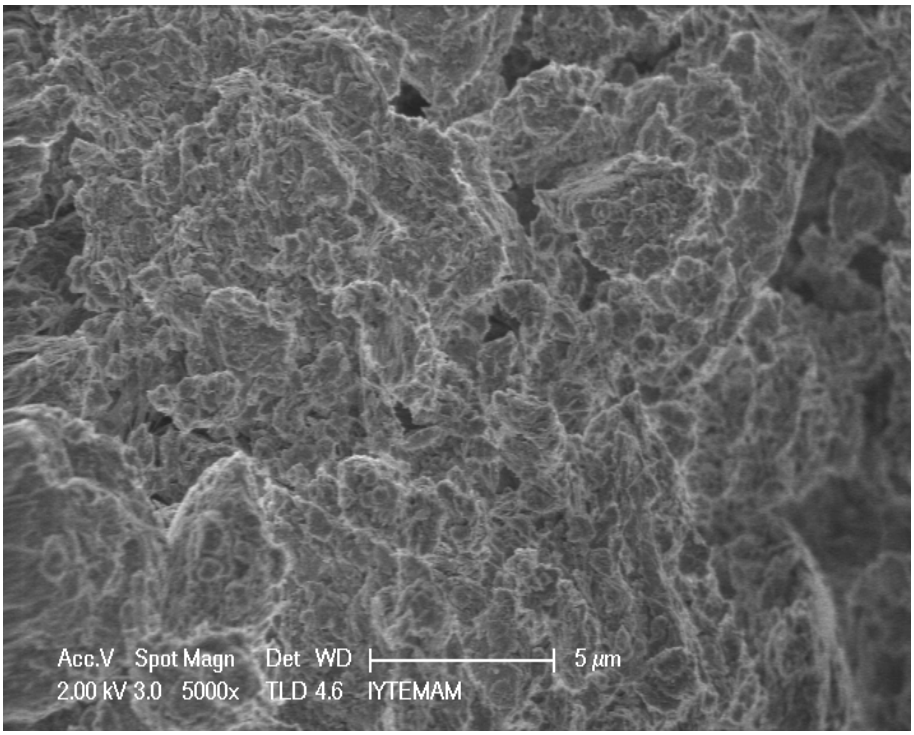

(a)

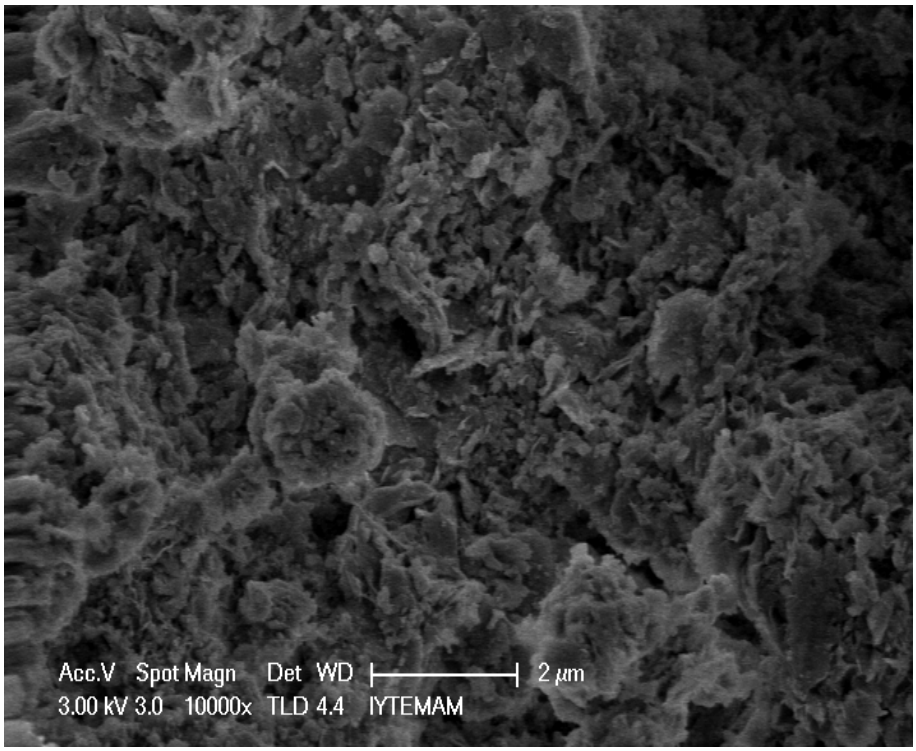

(b)

Figure 8.50. SEM Micrograph of PNBD-3% MMT nanocomposite magnification with (a) 5000× (b) 10000×.

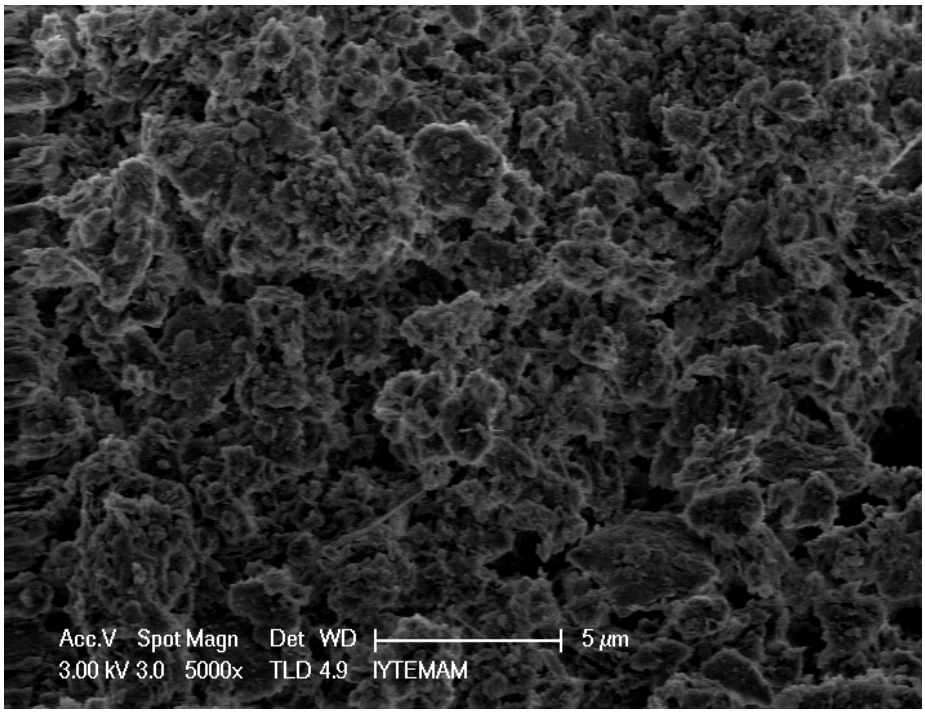

(a)

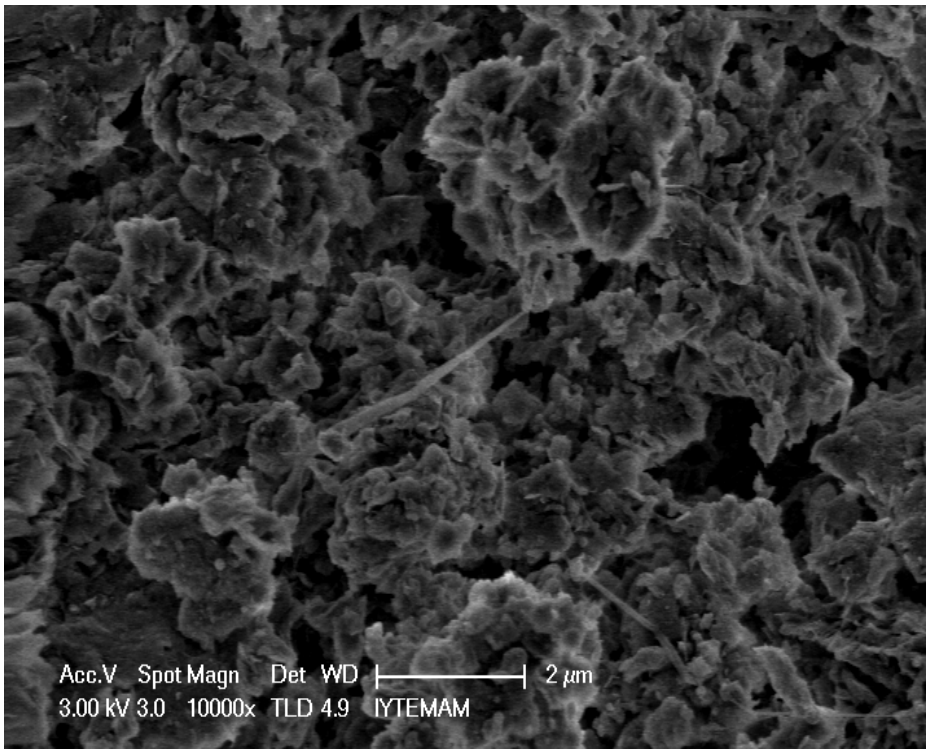

(b)

Figure 8.51. SEM Micrograph of PNBD-5% MMT nanocomposite magnification with (a) 5000× (b) 10000×.

8.7.5. TEM Analysis of Nanocomposites

To more clearly identify exfoliated structures of the nanocomposites, TEM images of the composites were obtained. The nanocomposite structure which are exfoliated and/or intercalated that can be decided with TEM analysis. The prepared 1%, 3% and 5% polynorbornadiene-clay nanocomposites of the TEM images was given in Figure 8.52, Figure 8.53, Figure 8.54, respectively.

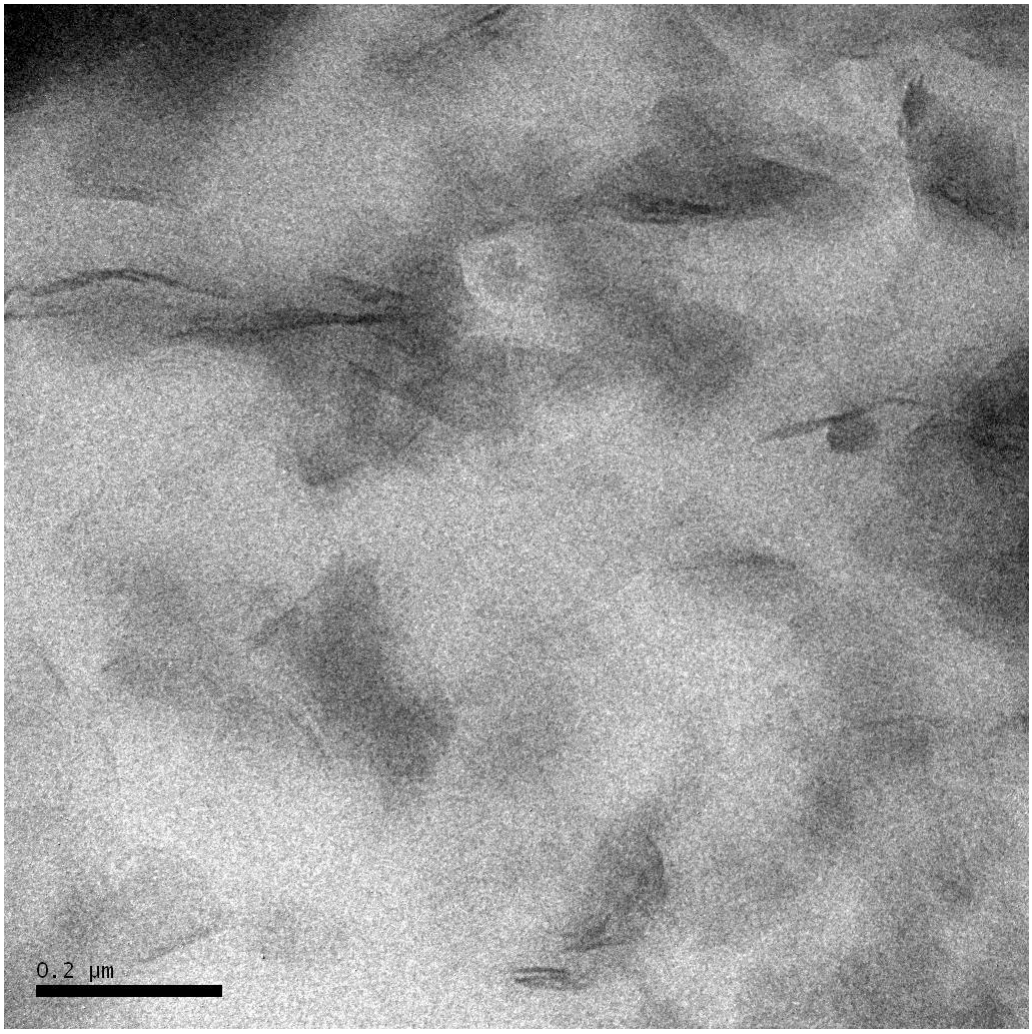

Figure 8.52. TEM Micrograph of PNBD-1% MMT nanocomposite.

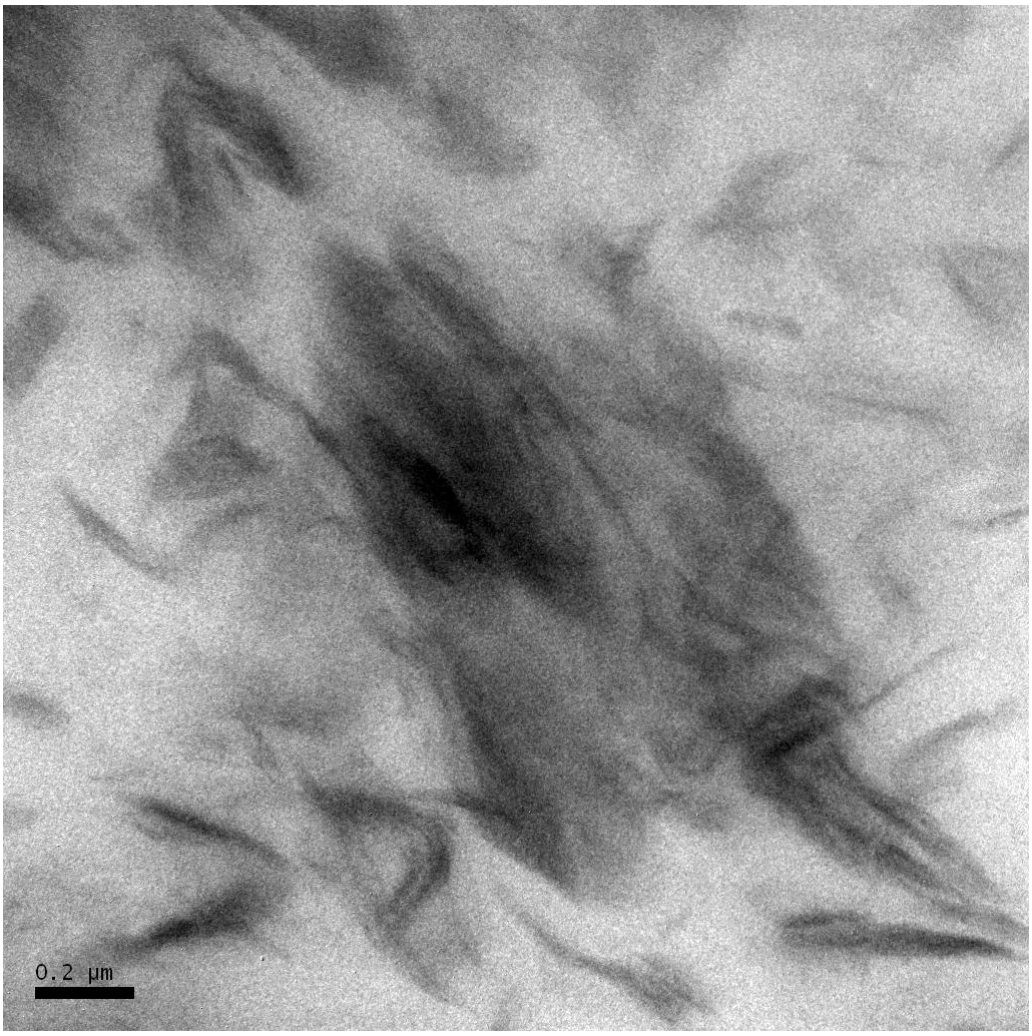

Figure 8.53. TEM Micrograph of PNBD-3% MMT nanocomposite.

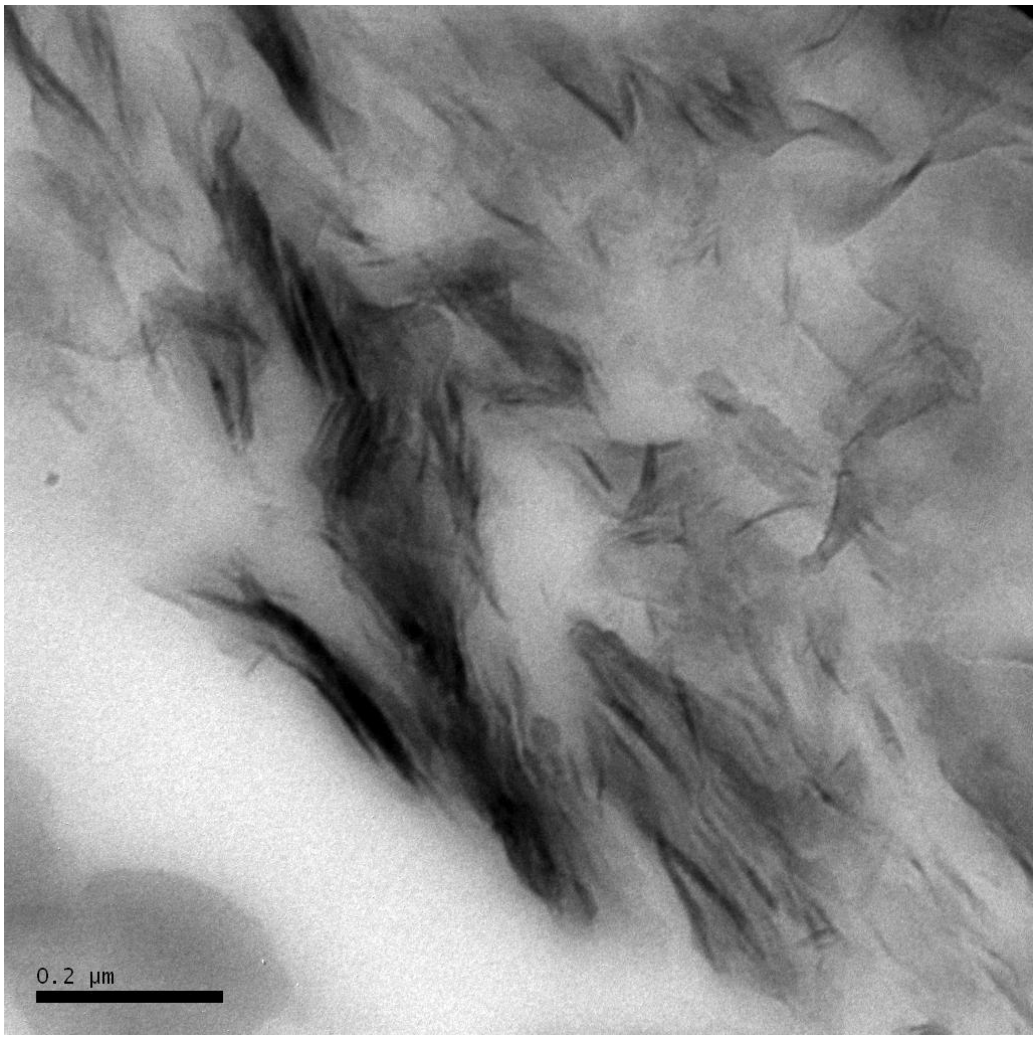

Figure 8.54. TEM Micrograph of PNBD-5% MMT nanocomposite.

As shown in Figure 8.52-54, where dark stripes represent the clay layers and the gray/white area represents the polymer matrix. It is clear at low content of clay that the exfoliated clay platelets are distributed in the polymer matrix more homogeneously and randomly (Figure 8.52). The size of the clay layers is ~3 nm thick and under 200 nm long. Individual silicate layers, along with two and three layer stacks, are exfoliating in the polymer matrix. For higher content of the clay (Figure 8.53 and 8.54), it is revealed that some of the clay domains actually consist of multiple layers, indicating that the clay exfoliation did not reach the single-layer-exfoliation condition. Some larger intercalated particles can also be identified. This is probably because the charge of the pristine clay layer is not locally constant but varies from layer to layer.

Eventually, the clay platelets for PNBD-1%MMT nanocomposite dispersed more than other nanocomposites. This observation was also consistent with the XRD results assigning the exfoliation to the same composite.

8.7.6. Dielectric Properties of Nanocomposites

The dielectric properties of prepared 1%, 3% and 5% polynorbornadiene-clay nanocomposites were investigated. Also, dielectric properties of polynorbornadiene were investigated to compare dielectric properties of the nanocomposites. For this purpose, the thickness of the polymer and the nanocomposite films were prepared as 60-80 μm. These films were kept under vacuum for a night before measuring. Dielectric properties were carried out as calculation of dielectric constants and measuring of dielectric losses (tan δ). For the purpose of calculating of dielectric constant (ε_r) in the range of 100 Hz-1 MHz frequency, the capacitance (C) values were measured by the LCR meter. Dielectric constant (ε_r) was calculated by the following equation (8.1):

$$C = \varepsilon_r \varepsilon_o (A/d) \qquad (8.1)$$

In the equation 8.1, ε_o is the vacuum permeability as 8.85×10^{-12} Fm^{-1}, A is the area of electrodes, d is the thickness of the sample.

Nanocomposite samples containing different percentage of clay (1%, 3% and 5%) change with the dielectric constant were shown in Figure 8.55 at constant frequency (10 kHz) and a constant temperature (25 ^{o}C). According to this figure, the dielectric constant decreased with increasing percentage of clay. The dielectric constant (ε_r) of clay is around 9 at the 10 kHz frequency (Israel et al., 2008). The dielectric constant of synthesized PNBD is around 5.5 at 10 kHz. The dielectric constants of nanocomposites were observed to decrease according to the pure polymer. The main objective of this project is to prepare polynorbornadiene-clay nanocomposites that have lower dielectric properties than the polynorbornadiene. Thus, materials that have lower dielectric constant properties were obtained that can be used in particularly electric-electronic industry.

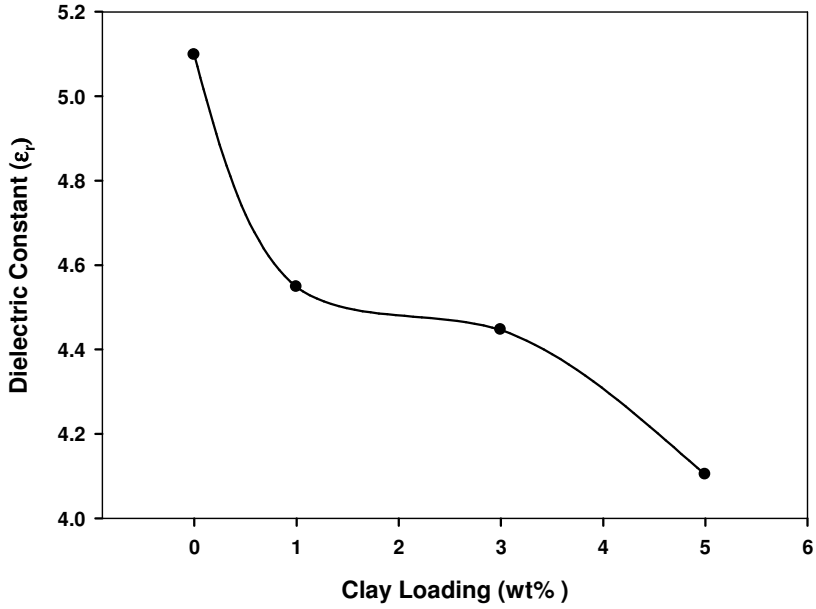

Figure 8.55. The change of Dielectric Constant with the clay loading for PNBD and Nanocomposites (10 kHz-25°C).

The change of dielectric constant (ε_r) with the frequency for polynorbornadiene-clay nanocomposites and pure PNBD were given at Figure 8.56.

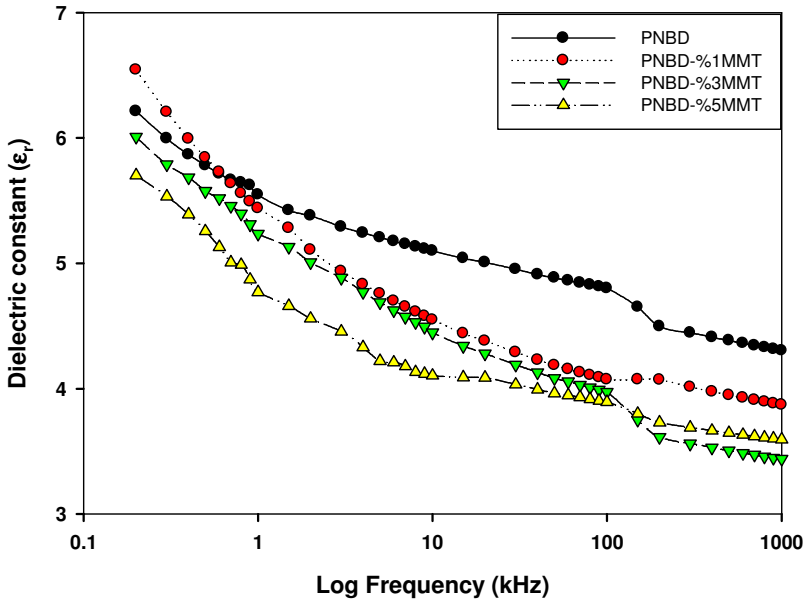

Figure 8.56. The change of Dielectric Constant with the frequency for PNBD and Nanocomposites.

As shown in Figure 8.56, the dielectric constant of nanocomposites and PNBD decreased as the intercalated clay increased for various frequencies. The decrease is significant and related to the content of clay and frequencies. It is believed that the reduced polarization of dipole orientation is largely responsible for this decrease due to the nanoscopic-confinement effects in the randomly exfoliated and intercalated layer structures. At some literature was reported that, a similar effect with organic-inorganic composites where the polymer is confined within 1.5-2.0 nm of the layered-silicate inorganic host (Anastasiadis et.al., 2000). This confinement effect is directly reflected in the local re-orientation dynamics. It might be understood that the decrease of dielectric constant at low frequencies of nanocomposite materials is due to this confinement effect. The dipole orientation from the ring of PNBD is constrained and does not move easily due to the confinement of clay at the nanoscale level.

The variation of dielectric loss (tan δ) for nanocomposite samples containing different percentage of clay (1%, 3% and 5%) and pure polymer, at constant frequency (10 kHz) and constant temperature (25^0C) is given in Figure 8.57. Polynorbornadiene-clay nanocomposites exhibited lower dielectric losses compared to pure polymer. In addition, the results obtained from this study, with the increasing of the percentage of clay used in the nanocomposite, dielectric loss (tan δ) was decreasing. This result is preferred for the possibility and the place of use of nanocomposites in the industry.

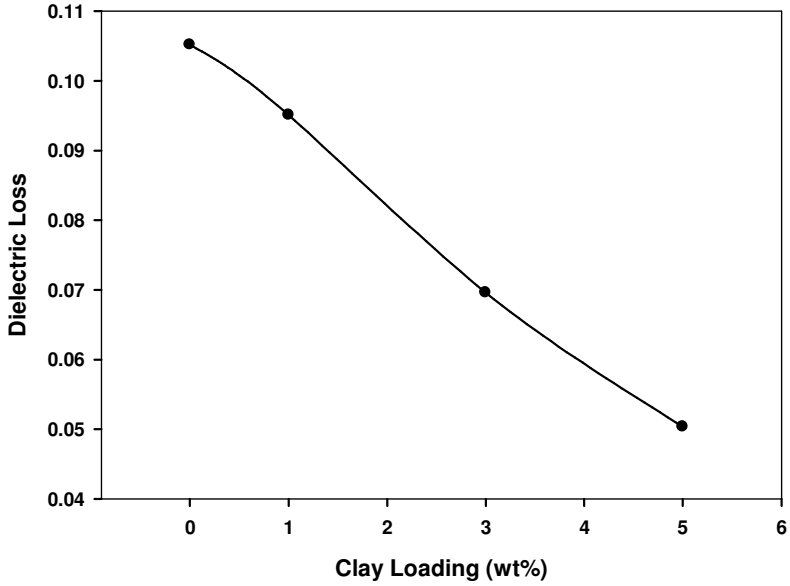

Figure 8.57. The change of Dielectric Loss with the clay loading for PNBD and Nanocomposites (10 kHz-25°C).

Dielectric loss (tan δ) of prepared 1%, 3% and 5% polynorbornadiene-clay nanocomposites and pure polymer in the frequency range was shown in Figure 8.58. The dielectric losses decreased with increasing applied frequency. The dielectric losses were approximately constant at high frequencies (MHz, etc.).

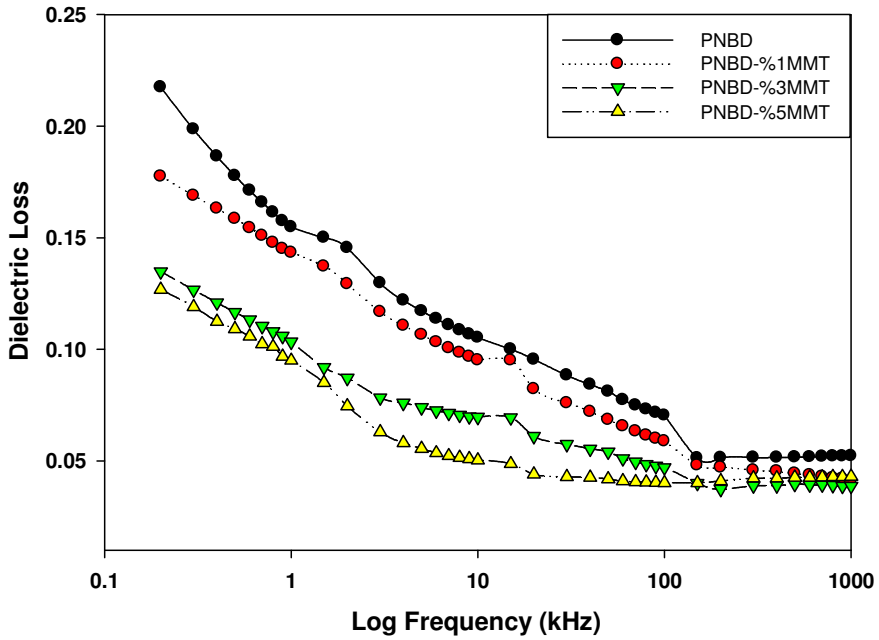

Figure 8.58. The change of Dielectric Loss with the frequency for PNBD and Nanocomposites.

9. CONCLUSIONS

For the assessment of synthesis of Ruthenium complex, firstly the ligand containing a quaternary ammonium salt was synthesized in Ar atmosphere with 80% yield. The characterization of this ligand was carried out by ^{1}H NMR and FTIR spectroscopies. Similarly, the Ruthenium salt and Ruthenium complex were synthesized and characterized by ^{1}H NMR, FTIR, TG and DTG methods.

Characterization of the montmorillonite was achieved by FTIR, XRD, TG and DTG methods. The basal spacing value (d_{001}) of montmorillonite was calculated as 11.4 Å. The characteristic absoption bands were obtained at about 3622, 1630, 3400, 1150 and 915 cm^{-1}, respectively from FTIR spectrum. From TG-DTG thermograms, the weight loss of unmodified montmorillonite was found as 8.5 wt % that have volatile materials. The maximum peak temperature of DTG thermogram was about 645 ^{o}C.

The montmorillonite was modified by Ruthenium complex according to cation exchange process and the modification conditions were optimized. The interlayer spacing of the silicate layers for modified montmorillonite was determined with X-Ray Diffraction Spectrometers. The basal spacing was expanded to 18.72 Å. Characterization of the modified montmorillonite was achieved by also FTIR, TG and DTG methods. The characteristic absoption bands of montmorillonite and Ruthenium complex together were obtained from FTIR spectrum. According to TG thermogram, the weight loss of modified montmorillonite was found as 26 wt % due to the organic materials, Ru complex, as a modificator at 1000 ^{o}C. The difference of unmodified montmorillonite, it was indicated that 17.5 wt % modificator was hold on to the montmorillonite. This result was compatible with that calculated of amount of modificator from CEC of the montmorillonite.

The norbornadiene was polymerized at different polymerization conditions. Then, the polymer was precipitated in large amount of vigorously stirred methanol by adding dropwise. But the polymer could not be isolated in high yield with only using catalyst. Trimethylsilydiazomethane was used as a co-catalyst in polymerization reactions as in several literatures. The effect of the ratio of [C] / [M], temperature, reaction time, precipitation reagent, quantity of solvent,

type of solvent and quantity of co-catalyst were investigated and optimize polymerization conditions were determined. Eventually, polymerization was carried out 1/1000 [C] / [M] ratio, in 3 mL dry dichloromethane, with 1 mL trimethylsilydiazomethane as a co-catalyst, at reflux temperature, for 6 hours and with 80% yield.

Characterization of the polynorbornadiene was achieved by FTIR, ^{1}H NMR, GPC, TG and DTG methods. According to GPC trace, M_n=34320 g/mol (the number average molecular weight), M_w= 121380 g/mol (weight-average molecular weight) and M_w/M_n=3.53 (PDI) results were obtained. The maximum peak temperature was obtained about 425 ^{o}C from DTG thermograms.

The polynorbornadiene-clay nanocomposites were prepared at different clay concent (1%, 3% and 5%) with in-situ polymerization method. Characterization of the nanocomposites was achieved by XRD, FTIR, TG, DTG, SEM and TEM methods. From XRD patterns, there is a lack of any diffraction peak in 2θ=4-10^0 as opposed on the diffraction peak at 2θ=4.71^0 (d_{001}=18.7 Å) for organophilic clay, indicating the possibility of having exfoliated silicate nanolayers of organophilic clay dispersed in a PNBD matrix. For the PNBD-1%MMT and PNBD-3%MMT nanocomposite, an exfoliated structure was obtained with absence of any d_{001} reflection in the XRD region. The existence of exfoliation may be due to good compatibility of PNBD with monomer at low concentration that might result from interaction of clay surface with the PNBD. On the other hand, PNBD-5%MMT exhibited small and broad peaks that might be probably resulting from partially exfoliated or intercalated structures. It was indicating that there is a small amount of organoclay existing in the form of an intercalated layer structure.

According to TG thermograms of the all nanocomposites and polynorbornadiene, all nanocomposite structures exhibited enhanced thermal stabilities compared to the pure polymer, PNBD. From the DTG data, it is clear that the maximum peak temperature (T_d) and residual weight after complete volatilization both increased. The maximum peak temperatures of the nanocomposites are higher than pure PNBD, and shift toward higher temperature as the amount of Na-MMT increases, indicating an enhancement of the thermal stability upon intercalation. The maximum peak temperatures of the PNBD,

PNBD-1% MMT, PNBD-3% MMT and PNBD-5% MMT were 440, 450, 530, 570 ^{o}C, respectively. The maximum peak temperature (in air) increased by 130 ^{o}C in comparison of PNBD with the PNBD-5% MMT nanocomposite. This enhancement of the thermal stability may be caused by the 'barrier effect' of the montmorillonite layer structure, which hinders mobility of the small molecules produced during the thermal degradation of the PNBD.

The surface morphology of the nanocomposites are compared by SEM analyses. For the PNBD-3%MMT and PNBD-5%MMT nanocomposites, one can see big aggregated particles together with small aggregates which may be attributed to intercalated or partially exfoliated structure. This may be most probably due to the poor interaction of MMT layers with polymer matrix in the interlayer galleries. On the other hand, PNBD-1%MMT nanocomposite has relatively small clusters of the clay particles that are homogeneously dispersed in the PNBD matrix.

From the TEM images, it is clear at low content of clay that the exfoliated clay platelets are distributed in the polymer matrix more homogeneously and randomly. The size of the clay layers is ~3 nm thick and under 200 nm long. Individual silicate layers, along with two and three layer stacks, are exfoliating in the polymer matrix. For higher content of the clay (3% and 5 %), it is revealed that some of the clay domains actually consist of multiple layers, indicating that the clay exfoliation did not reach the single-layer-exfoliation condition. Some larger intercalated particles can also be identified. This is probably because the charge of the pristine clay layer is not locally constant but varies from layer to layer.

Finally, the dielectric properties of prepared 1%, 3% and 5% polynorbornadiene-clay nanocomposites were investigated. Also, dielectric properties of polynorbornadiene were investigated to compare dielectric properties of the nanocomposites. Dielectric properties were carried out as calculation of dielectric constants and measuring of dielectric losses (tan δ) in the range of 100 Hz-1 MHz frequency. The dielectric constant decreased with increasing percentage of clay. The dielectric constant (ε_r) of clay is around 9 at the 10 kHz frequency. The dielectric constant of synthesized PNBD is around 5.5 at

10 kHz. The dielectric constants of nanocomposites were observed to decrease according to the pure polymer.

The dielectric constant of nanocomposites and PNBD decreased as the intercalated clay increased for various frequencies. The decrease is significant and related to the content of clay and frequencies. It is believed that the reduced polarization of dipole orientation is largely responsible for this decrease due to the nanoscopic-confinement effects in the randomly exfoliated and intercalated layer structures.

Polynorbornadiene-clay nanocomposites exhibited lower dielectric losses compared to pure polymer. In addition, the results obtained from this study, with the increasing of the percentage of clay used in the nanocomposite, dielectric loss (tan δ) was decreasing. The dielectric losses decreased with increasing applied frequency. The dielectric losses were approximately constant at high frequencies (MHz, etc.).

Summarily, the polymer-clay nanocomposites were produced by means of an economical single-step i.e. in situ polymerization method that clay layers were dispersed in polymers matrix and enhancement of thermal stability and dielectric properties.

REFERENCES

Alexandre, M., Beyer, G., Henrist, C., Cloots, R., Rulmont, A., JerGme, R., and Dubois, P., 2001, Preparation and Properties of Layered Silicate Nanocomposites Based on Ethylene Vinyl Acetate Copolymers, *Macromol Rapid Comm.*, 22, 643-646p.

Bai Y., Chiniwalla P., Kohl P.A. and Bidstrup-Allen S.A., 2001, Photosensitive Polynorbornene as a Dielectric Material for Packaging Applications, *International Symposium on Advanced Packaging Applications*, 322-326p.

Bazan, G.C., Schrock, R.R., Khosravi, E., Feast, W.J. and Gibson, V.C. 1989, Living Ring-Opening Metathesis Polymerization of 2,3-Difunctionalized-Norbornodiences by Mo(CH-t-Bu)CN-2,6-C_6H_3-i-Pr_2(O-t-Bu)$_2$), *Polym. Commun.,* 30, 258-268p.

Bazan, G.C., Khosravi, E., Schrock, R.R., Feast, W.J., Gibson, V.C., O'Regan, M. B., Thomas, J.K. and Davis, W.M., 1990, Living ring-opening metathesis polymerization of 2,3-difunctionalized norbornadienes by Mo(:CHBu-tert)(:NC6H3Pr-iso2-2,6)(OBu-tert)2, *J. Am. Chem. Soc.* 112, 8378-8387p.

Bharadwaj, R.K., 2001, Modeling the barrier properties of polymer-layered silicate nanocomposites, *Macromolecules*, 34, 1989–1992p.

Biagini, S. C. G., Gibson, V. C., Giles, M. R., Marshall, E. L. and North, M., 1997, Synthesis of Peniciline derived polymers utilizing ring-opening metathesis polymerisation methodology., *Chem. Commun*., 1097-1195p.

Biswas, M. and Sinha Ray, S., 2001, Recent progress in synthesis and evaluation of polymer–montmorillonite nanocomposites, *Adv Polym Sci*, 155, 167–221p.

Bourbigot, S., LeBras, M., Dabrowski, F., Gilman, J. W. and Kashiwagi, T., 2000, PA-6 clay nanocomposite hybrid as char forming agent in intumescent formulations, *Fire Mater*, 24, 201–208p.

Brow, T.L. and Lee, K.J., 1993, Ligand steric properties., *Coord. Chem. Rev*. 128, 89-98p.

REFERENCES (Continue)

Chen, J.S., Poliks, M.D., Ober, C.K., Zhang, Y., Wiesner, U. and Giannelis, E.P., 2002, Study of the interlayer expansion mechanism and thermal-mechanical properties of surface-initiated epoxy nanocomposites, *Polymer*, 43, 4895–4904p.

Czelusniak I. and Szymanska-Buzar T., 2004, Metathesis polymerization of norbornene and norbornadiene in the presence of tert-butylacetylene initiated by tungsten(II) and molybdenum(II) complexes, *Applied Catalysis A:General*, 277, 173-182p.

Dabrowski, F., Bourbigot, S., Delbel, R. and Bras, ML., 2000, Kinetic molding of the thermal degradation of polyamide-6 nanocomposite, *Eur Polym J* , 36, 273–284p.

Delaude, L., Demonceau, A. and Noels, A.F., 1999, Highly Stereoselective Ruthenium-Catalyzed Ring Opening Metathesis Polymerization of 2,3-Difunctionalized Norbornadienes and their 7-Oxa analogues, *Macromolecules*, 32, 7, 2091-2103p.

Demonceau, A., Stumpf, A. W., Saive, E. and Noels, A. F., 1997, Novel Ruthenium-Based Catalyst System for The Ring-Opening Metathesis Polymerisation of Low-Strain Cyclic olefins., *Macromolecules*, *30*, 3127-3136p.

Finkelshtein, E.Sh., Gringolts, M.L., Ushakov, N.V., Lakhtin, V.G., Soloviev, S.A. and Yampol'skii, Yu.P., 2003, Synthesis and gas permeation properties of new ROMP polymers from silyl substituted norbornadienes and norbornenes, *Polymer* 44, 2843–2851p.

Gamez P., Steensma R.H., Driessen W.L. and Reedijk, 2002, J. *Inorganica Chimica Acta*, 333, 51-56p.

Ghosh, A.K. and Hussain, K. A., 1998, Convenient synthesis of novel macrocyclic urethanes: alkoxycarbonylation of amines and ring-closing metathesis strategy, *Tetrahedron Lett.*, 39, 1881-1884p.

Giannelis, E.P., 1998, Polymer-layered silicate nanocomposites: synthesis, properties and applications, *Appl Organomet Chem*, 12, 675–680p.

REFERENCES (Continue)

Giannelis, E.P., Krishnamoorti, R. and Manias, E., 1999, Polymer-silicate nanocomposites: model systems for confined polymers and polymer brushes, *Adv Polym Sci*, 138, 107–147p.

Gilman, J.W., Kashiwagi, T. and Lichtenhan, J.D., 1997, Flammability studies of polymer-layered silicate nanocomposites, *SAMPE J*, 33, 40–45p.

Gilman, J.W., Jackson, C.L., Morgan, A.B., Harris, Jr. R., Manias, E., Giannelis, E.P., Wuthenow, M., Hilton, D. and Phillips, S.H., 2000, Flammability properties of polymer-layered silicate nanocomposites. Propylene and polystyrene nanocomposites, *Chem Mater*, 12, 1866–1873p.

Gloaguen, J. M. and Lefebvre, J. M., 2001, Plastic deformation behaviour of thermoplastic/clay nanocomposites, *Polymer*, 42, 5841-5847p.

Grove N.R., Kohl P.A., Bidstrup-Allen S.A., Jayaraman S. and Shick R., 1999, Functionalized Polynorbornene Dielectric Polymers: Adhension and Mechanical Properties, *Journal of Polymer Science :Part B:Polymer Physics* , 37, 3003-3010p.

Grubbs, R. H., Miller, S. J. and Fu, G. C., 1995, Ring-Closing Metathesis and Related Processes in Organic Syenthesis., Ring Closing diene Metathesis in Organic Synthesis., *Acc. Chem. Res*., 28, 446-452p.

Hackett, E., Manias, E. and Giannelis, E.P., 1998, Molecular Dynamics simulations of organically modified layered silicates, *J Chem Phys*, 108, 7410–7415p.

Hafner, A., Van der Schaaf, P. A. and Mühlebach, A., 1996**,** Recent Developments in Ring Opening Metathesis Polymerization, A. *Chimia*, *50*, 131-134p.

Hasegawa, N., Okamoto, H., Kawasumi, M., Kato, M., Tsukigase, A., and Usuki A., 2000, Polyolefin-clay hybrids based on modified polyolefins and organophilic clay, *Macromolecular Materials and Engineering*, 280(1), 76-79p.

He´Risson, J.-L. and Chauvin, Y., 1970, *Makromol. Chem*., 141, 161-176p.

REFERENCES (Continue)

Hiroi, R., Sinha Ray, S., Okamoto, M. and Shiroi, T., 2004, Organically modified layered titanate: a new nanofiller to improve the performance biodegradable polylactide, *Macromol Rapid Commun*, 25, 1359–1363p.

Huang, X. and Brittain, W. J., 2001, Synthesis and Characterization of PMMA Nanocomposites by Suspension and Emulsion Polymerization, *Macromolecules*, 34, 3255-3260p.

Ivin, K. J. and Mol, J. C., 1997, Olefin Metathesis and Metathesis Polymerization; Academic Press, San Diego.

Jeon, H. G., Jung, H., and Hudson, S. D., 1998, Morphology of polymer/silicate nanocomposites, *Polymer Bulletin*, 41, 107-113p.

Kawasumi, M., Hasegawa, N., Usuki, A. and Akane, O., 1998, Nematic liquid crystal/clay mineralcomposites, *Mater. Eng. Sci. C*, 6, 135-143p.

Ke, Y., Long, C. and Qi, Z., 1999, Crystallization, Properties, and Crystal and Nanoscale Morphology of PET–Clay Nanocomposites, *J. Appl. Polym. Sci*, 71, 1139-1146p.

Kinoshita, A., Sakakibara, N. and Mori, M., 1997, Novel 1,3-Diene Synthesis from Alkyne and Ethylene by Ruthenium-Catalyzed Enyne Metathesis, *J. Am. Chem. Soc.,* 119, 12388-12389p.

Krishnamoorti, V.R. and Giannelis, E.P., 1996, Structure and dynamics of polymer layered silicate nanocomposites, *Chem Mater*, 8, 1728–1734p.

Lagaly, G., 1986, Interaction of alkylamines with different types of layered compounds, *Solid State Ionics,* 22, 43–51p.

Laus, M., Camerani, M., Lelli, M., Sparnacci, K., Sandrolini, F., and Francescangeli, O., 1998, Hybrid nanocomposites based on polystyrene and a reactive organophilic clay, *J. Mater. Sci*., 33, 2883-2888p.

Leeuwenburgh, M. A., Van der Marel, G. A. and Overkleeft, H. S., 2003, Olefin metathesis in glycovbiology: New routes towards diverse neoglycoconjugates., *Curr. Opin. Chem. Biol.,* 7, 757p.

LeBaron, P.C., Wang, Z. and Pinnavaia, T.J., 1999, Polymer-layered silicate nanocomposites: an overview, *Appl Clay Sci*, 15, 11–29p.

REFERENCES (Continue)

Liu, L., Qi, Z., and Zhu, X., 1999, Studies on Nylon 6/Clay Nanocomposites by Melt-Intercalation Process, *J. Appl Polymer Sci,* 71, 1133-1138p.

Loo, L.S. and Gleason, K.K., 2003, Fourier transforms infrared investigation of the deformation behavior of montmorillonite in nylon 6/nanoclay nanocomposites, *Macromolecules*, 36, 2587–2590p.

Love, J.A., Sanford, M.S., Day, M.W. and Grubbs, R.H., 2003, Synthesis, Structure and Activity of Enhanced Initiators for Olefin Metathesis*, J. Am. Chem.Soc*. 125, 10103-10113p.

Manning, D. M., Hu, X., Beck, P. and Kiessling, L. L., 1997, Synthesis of Sulfated Neoglycopolymers: Selective P-selection inhibitors, *J. Am. Chem. Soc.*, 119, 3161-3170p.

Mitchell, C.A., Bahr, J.L., Arepalli, S., Tour, J.M. and Krishnamoorti, R., 2002, Dispersion of functionalized carbon nanotubes in polystyrene, *Macromolecules,* 35, 8825–8830p.

Magonov, S. and Yer ina, N.A., 2005, In Microscopy for Nanotechnology, Kluwer Academic Press, New York, 113p.

Makovetsky K.L., 1999, *Polym Sci Ser B*, 41, 269p.

Matos J.M.E. and Lina-Neto B.S., 2004, Piperidine as ancillary ligand in the novel [$RuCl_2(PPh_3)_2$(piperidine)] complex for metathesis polymerization of norbornene and norbornadiene, *Journal of Molecular Catalysis A:Chemical*, 22, 81-85p.

Messersmith, P.B. and Giannelis, E.P., 1995, Synthesis and barrier properties of poly(1-caprolactone)-layered silicate nanocomposites, *J Polym Sci, Part A: Polym Chem,* 33, 1047–1057p.

Messersmith, P. B., and Giannelis, E. P., 1994, Synthesis and characterisation of layered silicate-epoxy nanocomposites, *Chem. Mater*., **6**, 1719-1725p.

Messersmith, P. B., and Giannelis, E. P., 1995, Synthesis and barrier properties of poly(ε-caprolactone)- layered silicate nanocomposites, *J. Appl. Polym. Sci. Part A*, 33, 1047-1057p.

Michler, G.H., and Balta-Call, F.J., 2005, Mechanical Properties of Polymers Based on Nanostructure and Morphology, CRC PressTaylor & Francis, Boca Raton and New York.

REFERENCES (Continue)

Mohanty, A.K., Drzal, L.T. and Misra, M., 2003, Nano-reinforcement of bio-based polymers-the hope and reality, *Polym Mater Sci Eng*, 88, 60–61p.

Morgan, A.B., Gilman, J.W., and Jackson, C.L., 2001, Characterization of the Dispersion of Clay in a Polyetherimide Nanocomposite, *Macromolecules*, 34, 2735-2741p.

Murdzek, J. S. and Schrock, R. R., 1987, Low polydispersity homopolymers and block copolymers by ring opening of 5,6-dicarbomethoxy norbornene., *Macromolecules,* 20, 2640-2547p.

Nguyen, S. T., Johnson, L. K., Grubbs, R. H. and Ziller, J. W., 1992, Ring opening metathesis polymerisation (ROMP) of norbornene by a group VIII carbene complex in protic media., *J. Am. Chem. Soc*., 114, 3974-3980p.

Nguyen, S. T., Johnson, L. K., Grubbs, R. H. and Ziller, J. W., 1993, Catalytic ring-closing metathesis of functionalized dienes by a ruthenium carbene complex, *Am. Chem. Soc.,* 115 (21), 9858p.

Noels, A.F. and Demonceau, A., 1998, *In Metathesis Polymerization of Olefins and Polymerization of Alkynes*; Imamoglu, Y., Ed.; Kluwer: Dordrecht, 29-46p.

Odıan G., 2004, Principles of Polymerization, fourth edition, John Wiley Interscience, New York, 544p.

Okada, A., Kawasumi, M., Usuki, A., Kojima, Y., Kurauchi, T., and Kamigaito O., 1990, Nylon 6-clay hybrid, *Mater. Res. Soc. Proc*., 171, 45-50p.

Okada, A., Kawasumi, M., Usuki, A., Kojima, Y., Kurauchi, T. and Kamigaito, O., 1990, Synthesis and properties of nylon-6/clay hybrids. In: Schaefer DW, Mark JE, editors. Polymer based molecular composites. MRS Symposium Proceedings, Pittsburgh, 171, 45–50p.

Opstal, T., Couchez, K. and Verpoort, F., 2003, Easily Accessible Ring Opening Metathesis and atom Transfer Radical Polymerization Catalysts based on Arene, Norbornadiene and Cyclooctadiene Ruthenium Complexes Bearing Schiff Base Ligands, *Adv. Synth. Catal*., 345, 393-401p.

REFERENCES (Continue)

Oriakhi, C.O., Farr, I.V. and Lerner, M.M., 1997, Thermal characterization of poly(styrene sulfonate)/layered double hydroxide nanocomposites, *Clays and Clay Minerals,* 45, 194p.

Oriakhi, C.O., Nano sandwiches**.,** 1998, *Chem. Br.*, 34, 59-65p.

Peetz R.M., Moustafa A.F. and Kennedy J.P., 2003, Cationic Polymerization of Norbornadiene, *Journal of Polymer Science: Part A: Polymer Chemistry*, 41, 732-739p.

Pitarch, M., McKee, V., Nieuwenhuyzen, M. and McKervey, M. A., 1998, Synthesis of Bridged, Multifunctional Calixarenes via Ring Closing Metathesis, *J. Org. Chem.*, 63, 946-951p.

Schneider, M. F., Lucas, N., Velder, J. and Blechert, S., 1997, Selektive ring öffnende olefin metathese mit funktional isierten monosubstituierten olefinen *Angew.Chem., Int. Ed. Engl*., 36, 257-259p.

Schrock, R. R., Murdzek, J. S., Bazan, G. C., Robbins, J., DiMare, M. and O'Regan, M., 1990, Synthesis of molybdenum imido alkyidine complexes and some reactions involving acyclic olefins., *J. Am. Chem. Soc.,* 112, 3875-3880p.

Schrock, R. R., DePue, R., Feldman, J., Schaverien, C. J., Dewan, J. C. and Liu, A. H., 1988, Preparation and reactivity of several alkylidene complexes of the type W(CHR')(N-2,6-C6H3-iso-Pr2)(OR)2 and related tungstacyclobutane complexes. Controlling metathesis activity through the choice of alkoxide ligand, *J. Am. Chem. Soc*., 110 (5), 1423p.

Schrock, R. R., 1990, Living ring-opening metathesis polymerization catalyzed by weel characterized transition-metal alkylidene complexes., *Acc. Chem. Res.,* 23, 158-165p.

Schwab, P., France, M. B., Ziller, J. W. and Grubbs, R. H., 1995, A Series of Well-Defined Metathesis Catalysists Synthesis of $[RuCl_2(=CHR')(PR_3)_2]$and ıts Reactions., *Angew. Chem., Int. Ed. Engl*., 34, 2039-2041p.

REFERENCES (Continue)

Seligson, A.L. and Trogler, W.C., 1991, Cone angles for amine ligands. X-ray crystal structures and equilibrium measurements for ammonia, ethylamine, diethylamine, and triethylamine complexes with the [bis(dimethylphosphino)ethane]methylpalladium(II) cation, *J. Am. Cem. Soc.* 113, 2520p.

Sinha Ray, S., Yamada, K., Okamoto, M. and Ueda, K., 2002, New polylactide/layered silicate nanocomposite: a novel biodegradable material, *Nano Lett*, 2, 1093–1096p.

Sinha Ray, S. and Okamoto, M., 2003, Polymer/layered silicate nanocomposites: a review from preparation to processing, *Prog Polym Sci*, 28, 1539–1641p.

Stewart, R., 2006, In Plastics Engineering, SPE Brook-field CN, 12p.

Stumpf, A. W., Saive, E., Demonceau, A. and Noels, A. F., 1995, Ruthenium-based catalysts fort he ring opening metathesis polymerisation of low-strain cyclic olefins and of functionalised derivatives of norbornene and cyclooctane., *J. Chem. Soc., Chem. Commun*., 1127-1128p.

Suh, D. J., Lim, Y.T. and Park, O.O., 2000, The property and formation mechanism of unsaturated polyester-layered silicate nanocomposite depending on the fabrication methods, *Polymer*, 41(24), 8557p.

Szymanska-Buzar, T., Glowiak, T. and Czelusniak, I., 2001, The initiation of ring-opening metathesis polymerization of norbornadiene by seven-coordinate molybdenum(II) compounds. X-ray crystal structure of [Mo(μ-Cl)($SnCl_3$)$(CO)_3$(η^4-NBD)], *Journal of Organometallic Chemistry*, 640, 72-78p.

Theng, B.K.G., 1979, Formation and properties of clay–polymer complexes, Elsevier, Amsterdam.

Trnka, T.M. and Grubbs, R.H., 2001, The Development of L_2X_2Ru CHR Olefin Metathesis Catalysts: An Organometallic Success Story, *Acc. Chem. Res*. 34, 18-29p.

REFERENCES (Continue)

Usuki, A., Kojuma, Y., Kawasumi, M., Okada, A., Fukushima, Y., Kurauchi, T. and Kamigaito, O., 1993, Synthesis of Nylon 6- Clay Hybrid, *J Mater Res*, 8, 1179-1185p.

Vaia, R.A., Teukolsky, R.K. and Giannelis, E.P., 1994, Interlayer structure and molecular environment of alkylammonium layered silicates, *Chem. Mater.,* 6, 1017–1022p.

Vaia, R.A. and Giannelis, E.P., 1997, Lattice of polymer melt intercalation in organically-modified layered silicates., *Macromolecules,* 30, 7990–7999p.

Vaia, R.A., Price, G., Ruth, P.N. and Nguyen, H.T., 1999, Polymer/layered silicate nanocomposites as high performance ablative materials. *J.Appl Clay Sci,* 15, 67–92p.

Vaia, R.A. and Wagner, H.D., 2003, Desk Reference of Polymer Characterization and Analysis, Oxford Press, ACS, 490p.

Vaia, R.A. and Wagner, H.D., 2004, Polymer Nanocomposites: Framework for the Future, *Mater. Today Nov*., 32-37p.

VanderHart, D.L., Asano, A, and Gilman, J.W., 2001, NMR measurements related to clay dispersion quality and organic-modifier stability in nylon 6/clay nanocomposites, *Macromolecules*, 38, 3819–3822p.

Wagener, K. B., Boncella, J. M. and Nel, J. G., 1991, Acyclic Diene Metathesis (Admet) Polymerization, *Macromolecules,* 24, 2649-2657p.

Wallenberger, F.T. and Weston, N.E., 2004, Eds. Natural Fibers, Plastics and Composites, Kluwer Academic, Boston.

Weimer, M. W., Chen, H., Giannelis, E. P., and Sogah, D. T., 1999, Direct synthesis of dispersed nanocomposites by in-situ living free radical polymerisation using a silicate-anchored initiator, *J. Am. Chem. Soc*., 121, 1615-1616p.

Wilson Jr., O., C., Olorunyolemi, T., Jaworski, Borum, A., L., Young, D., Siriwat, A., Dickens, E., Oriakhi, C. and Lerner, M., 1999, Surface and interfacial properties of polymer-intercalated layered double hydroxide nanocomposites., *Appl. Clay Sci.,* 15, 265p.

REFERENCES (Continue)

Yano, K., Usuki, A., Okada, A., Kurauchi, T. and Kamigaito, O., 1993, Synthesis and properties of polyimide–clay hybrid, *J. Polym. Sci, Part A: Polym Chem*., 31, 2491–2493p.

Zanetti, M., Camino, G., Thomann, R., and Miilhaupt, R., 2001, Synthesis and thermal behaviour of layered silicate-EVA nanocomposites, *Polymer*, 42, 4501-4507p.

Zumbrunnen, D.A., Inamdar, S., Kwon, O. and Verma, P., 2002, Chaotic Advection as a Means to Develop Nanoscale Structures in Viscous Melts, *Nano Lett*., 2, 1143p.

Esra Evrim YALÇINKAYA

Personal Information

1. Date / Place of Birth : 18.02.1980 - Erzurum, TURKEY
2. Sex : Female
3. Nationality : Turkish Republic
4. e-mail: esra.evrim.saka@ege.edu.tr

Education

2005 - E.U. Institute of Natural and Applied Science, Izmir, TURKEY **Ph.D. in Physical Chemistry,** The subject of PhD. Thesis "Polymer Clay Nanocomposites"

2002-2005 E.U. Institute of Natural and Applied Science, Izmir, TURKEY **MSc. in Physical Chemistry,** The subject of MSc. Thesis "The Effects of the Ionic strength, Ion Species and pH on the Electrokinetic Properties of the Montmorillonite"

1998 - 2002 E.U. Faculty of Science Chemistry Dept. Izmir, TURKEY **BSc. in Chemistry**

Publications

DURMAZ, Y. Y.; KARAGOZ, B.; BICAK, N., ODACI DEMİRKOL, D.; **YALCINKAYA, E. E.;** TIMUR, S.; YAGCI, Y., "Modification of Polydivinylbenzene Microspheres by a Hydrobromination/Click-Chemistry Protocol and their Protein-Adsorption Properties", *Macromolecular Bioscience,* 11 (**2011**) 141-150.

MAVIOGLU AYAN, E., TOPTAS, A., KIBRISLIOGLU, G., **SAKA YALCINKAYA, E.E.,** YANIK, J., ''Biosorption of Dyes by Natural and Activated Vine Stem. Interaction between biosorbent and dye'', *Clean-Soil Air Water,* 39 (4)(**2011**), 406-412.

YALCINKAYA, E.E..; GULER, C., ''Electrokinetic Properties of Acid-Activated Montmorillonite Dispersions", *Separation Science and Technology*, 45(5) (**2010**) 635-643.

SAKA, E.E..; GULER, C., "The effects of electrolyte concentration, ion species and pH on the zeta potential and electrokinetic charge density of montmorillonite", *Clay Minerals*, 41 (**2006**) 853-861.

Employment

Research Assistant, Ege University, Faculty of Science, Department of Chemistry, Division of Physical Chemistry, 2002-

Projects

2007 – **Ege University, Research Funds**, 2008 / FEN / 046

2008 - 2010 **TUBITAK-TBAG** (108T101)

2004 - 2005 **Ege University, Research Funds**, 2004 / FEN / 053

Scholarship

The Scientific and Technological Research Council of Turkey (TUBITAK-BAYG), National PhD Fellowship Programme, 2006-2010, 4 years.

Courses, Congress and Conferences

Seleci, M., Ag, D., Odaci Demirkol, D., **Yalcinkaya, E.E**., Timur, S., 'Use of montmorillonite clay as biosensing material', *10th workshop on biosensors and bioanalytical microtechniques in environmental and clinical analysis,* June **2011**, GERMANY.

Mavioğlu Ayan, E., Kıbrıslıoğlu, G., Toptaş, A., **Yalçınkaya, E.E.,** Yanık, J., 'Biomass as a Low-cost Sorbent', *The Fourth International Student Conference on Advanced Science and Technology ICAST,* 25-26 May **2010**, İzmir, TURKEY

Yalcınkaya, E.E., Guler, C., "Electrokınetıc propertıes of acid activated montmorıllonıte dıspersıons", *23rd European Colloid and Interface Society (ECIS) Conference,* 6-11 September **2009**, Antalya, TURKEY

Yalcınkaya, E.E., Guler, C., "modificatıon of montmorillonite with new alkylammonıum based ruthenıum complex", *23rd European Colloid and Interface Society (ECIS) Conference,* 6-11 September **2009**, Antalya, TURKEY

Yalcınkaya, E.E., Guler, C., "Synthesis of polynorbornadiene with ring opening methatesis polymerization by using new Ru-based catalyst", *European Polymer Congress*, 12–17 July **2009**, Graz, AUSTRIA.

Yalcınkaya, E.E., Nato Advanced Study Institute (Ası); New Smart Materıals Vıa Metal Medıated Macromolecular Engıneerıng: From Complex To Nano Structures, 1-12 September **2008**, Antalya, TURKEY

Saka E.E.., Guler, C., "The Effects Of The Hıgh Valence Catıon Specıes And Concentratıon on The Zeta Potentıal And Electrokınetıc Charge Densıty of The Montmorıllonıte", *XIII. National Clay Symposium,* **2007**, Isparta, TURKEY.

Saka E.E.., Guler, C., "The Effects of The pH, Ionic strength and Ion Specıes on the Zeta Potentıal of The Montmorıllonıte", *XIX. National Congress on Chemistry,* **2005**, İzmir, TURKEY.

Saka E.E.., Guler, C., "The effects of pH and Ionic strength on the zeta potential of Montmorillonite ", *XVIII. National Congress on Chemistry*, **2004**, Kars, TURKEY.

Research Interests

Polymer clay nanocomposites, clays, polymerization, dielectric properties, zeta potential